Ultrasound Testing System for the Detecting of the Shape and Growth of a Vapor Chamber in the VAPEX Process

This Thesis

Submitted to the Faculty of Graduate Studies and Research

in Partial Fulfillment of the Requirements for the

Degree of Masters of Applied Science in

Electronic Systems Engineering at the

University of Regina

by

Wenjin Zhou

Regina, Saskatchewan

July 2011

UNIVERSITY OF REGINA

FACULTY OF GRADUATE STUDIES AND RESEARCH

SUPERVISORY AND EXAMINING COMMITTEE

Wenjin Zhou, candidate for the degree of Master of Applied Science in Electronic Systems Engineering**,** has presented a thesis titled, ***Ultrasound Testing System for the Detecting of the Shape and Growth of a Vapor Chamber in the VAPEX Process,*** in an oral examination held on June 30, 3011. The following committee members have found the thesis acceptable in form and content, and that the candidate demonstrated satisfactory knowledge of the subject material.

External Examiner:	Dr. Peng Luo, Saskatchewan Research Council
Supervisor:	Dr. Raman Paranjape, Electronic Systems Engineering
Committee Member:	Dr. Mehran Mehrandezh, Industrial Systems Engineering
Committee Member:	Dr. Paul Laforge, Electronic Systems Engineering
Committee Member:	*Dr. Koorosh Asghari, Petroleum Systems Engineering
Chair of Defense:	Dr. Troni Grande, Department of English

*Not present at defense

ABSTRACT

Acoustic wave detection systems are designed to estimate distances based on the measurement of the time of arrival (TOA) of an ultrasonic wave. It has been used in diagnoses and treatments in areas such as medicine, dentistry, civil engineering, and many other industrial applications. It has also been applied in the oil industry for pipeline inspection and fluid velocity measurement.

In this study, a comprehensive experimental program was designed and conducted to evaluate the feasibility of using acoustic waves for detection and monitoring of vapor chamber growth and pressure front movement in porous media during vapor chamber expansion in the VAPEX process. Vapor extraction is a potential nonthermal recovery process used to improve the recovery factor from heavy oil and bitumen reservoirs. In this process, a mixture of light hydrocarbon vapors close to its dew-point, such as propane or butane, is injected into the reservoir through a horizontal injection well. As the solvent vapor comes into contact with the heavy oil, it dissolves in the oil and reduces its viscosity. The mobilized oil then drains into the second horizontal production well. After the breakthrough of the vapor chamber from injection to production well, the vapor chamber begins to grow and more oil becomes mobilized by interaction with the solvent chamber.

The simulated VAPEX chamber in this study was conducted by using different sized air balloons buried in a water- or oil-saturated sand pack. The ultrasound receivers

were placed on the physical model to detect the acoustic signals from the transducers. A Matlab^{TM} based program was developed to do the signal processing using wavelet signal transform technique to extract the position of the echo signal from the signal record; the size and shape of the air balloons were determined based on the TOF of the ultrasonic signal record. The results of the measurements and simulations show that ultrasound detection system is applicable to test the shape and growth of simulated VAPEX chamber in a lab scale; the image results of the simulated lab model are reliable. It is the first time that such a technique has been proposed for this purpose and it was proven effective on a laboratory scale.

ACKNOWLEDGMENTS

I wish to acknowledge the following persons or organizations:

- Dr. Raman Paranjape, my academic advisor, for his excellent guidance, valuable advice and constant encouragement during my Master's degree program.
- Dr. Koorosh Asghari, my research advisor, for his supervision, trust, and support throughout the experimentation for this research work;
- My past and present research group members, Dr. Mehran Mehrandezh, Mr. Rui Zhou, Mr. Chayatat Ratanasawanya, for their useful technical discussions during my thesis study. In particular, I am grateful to Mr. Farid Ahmadloo for his technical assistance and suggestions in this thesis research;
- Petroleum Technology Research Centre (PTRC).
- Faculty of Graduate Studies and Research (FGSR) at the University of Regina.
- My parents for their constant support and inspiration throughout my entire education.

TABLE OF CONTENTS

LIST OF FIGURES

LIST OF TABLES

LIST OF APPENDICES

NOMENCLATURE

Notations

Z	Acoustic Impedance, [M L^{-2} T^{-1}]; N s/m^3 or Pa s/m
ρ	Material Density, [M L^{-3}]; kg/m^3
v	Sound Speed, [L T^{-1}];
d	Distance, m
t	Time, s
ψ	Mother Wavelet
a	Scale Index
b	Position Index in Wavelet Transform
W	Continuous Wavelet Transform
P	Position Index for the Peak Signal
f	Sampling Frequency
C	Wavelet Transform Coefficient

Acronyms

TOA	Time of Arrival
TOF	Time of Flight
AI	Acoustic Impedance
CWT	Continuous Wavelet Transform
DWT	Discrete Wavelet Transform
VAPEX	Vapor Extraction
NDT	Non-destructive Detection
SONAR	Sound Navigation And Ranging
RADAR	Radio Detection and Ranging

1. Introduction

The VAPEX process is an attractive enhanced oil recovery (EOR) process due to its low energy requirements, lesser environmental impact, and significantly lower operational costs. In this process, a solvent is injected into a heavy oil or bitumen reservoir close to its dew-point pressure. After the breakthrough of gas to the production well, a solvent chamber forms around the injection and production wells. Through the expansion phase of the solvent chamber, the oil comes into contact with the solvent, which becomes miscible with the oil in order to increase its mobility. Then, the mobilized oil flows due to gravity into the parallel horizontal well.

One of the challenging aspects of VAPEX process is in-situ monitoring of solvent chamber formation and growth during the process. This can provide a unique opportunity to have better control on vapor chamber growth and to potentially optimize the process. In this thesis, the use of underground sound navigation and ranging (SONAR) is proposed as a non-destructive technique to determine the shape and growth rate of a vapor chamber in an experimentally simulated VAPEX process.

1.1. VAPEX Process

VAPEX process was proposed by Dr. Butler in the early 1990s [66]. VAPEX is an EOR method for the extraction of heavy oil and bitumen using solvent injection in a vapor state (e.g. butane, propane). During this process, the dissolution of solvent into the

oil phase significantly reduces its viscosity, and as a result increases the mobility of the oil. The solvent is typically injected into a horizontal well configuration similar to the steam assisted gravity drainage (SAGD) process (Figure 1.1). Recently, VAPEX has received considerable attention because of the abundance of heavy oil and bitumen resources in Canada and increasing energy demands. It is estimated the oil-in-place in Canadian reserves is more than 400 billion m^3, which is approximately twice that of the total conventional oil reserves of all Gulf nations. These reserves are in the sand and carbonate formations in Athabasca, Cold Lake, Peace River and Wabasca [52].

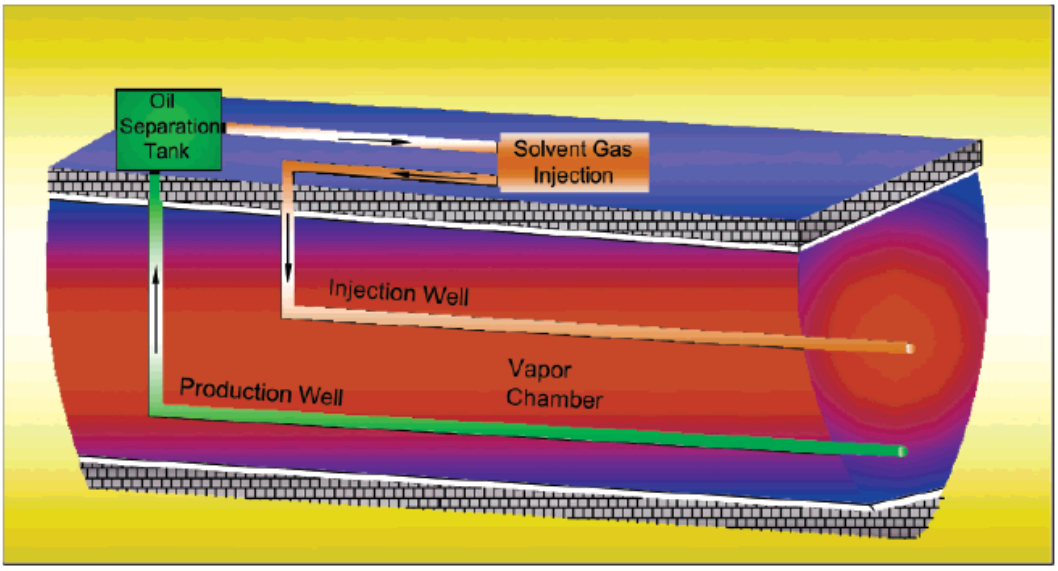

Fig. 1. 1. Typical heavy oil reservoir in VAPEX process [52]

VAPEX is typically implemented in the horizontal configuration of an injection well above a production well. It is located inside a heavy oil and bitumen reservoir, between two impermeable rock layers called the overburden and the underburden (Figure 1.2). Solvent diffusion and dissolution on the edge of the vapor chamber reduces the viscosity of heavy oil and also provides for in-situ upgrading of the oil through a

de-asphalting process. Thus, using the forces of gravity, the oil can flow to the underlying production well.

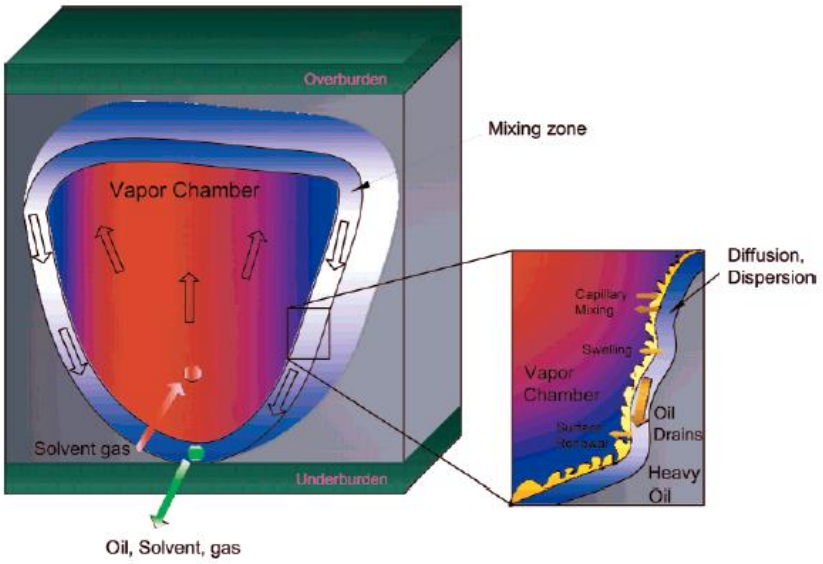

Fig. 1. 2. Concept of VAPEX [52]

Although the VAPEX process requires no fresh water and less capital and energy than other thermal recovery techniques, it has several shortcomings that negatively impact its performance. A few of its shortcomings are slow mixing of solvent with heavy oil and bitumen resulting in a long startup time and low initial oil recovery rates, de-asphalting of heavy oil which potentially leads to formation damage, specific arrangements of wells, and monitoring and control of the vapor chamber.

Currently, there are few techniques (e.g. micro seismic) for monitoring the growth of the vapor chamber during the VAPEX process which could be beneficial with regard to a better understanding and consequently more successful implementation of VAPEX technology. Advantages of monitoring the vapor chamber growth at different stage of the process are:

1. A better understanding of the production mechanisms during the VAPEX process by determining more representative values for diffusion and dispersion phenomena in VAPEX.
2. Understanding the growth rate of the vapor chamber can assist in a better evaluation of the solvent chamber growth, monitoring of the effect of formation heterogeneity on the efficiency of the process, and control the optimization of the process.
3. Determination of the sweep efficiency of the process and a more accurate determination of the un-swept zone in the reservoir with regard to future infill drilling or modification of well patterns.

1.2. Acoustic Detection Techniques

Acoustic detection techniques, which are also called acoustic detection methods, are viewed as nondestructive methods which analyze the acoustic wave's characteristics in order to measure the shape and/or location of an object within an environment. An analysis of a reflected acoustic signal's characteristics can assist in localizing the interface between materials. An important concept in acoustics is acoustic impedance, which is the acoustic property of a material. The following equation illustrates acoustic impedance:

$$Z = v \times \rho, \qquad [1.1]$$

where Z is the characteristic acoustic impedance ([M·L^{-2}·T^{-1}]; N s/m^3 or Pa s/m), ρ is the

density of the medium ([M L^{-3}]; kg/m^3), and v is the speed of sound propagating through the material ([L T^{-1}]; m/s).

The reflection of acoustic waves occurs when there is a change in acoustic impedance between two adjacent materials. Thus, the reflected signal can be used to determine the presence of any abnormality or discontinuity in a solid body. At the same time, the reflected surface of a different material will not change the sound wave's properties, which means the shape of the reflected signal is in complete accordance with the incoming signal. The angle between the reflected acoustic signal and the reflective surface is equal to the angle between the incoming acoustic wave and reflective surface. If the incoming acoustic signal is perpendicular to the border of the two adjacent materials, the reflected acoustic signal will reflect along the incoming path in the reverse direction. The reflected signal can also be called an echo signal and the object that reflects the sound wave is called the reflector. Acoustic detection techniques transmit acoustic signals, record reflected signals, and analyze the records in order detect objects in the environment. The type of acoustic signal used in an acoustic system is usually a pulse shaped signal due to its strong discontinuity, which makes the signal clearer and therefore easier to extract. The acoustic transducer used as a signal transmitter and receiver is an apparatus with the capability of converting electrical energy into acoustic energy and back again [54]. This device is also called a probe in an ultrasound system. It is attached to the surface of an object and transmits pulses into the object. It receives an echo pulse if there is any other material or object inside the object being examined. At the

same time, an analyzer measures the TOA (time of arrival) of the echo signal and calculates the TOF (time of flight) of the ultrasonic signal, which is the time interval between the transmitted pulse and the received echo pulse. The distance between the surface of the object to which the probe is attached and the detected material/object in the measured object is calculated using the following equation:

$$d = \frac{t \times v}{2} \qquad [1.2]$$

where d is the distance between the surface of the object to which the probe is attached and the reflector in the object (m), t is the time interval between the transmitted pulse and the echo pulse (s), and v is the speed of sound (m/s). The speed of sound is a critical element in the system. Usually, the speed of sound through a medium is not known, so it is necessary to perform a prerequisite experiment before the detection system can be used for quantitative measurements. Figures 1.3 and 1.4 show how the system is used to measure an object underwater and the theoretical signal that would be collected from the probe, respectively.

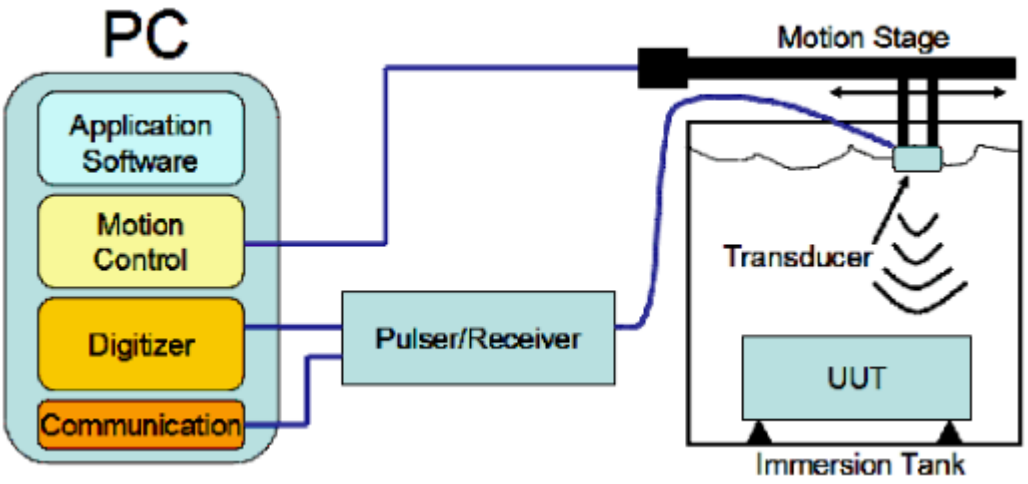

Fig. 1. 3. Ultrasound system for an underwater object [7]

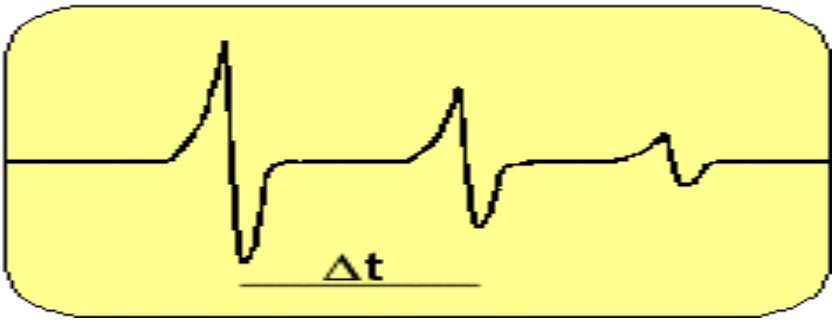

Fig. 1. 4. Theoretical ultrasound signal [7]

Figure 1.4 shows a theoretical ultrasonic pulse signal collected at the transducer, which is composed of the transmitted pulse and two echoed pulses. The first pulse is the transmitted signal and the remaining two signals are the echo pulses, which are wider with lower amplitudes due to attenuation and path loss during the propagation process.

Since the acoustic detection system is based on the sound wave's reflective properties, it is also called the pulse-echo detection system. It has various industrial applications such as crack detection on bridges, water depth measurements and SONAR systems. The main purpose of this thesis is to apply acoustic experimentation within a

simulated laboratory situation, combining both distance measurements and a transducer's measured position in order to attain the shape of the vapor chamber during the VAPEX process.

1.3. Purpose and Scope of Thesis

The purpose of this thesis is to explore the feasibility of using a pulse-echo detection system for the detection of the vapor phase in a porous media using a lab-scale experimental model. The main research objectives of this study are:

1. To design and manufacture an experimental set-up and perform preliminary measurements using known environments (i.e., oil- and water-saturated sand packs) in order to validate the system.
2. To measure the speed of sound in water to validate the measurements in this study against the reported speed of sound in water in the lecture.
3. Experimental simulation of VAPEX process in porous media using two different fluids (i.e., water and oil).
4. To conduct measurements using different ultrasound transducers at different frequencies to determine the trade-off between the distance of propagation and the precision of resolution.
5. To measure the speed and attenuation of sound through water- and oil-saturated sand packs in order to assess the depth propagation characteristics.

6. To conduct a scattering shape measurement to determine the spatial sampling rate of the system.
7. To find the most suitable signal processing algorithm with which to analyze the collected ultrasonic data.
8. To conduct a series of measurements to detect specific and random shapes in the sand pack.
9. To create a representation of the shape of various buried objects in the two different media using the collected ultrasonic data.

1.4. Thesis Outline

This thesis is comprised of six chapters. Chapter 1 introduces the subject matter of the thesis' research and lists the major research objectives. Chapter 2 provides a literature review of industrial applications of ultrasound techniques. Additionally, it includes a signal processing algorithm used to analyze and process ultrasonic signals. Chapter 3 presents the experimental program, including the experimental set-ups, the prerequisite measurements and the selection of a suitable transducer for the imaging experiments. Chapter 4 outlines the details of the signal processing algorithm used to process the ultrasound data. It also details major difficulties in extracting the information from the ultrasound signal record and how to address them using a signal processing algorithm. Chapter 5 presents a set of experimental data which was conducted to measure the shape of different objects in both water- and oil-saturated sand packs. The improvement of the

accuracy and resolution of imaging of the simulated vapor chambers are also discussed in this chapter. Finally, Chapter 6 summarizes the major findings in this study and provides a list of recommendations for future studies.

2. Literature Review

Although acoustic testing for monitoring the vapor chamber in the VAPEX process is a new area of research, there are other acoustic theory-based testing systems such as exploration seismology and ultrasonic well logging, which are applied in the oil industry.

2.1. Exploration Seismology

Exploration seismology is a major application of wave-based measurements in the oil industry. 'Seismic' refers to vibrations within the earth. The P seismic wave (whose compressions and rarefactions act on the soil in the vertical direction) is essentially a low-frequency sound wave. The P wave partially reflects as it travels downward through different layers in the soil. Its application to exploration began in searches for underground oil reserves [55]. Exploration seismology involves a manmade vibration or explosion above ground. Subsoil energy is transmitted by acoustic sources (e.g. dynamite, air gun, or vibroseis). Data is collected using hydrophones (in water) or geophones (on the ground). A key aspect in these seismic techniques is the measurement of the sound's propagation characteristics as it travels through a boundary. The sound signals, which are collected using geophones or hydrophones, produce images of the earth media [56]. Thus, the underground structure can be determined by analyzing the reflected signals. At the first stage of the seismic technique, two types of seismic data analyses are applied. The

first is refraction seismology, which analyzes the geological structure with the refraction phenomenon as the sound wave travels through different types of soil or rock, which in turn leads to a different speed of sound [57]. The second seismic data analysis approach is called reflection seismology which uses a reflected seismic wave; it is dependent upon the difference in the adjacent materials' acoustic impedance, which determines the geological structure [58]. The reflection data can be analyzed and interpreted relatively easily but it cannot provide an accurate result unless the seismic velocity in each rock layer is higher than the one above it [59]. Hence, reflection seismic analysis is not frequently used in the oil industry.

Reflected seismic signals create a representation of the subsurface structure. The geophones are always fixed in-line. When the source is set on the same line as the geophones, a two-dimensional (2D) profile can be generated. If the source moves around the lines, causing the reflected signals to be recorded out of the plane of the in-line profile, then a three-dimensional (3D) image is possible [66]. The key to reducing domestic oil and gas exploration costs in the oil industry is a fast, accurate imaging of complex, oil-bearing geology such as over thrusts and salt domes [4]. If accurate 3D seismic imaging beneath salt domes is possible, the number of known oil reserves could significantly increase. Twenty-seven years ago, the first 3D time lapse seismic data was acquired from onshore Texas to monitor an enhanced oil recovery (EOR) fire-flood project [1]. The development of research in its application led to an analysis of 3D seismic data aimed at identifying and locating hydrocarbon deposits, drilling fewer wells

for better oil and gas recovery, characterizing hydrocarbon reservoir boundaries, subsurface formations, lithology, and depth, and estimating porosity and drilling locations [2]. BP began applying 4-D seismic activity, or time-lapse seismic activity, in the 1990's for effective reservoir management and infill drilling campaigns in late-life water-flood fields and newer, more complex fields [1]. 4D seismic technologies is an important subject in the petroleum industry, enabling exploration with more than 3D seismic data [5]. In Draugen Field, situated offshore from Norway, 4D seismic interpretation plays a key role in reservoir management [6]. At the same time, all 4D interpretations conducted so far have indicated the need for simulation model changes (such as modified reservoir volumes in certain areas), a revision of fault transmissibility and improved relative permeability characteristics. Quantitative 4D seismic data has been incorporated into the history matching procedure [5], and 4D seismic amplitude data was also included in a history matching procedure [7] [8]. Production history and 4D seismic data are usually incorporated into reservoir models through an interactive process [9]. At the same time, 4D seismic data can reflect a water saturation difference (time-lapse). Hence, 4D seismic data could point out discontinuities not originally apparent in static data [10]. With the arrival of information technology, the Vallhall oilfield initiated continuous monitoring with permanently installed cables at the bottom of the ocean and conducted monthly surveys which differ from non-continuous traditional 4D seismic data collection [11] that applies time lapse monitoring with an annual repetition interval. To analyze the seismic data, two main approaches are used, Wavelet transforms and Fourier transform. The

variation of frequency content with time is an important seismo-stratigraphic indicator [3]. Instead of describing a signal with time or frequency alone, the wavelet transform can be used to transform a recorded seismic reflection to the frequency domain, sample and interpret the frequency content of a spike, and use the same sample indices to locate the spike in the original temporal signal. As a result, the location of the subsurface stratifications, marked by spikes in the seismic reflections, can be mapped [3].

2.2. Well-logging Techniques

The acoustic system is applied to the well-logging technique using a sonic tool to transmit sound energy through the rocks of the bore wall [12]. In the oil and gas industry, the rock and fluid properties are recorded in an effort to find hydrocarbon zones in the areas intersected by a borehole. The purpose of well-logging, or borehole logging, is to gain detailed information regarding the formations penetrated by a borehole [13]. Acoustic well-logging is used to determine the wave velocity of a formation as introduced by Summers and Broding in 1952. The full waveform is recorded in order to determine the propagation velocities of the different types of waves and measure certain petro-physical properties to obtain lithological information [61]. Normally, a sonic tool consists of two modules. The transmitter is contained in one of the modules and two or more receivers are in the other. To reduce the direct sound energy transmitted along the tool, there is a rubber connection between the transmitter section and the receiver section. Figure 2.1 shows the construction of the sonic well-logging tool.

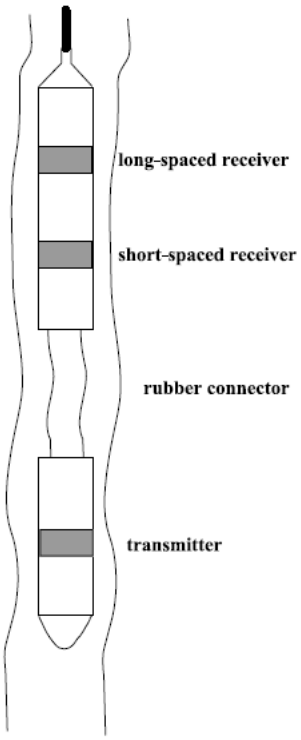

Fig. 2. 1. Schematic diagram of a sonic tool with a transmitter and two receivers [64]

When the sonic tool is placed in the borehole, sound energy is injected into the formation by the transmitter and a series of signals are received by the receiver. The TOF is measured to determine the density of the rock [13]. In sonic logging, the velocities of wave components (with or without their amplitudes) have been used to infer petro-physical or lithological properties such as mineralogy, fluid saturation, porosity, grain contacts, or rock types, such as sandstone, shale, and limestone in the surrounding formations [20] [21] [22] [23] [24]. The collected data is processed by a signal processing algorithm to extract necessary information such as the zero-crossing [25], the Karhunen-Loeve transform [26], the wavelet transform[20] [14] [15], the multiscale method [16] and the multiwave method [17].

2.3. Acoustics of Porous Media

Acoustic techniques are applied to porous media, such as sand and mud, to study the mechanisms of the sound's movement through the media. This technique assists with the detection of a mine and the estimation of the permeability of the reservoir [38].

2.4. Applications of Wavelet Transform to Acoustic Signals

In acoustic signal records, singularity and dynamics are the majority of signal information. Hence, the two key factors in signal processing are singularity analysis and dynamic behaviors. A wavelet is an excellent method for localizing singularities [18], which is important in measuring the TOF of a record in an acoustic system. To attain a more accurate measurement in the acoustic system, the peak signal should be carefully extracted from any background noise, eliminating strong interference on the reflected signal. A wavelet plays a large role in de-noising by damping or thresholding in the wavelet domain [19]. Sections 2.4.1 and 2.4.2 will introduce applications of wavelet transformation in transient signal localization and signal de-noising.

2.4.1. Transient Signal Localization

The application of a signal process on the acoustic record of the vapor chamber monitoring system is the same as applying an algorithm to other acoustic systems' data, such as sonic data from a well-logging system, data regarding the SONAR system, and signals from the seismic system and similar systems such as RADAR. In other words,

signal processing is focused more on the algorithm's capabilities to detect and classify short duration transients [27]. To localize the transient signal, a time-frequency characterization of the signal is required, which poses problems when using a Fourier transformation. A wavelet transformation maps a time series signal into a time-frequency domain showing the frequency components of the signal with the variation in time [62]. Therefore, it can easily locate the position of the singularity signal since it normally includes a high frequency component, which corresponds to a high wavelet transform coefficient. In the areas of seismic and well-log analysis, many researchers have shown wavelet transform is an effective way of processing acoustic data. Wavelet transformation has been applied to many types of acoustic systems. The reconstruction of seismic traces by wavelet transform has been found to be very effective in reservoir sand mapping and characterization [28]. The Morlet wavelet was used to analyze transient seismic signals, such as instantaneous amplitude, frequency and phase [29]. The wavelet transform in a frequency domain can be explained as a pair of high and low pass filters repeatedly applied to a signal trace. When it is being applied to the seismic trace, geophysical operations such as wave propagation can be readily derived in the wavelet domain [30]. Geological lithofacies groups were identified by applying the chart of the wavelet transform of their seismic reflection response [33] to conduct well-log analysis [34]. The wavelet decomposition was applied to the well-log and the detailed coefficient at each scale was analyzed. The larger coefficients were viewed as asymptotic structures, meaning there was a spike signal in the well-log. Wavelet transform was applied to the

well-log data in order to extract the features of the data [31]. A Morlet wavelet was used for the analysis process and resistivity and permeability data were applied to the logarithm of the signal. Following wavelet transformation of the signal with the Morlet mother wavelet, the faces of the well-log could be identified. Due to the wavelet's capabilities to identify breakdown points, the reservoir fluid was identified by applying wavelet transform to well-log data [32]. Therefore, in acoustic systems, wavelet transformation plays an important role in obtaining position information of a singularity in an acoustic signal record. In this study, acoustic signals will be applied to the VAPEX process in an effort to locate a solvent chamber.

2.4.2. De-noising by Wavelet Transform

Another important application of wavelet transform is de-noising of the acoustic record. Removing the background noise of an acoustic signal allows us to extract feature signals more accurately and avoids the loss of important information. Recently, researches have shown the wavelet transform, based on a de-noising algorithm, plays an effective role in reaching planned goals in the areas of seismic signal analysis and well-logging signal analysis. A comparison [36] shows the wavelet de-noising method is more adaptive and robust to the non-stationary and low noise signal ratio seismic signals than traditional methods, such as the use of linear pass-band filters, the efficiency of which is reduced when transients are close to the signals. Additionally, the Wiener filter is based upon the assumption of the stationary of the signal and noise and is not suitable for

non-stationary signals, such as seismic signals. To suppress the difficult-to-remove noise in the seismic data, a branch of wavelet transform-based 1D and 2D filters have been proposed by different researchers Deigahn and Watts (1998), Yu et al. (2002), Yu and Garossino (2005) and Abdul-Jauward and Khene (2000). A more promising 2D wavelet transform-based filter was produced by researchers [37]. In the oil industry, different researchers applied wavelet transform-based noise control to the well-log to predict the gas zone [35]. Wavelet decomposition was applied to the well-log traces; a threshold was applied to the frequency spectrum to filter out and isolate the high frequency components and recombine the signal components with a wavelet transform. This procedure removes the noise superimposed upon the well-log trace data. The noise in the density well-logging porosity and compensation neutron porosity data was removed before comparing the values to determine the location of the gas zone [35].

2.5. Acoustic Probing and Imaging

Acoustic probing and imaging systems are popular due to their nondestructive properties; we can “see” inside an opaque area without damaging it. Therefore, it has a wide range of applications in many areas of monitoring systems, such as medical diagnosis and industrial monitoring. For many years it has been applied to several industrial areas including flaw detection, underwater monitoring and water depth monitoring. An air gap between metal walls was detected by acoustic probing techniques [42], the conditions of fragile historic buildings were measured by NDT [43], and

wooden construction defects were detected by using acoustic NDT. NDT was also used to measure the thickness of concrete elements [45] and a laboratory inspected the welding on a branch of pipe, noting the chemical and volume control system so as to improve acoustic probing techniques in nuclear applications [46].

The basic theory of acoustic imaging systems is the same in any area. It consists of two major parts: the ultrasonic transducer and a personal computer. Transducers transmit and receive acoustic signals to detect the distance between the transducer and a detected object, which reflects sound. At the same time, they send these sound waves to a personal computer. After the signal is processed, the output is shown on the computer screen. Acoustic imaging techniques are applied to many medical areas for the purpose of tumor diagnosis, cardiac malformation, fetal anomaly estimation, baby weight etc. [39, 40, 41]. Human organs such as the liver, heart, brain, lung as well as the fetus can be examined with an ultrasonic system. In the oil industry, both seismic data and well-log data could be used as an imaging signal source in order to estimate the structure of the ground and the conditions under the well. In the past several years, 2D seismic imaging has been all but entirely replaced [49]. At the Takutu sedimentary basin in Brazil, seismic data was used to image the basin's structure [50]. Well-logging data was used in image processing [47]. A reservoir off a Niagara reef was imaged using well-logging data [48]. Due to its successful applications and non-destructive properties, acoustic probing and imaging can be considered a potential technique for monitoring the vapor chamber evolution in different stages of the VAPEX process.

2.6. Problem Statement

As mentioned in the preceding sessions, acoustic systems have been used previously in many industrial areas, such as structure analysis by seismic techniques, crack and defect measurements, and localization in well-logging fields. It has also been applied in the analysis of porous media. Ultrasound imaging systems are used in many areas, such as imaging of human organs in 3D and underwater SONAR systems. Wavelet transform provides a strong time-frequency algorithm to deal with the signal's discontinuity localization and de-noising problems. Up to now, an acoustic system has never been used in the VAPEX process to monitor the growth of a vapor chamber. Studies regarding its successful applications in relevant areas show strong evidence suggesting the feasibility of its use in the VAPEX process. Hence, this thesis investigates the applicability of using acoustic technique for imaging an experimentally simulated vapor chamber in a lab scale physical model using representative sand and fluids.

For this purpose, propagation length measurements of an ultrasound signal through a medium were viewed as the prerequisite demand of the imaging experiment. The measurements include the penetration, attenuation, longest length traveled, and scattering shape measurements. The speed of sound through different mediums (i.e., sand packs) were also measured. A mother wavelet selection analysis was conducted before the application of wavelet transform and then the wavelet transform was applied prior to the imaging process. Finally, the collected ultrasound data was used to build 2D images

of the experimentally simulated vapor chambers. The calibration of the acoustic system makes its penetration ability a very important factor within the entire experiment process due to the structure of the sand mixture. The combination of small particles of sand has a strong scattering effect upon the acoustic waves. When the sand is mixed with oil, its high viscosity makes propagation of the acoustic wave difficult. Even if the acoustic wave could propagate through the medium successfully, the strong attenuation through the medium during the propagation limits the distance traveled by the acoustic wave, which may in turn reduce the resolution of the entire system. Hence, robust signal processing plays an important role in the study due to the structural factors of the medium. The reflected signals should be precisely localized even if there is strong attenuation or if they are superimposed with strong background noise. The precision of the signal positioning step leads to an accurate 2D image of the measured object.

3. Experiments

This chapter provides a detailed explanation of the experimental set-up and procedure. Meanwhile, a series of prerequisite experiments were conducted in order to calibrate the whole detection system and to measure the speed of sound through different media such as water, water saturated sand and oil saturated sand.

3.1. Experimental Set-up and Calibration

The first step of the experiment is to set up the equipment and perform the calibration. Transducers are calibrated at different frequencies and the pulser is operated in both modes (transmission mode and reflection mode).

3.1.1. Experimental Set-up

The experimental set-up is comprised of two modes (transmission and reflection modes), an ultrasound pulser, two transducers, a data-collection board and a personal computer. The ultrasound pulser can modify the amplitude, frequency, gain and attenuation of the transmitted signal. Transducers can work as transmitters or receivers. The data-collection board works as an interface between the ultrasound pulser and personal computer. It is used to collect the signals and transfer data to the computer. The output signals and the experimental results are displayed on the computer. An aquarium and a plastic container are used to hold several types of media (water, water saturated

sand, and oil saturated sand). The software programs used are MATLAB™ and Tracer DAQ™. Their purpose is to capture, store and analyze the signals. Figure 3.1 shows the schematic of the experimental set-up in this study.

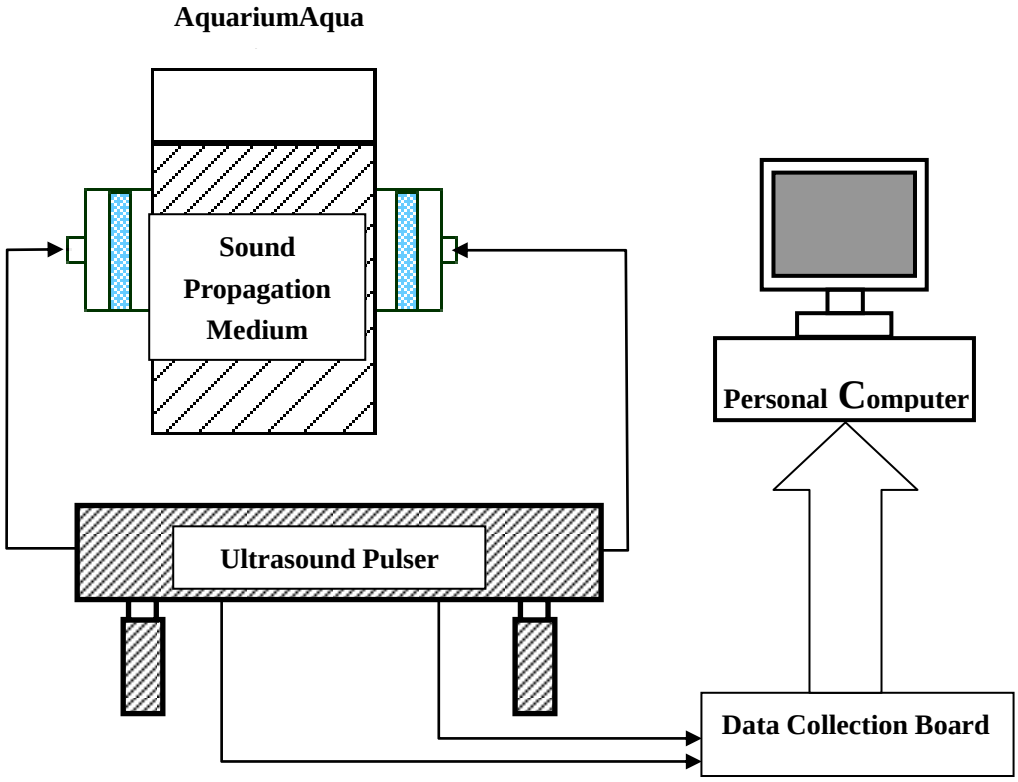

Fig. 3. 1. Ultrasound measurement system

3.1.2. Calibration

The ultrasound pulser has two working modes. The first is the transmission mode and the second is the reflection mode. To determine whether all the equipment and software is in working order, the actual system is connected as shown in Figure 3.2.

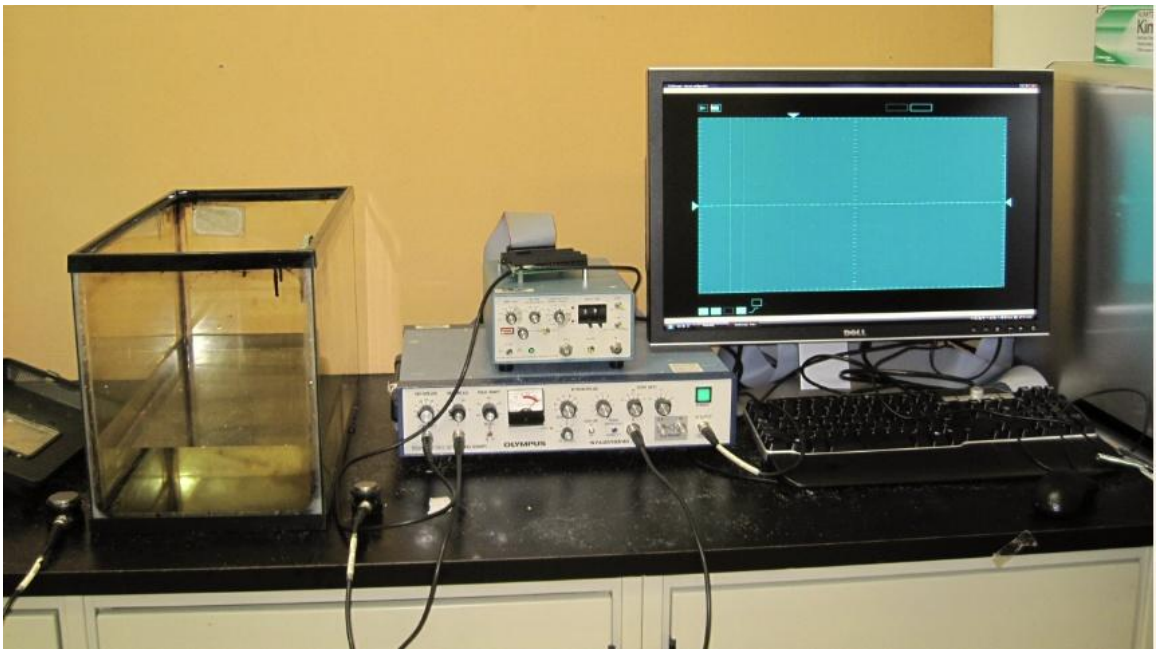

Fig. 3. 2. Experimental Set-up

The pulser is operated in both transmission mode and reflection mode. When the pulser is in transmission mode, two transducers must be acoustically coupled to the aquarium. One of the transducers operates as a transmitter to generate the ultrasonic signal, and the other transducer operates as a receiver to collect the ultrasonic signals after they propagate through the object. When the system is set to reflection mode, only one transducer is required, which must be attached to the detected object's surface in order to function as both a transmitter and receiver. The signal received from the transducer is the echo signal from the surface of an object which is different from the medium through which the ultrasound propagated. The surface can be the other side of the system or the reflector whose acoustic impedance is different from the medium through which the ultrasound is transmitted.

The transducer is attached to a glass tank filled with water in order to measure the

operation of the whole system. Figures 3.3 and 3.4 show the received signals from the receiver in transmission and reflection modes.

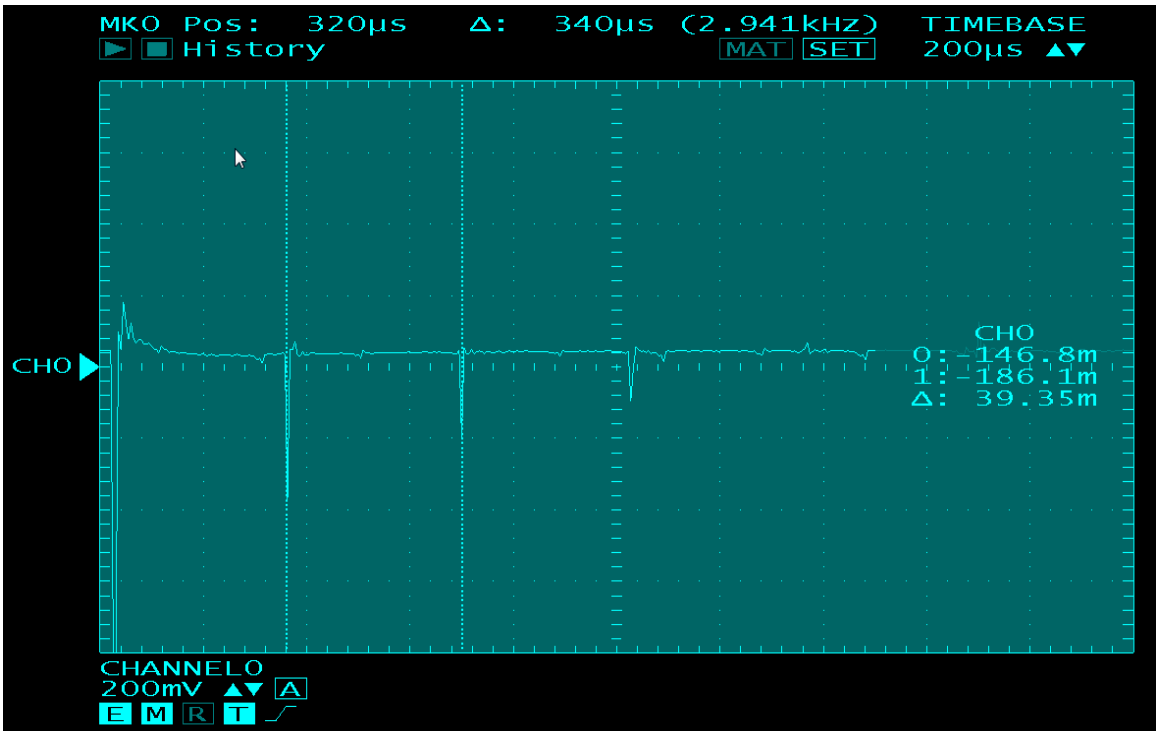

Fig. 3. 3. Signal from the reflection mode

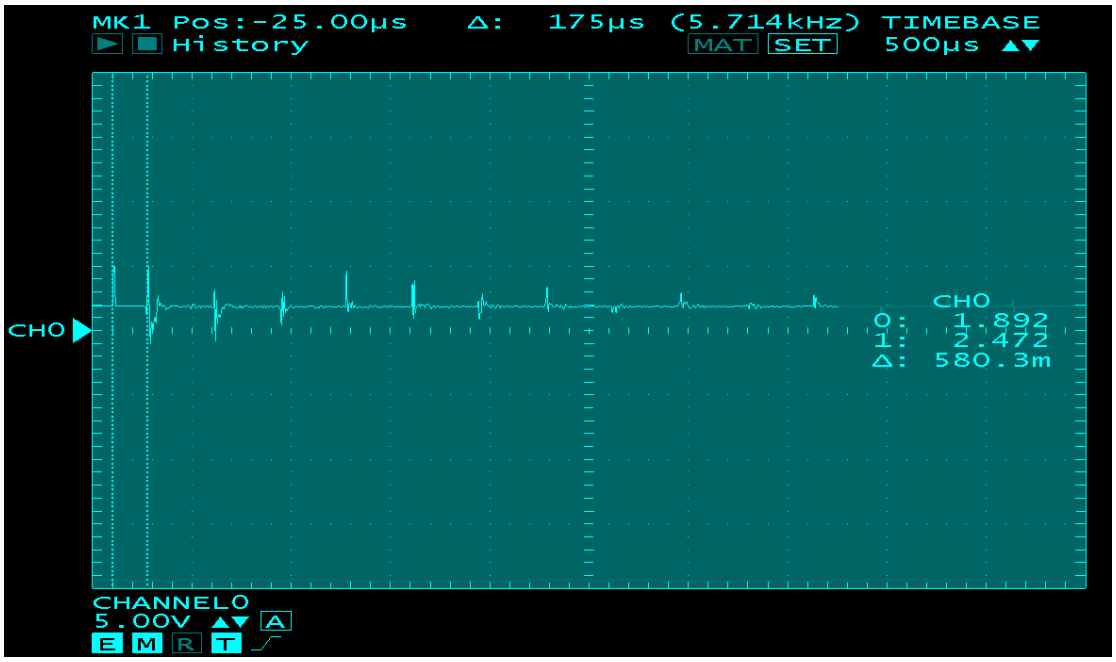

Fig. 3. 4. Signal from the transmission mode

The time duration between the first two peaks of Figure 3.3 indicates the time of

flight (TOF) in reflection mode. The object which reflected the transmitted signal is the aquarium's glass wall that is opposite the glass to which the transducer is attached. Thus, the distance the signal traveled is a 'round trip' between the two opposite glass walls. According to Figure 3.4, since the pulser is working in transmission mode, the TOF between the first two peaks is the amount of time the ultrasound signal took to travel from the surface, upon which the transmitter is attached, to the other surface upon which the receiver is attached. Hence, the distance the signal traveled in this time is a 'one-way trip' between the opposite glass walls. Therefore, the distance the ultrasound signal travelled though the water medium, from the transmitter to the receiver in the transmission mode, is half the distance the ultrasound signal traveled. Therefore, the TOF in transmission mode should be half the TOF in reflection mode. Note, the units of horizontal axis in Figure 3.3 are different than those of Figure 3.4 (ie. 200μs verses 500μs per unit time). We are able to observe from Figures 3.3 and 3.4 the time duration of the reflection mode is 340 μs, which is twice the TOF in transmission mode. The measurement results show the pulser and transducers are performing well with regard to future experiments.

3.1.3. Experimental Environment

As previously mentioned, there is a trade-off between the strong penetrating power of an ultrasound signal and the resolution of the ultrasound system when choosing the frequency of the transducer. The acoustic signal was transmitted through porous

media with characteristics very similar to those of heavy oil formations in oil fields. The experiments are conducted in either water saturated sand or oil saturated sand. In order to obtain the expected results when imaging a gas bubble in the simulated porous media, one must take into consideration two important factors that affect the results of this study. The first factor is the penetrating power of an ultrasound signal through the media. The second factor is the sensitivity of an ultrasound signal with a certain frequency, which is related to the resolution of the system. Three different types of transducers are used in this study: 50 kHz, 100 kHz, and 500 kHz. After a series of measurements using each frequency are taken in the lab, the 100 kHz ultrasound is selected with respect to conducting future experiments. It is difficult to distinguish the peak signal from the 50 kHz record and the ultrasound signal cannot travel far enough with a 500 kHz frequency. The pulser is placed in reflection mode to detect the distance between the air bubble and tank surface in order for the time interval to be measured and the distance calculated based on the time and speed. Therefore, 100 KHz is chosen as the frequency of the transmitted ultrasound signal and the transmitting frequency is 1 KHz (i.e. 1000 ultrasound signals are generated per second). Signal data is collected by the data acquisition toolbox in MATLAB^{TM} at a sampling rate of 500000 per second (i.e. 500 data points per transmitting period). The time interval between the two data points is 2 μs. The distance between the two data collection points is 1 cm (the selection of 1 cm as a spatial sampling rate is discussed in section 3.5.2.2.2).

3.2. Typical Transmitted and Received Signals

Several different shapes of transmitted ultrasound signals exist, such as pulse, triangular, and rectangular signals. The chosen shape of the transmitted signals depends on the media the signal is required to penetrate and the required resolution of the system. The shapes of ultrasound signals also depend upon the pulser which generates the ultrasound signal. The ultrasound pulse is selected for this system for its strong discontinuous properties, which can lead a more accurate measurement of the time intervals. Figure 3.5 shows the typical transmitted and received signals with their pulse shapes.

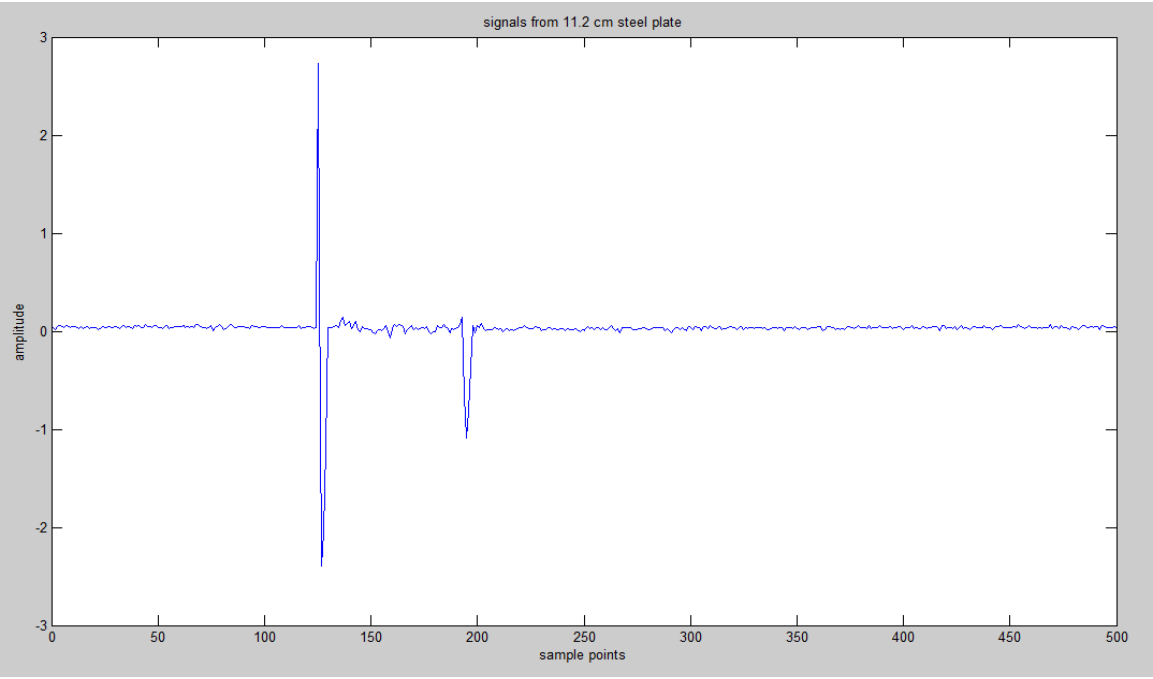

Fig. 3. 5. Typical transmitted and received signals

There are 500 samples in Figure 3.5, which represents a whole transmission period of the pulser. The first spike in Figure 3.5 is the transmission signal while the

second is the echo signal. The received echo signal is broader and weaker due to attenuation, absorption and energy loss during the propagation process. When the distance between the attached surface and the reflector is increased, the received signal weakens and widens until it cannot be distinguished easily from the background noise.

3.3. Attenuation and Multiple Reflections

Two phenomena observed in the received echo pulse are discussed in this section. The first is the attenuation, which is related to the digital processing step. The second is the multiple reflected pulses from different layers of different materials.

3.3.1. Attenuation

Attenuation is the gradual loss in intensity of an ultrasonic signal through a medium. It affects the propagation length of the ultrasonic wave in an ultrasonic system. Attenuation is a critical factor in an ultrasonic system because the reduction of the signals' amplitudes with increasing travel times leads to weaker echo signals, which are difficult to localize clearly. This difficulty in accurate localization impacts the quality of the obtained image. Moreover, the signal amplitude fades to the background noise level after it has traveled a certain distance, and as a result the ultrasonic signal can no longer be distinguished. Therefore, the attenuation of the ultrasound signal is related to the resolution of the whole system. Figures 3.6, 3.7, and 3.8 show the echo signals from the sand-steel plate interface with different distances between the attached surface and steel

plate. Five hundred data points are collected to obtain the echo signals, since the signals are sampled at 500 points at each transmitting period, and each set of 500 data points contain a whole transmitted and reflected signal set.

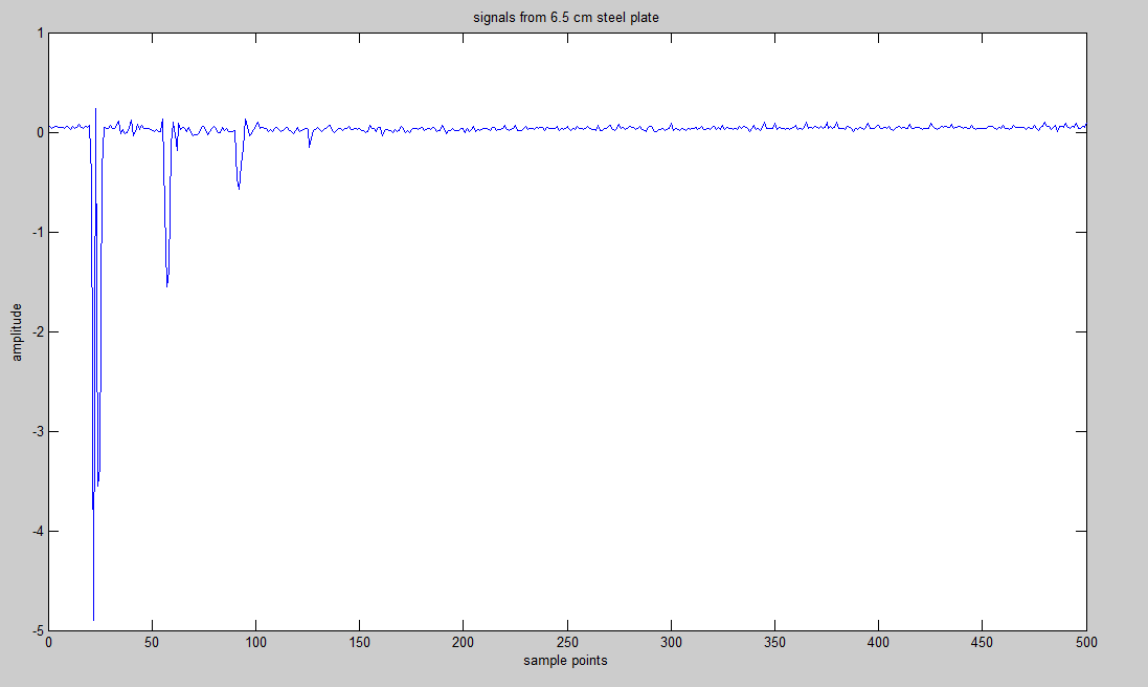

Fig. 3. 6. Reflected signals 6.5 cm away from the steel plate

In Figure 3.6, the steel plate is 6.5 cm away from the transducer and since the attached surface and steel plate are close, three echo signals are observed reflecting off the plate, as shown in Figure 3.6. The echoes become weaker and wider due to reflections between the attached surface and steel plate. Based on Figure 3.6, a functional relationship between the amplitude of the acoustic signal and the distance the signal travels can be generated. After measuring the amplitude of the transmitted signal and every reflection signal, the following equation can be defined:

$$A(d)=-5.4546e^{-0.073d} \qquad [3.1]$$

Where A is the amplitude of the acoustic signal, and d is the distance the signal travels.

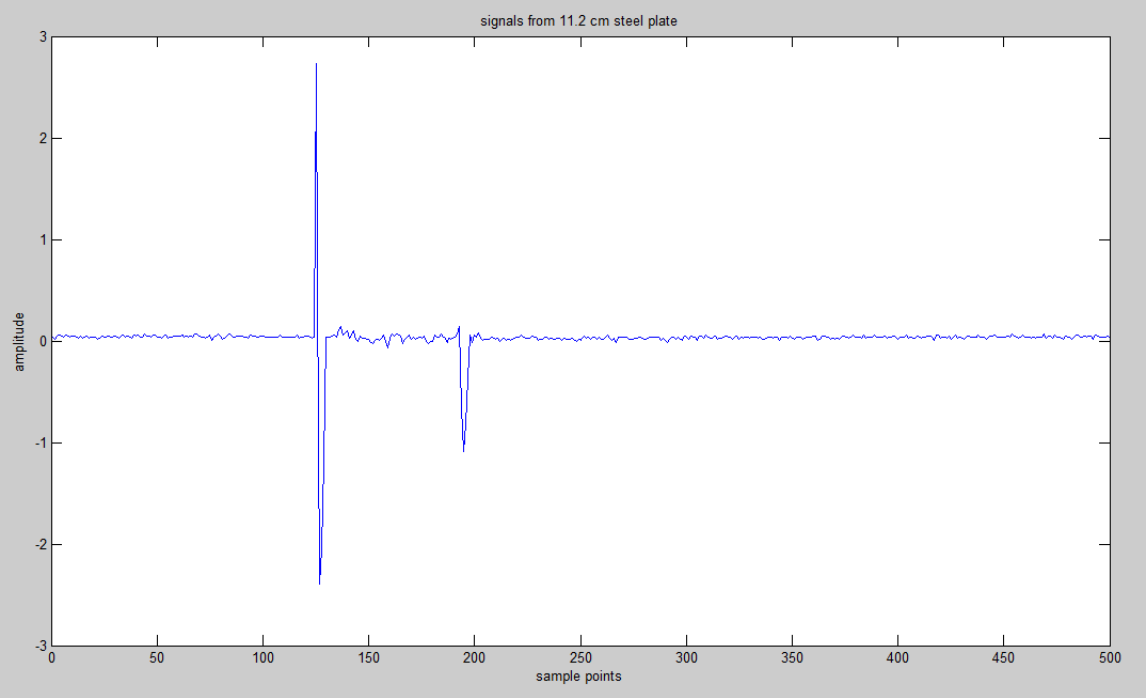

Fig. 3. 7. Reflected signal 11.2cm away from the steel plate

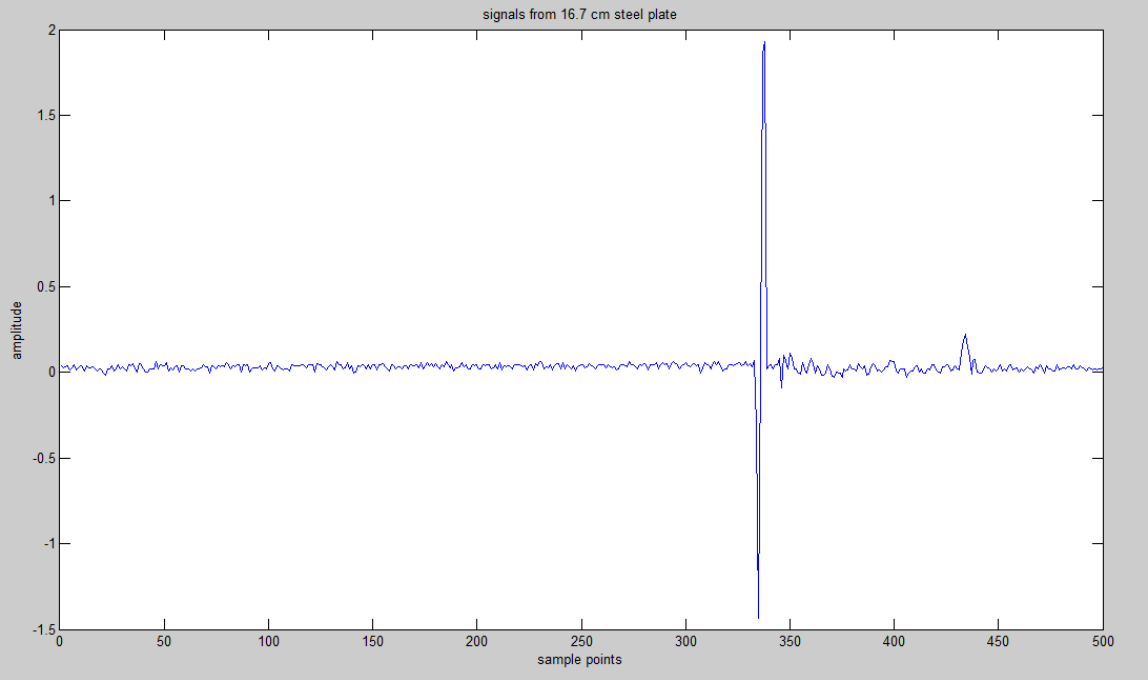

Fig. 3. 8. Reflected signal 16.7cm away from the steel plate

When the plate is moved further from the transducer, the reflected ultrasound signal is not strong enough to return from the steel plate a second time. This is observed in Figure 3.7, where the distance between the steel plate and transducer has been

increased to 11.2 cm. The limit is reached when the multiple echoes are attenuated and only one echo is received. In Figure 3.8, the echo from the steel plate, which is 16.7cm from the attached surface, is the furthest distance traveled by the signal, so the observed echo signal is the weakest and widest among the three measurements due to the strongest attenuation process led by the longest propagation length.

3.3.2. Multiple reflective layers

As mentioned in Chapter 2, sound reflection occurs at the interface between two different materials having two different acoustic impedances. The intensity of the echo signal depends on the difference between the acoustic impedances of the adjacent materials. The remaining signal power will travel through the interface. As long as the transmitted signal reaches another interface, which has two different acoustic impedance materials adjacent to each other, after penetrating the first material part of the signal will be reflected and the remaining signal power will continue to transmit as it did at the previous interface. Theoretically, we should get as many echo signals as the number of interfaces between two layers of the different materials. However, due to attenuation and path loss when the ultrasonic signal is propagating through the media, the signal may not be strong enough to return to the transducer.

The following experiment is set up to observe the multiple layer reflection phenomenon. The pulser is placed in reflection mode and the transducer is attached to the bottom of a beaker. There are three layers of materials in the beaker: the first from the

bottom is the water saturated sand, the second is water and the third is air. The transducer is attached to the beaker as shown in Figure 3.9.

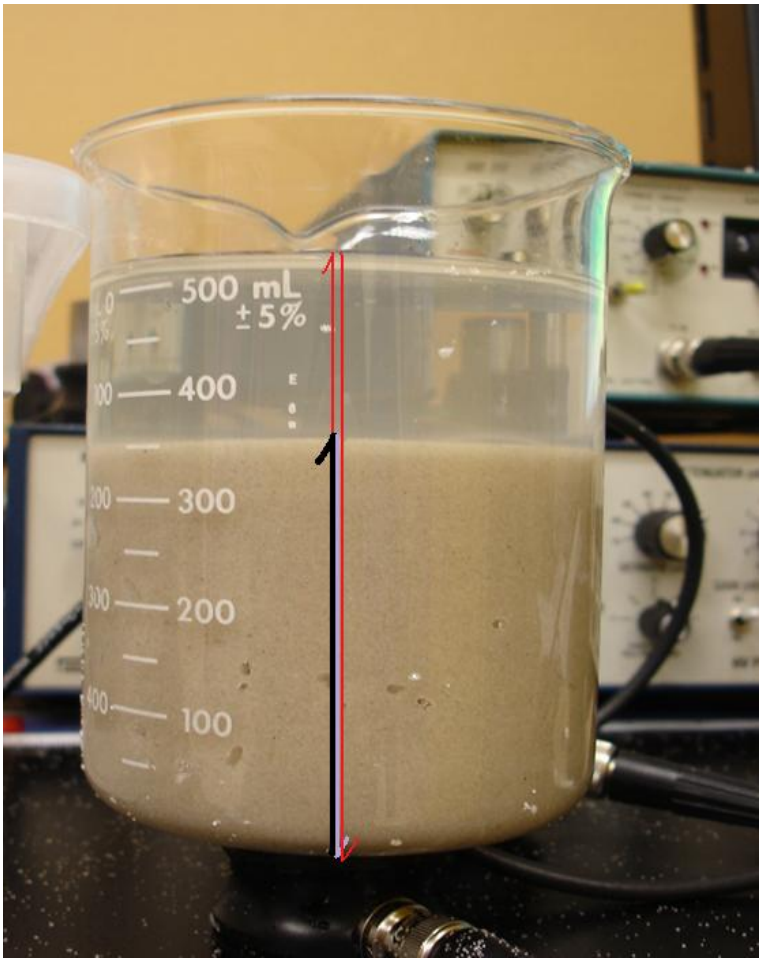

Fig. 3. 9. Multiple reflection test experimental set-up

According to Figure 3.9, two interfaces can be observed, which may lead to two echo signals. The first interface from the bottom is the water saturated sand/water interface. The second interface is the water/air interface. The signal obtained from this system is shown in Figure 3.10.

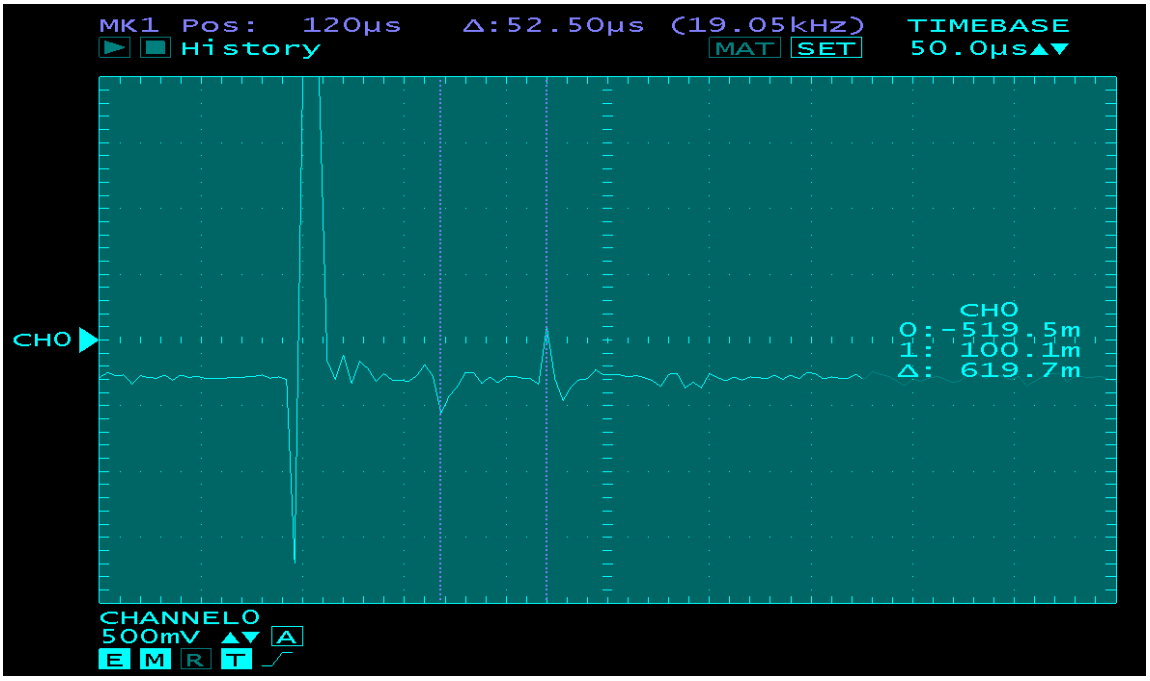

Fig. 3. 10. Initial multiple reflected signals

Two echo signals from this system can be distinguished in Figure 3.10. To illustrate that the second echo signal is not the second reflected signal from the interface between the water-sand and the water layers, more water is added to the beaker and the signals are shown in Figure 3.11.

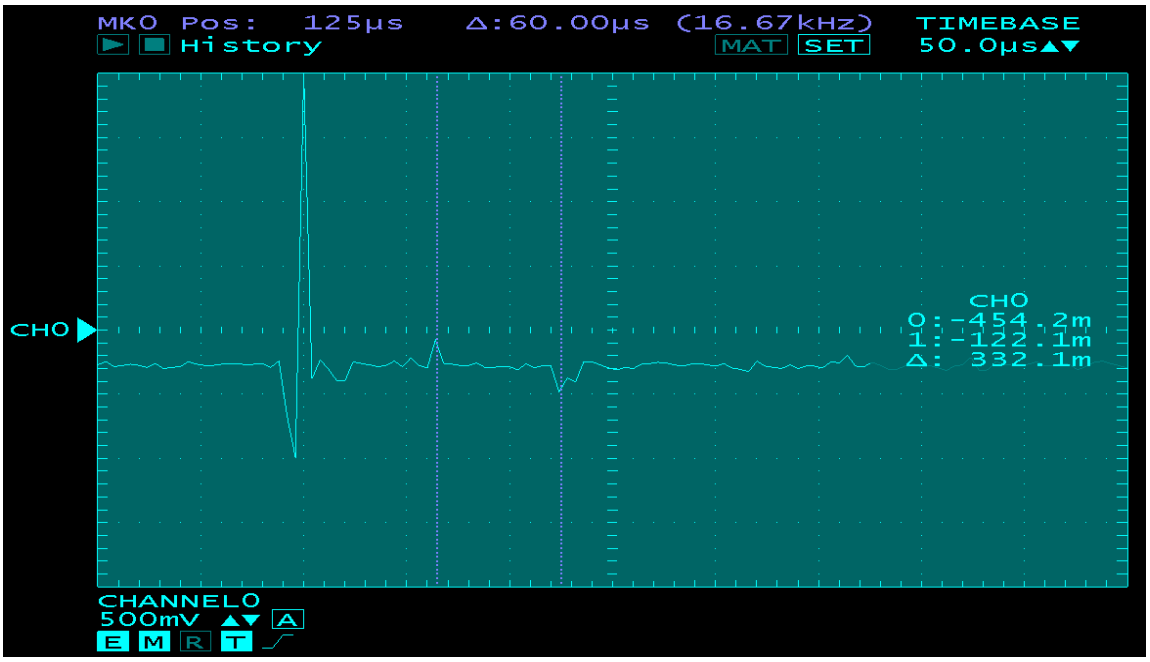

Fig. 3. 11. Second set of multiple reflected signals

The time intervals between the transmitted pulse and the first echo pulse in both experiments are the same because the depth of the water-sand layer did not change. The time interval between the two echo signals in the second experiment is longer than in the first due to more water being added to the beaker.

The echo signals help to measure the distances in the experiment and identify the location of the interface, which is very important to the interpretation of seismic data.

3.4. Speed of Sound Measurements through Different Media

The speed of sound is an important factor in an ultrasound system since it is necessary to multiply the measured time interval between the transmitted pulse and echo signal with the ultrasound speed through the media in order to calculate the distance between the transducer and reflector. This speed of sound measurement is fundamental to

the entire ultrasound imaging system. The speed of sound is affected by temperature, pressure, water saturation and various other factors. Therefore, some initial measurements must be taken to measure the actual ultrasound speed through various types of media. Prior to taking the imaging measurement, measurements of speed are performed on simulated porous media in a laboratory-scale model. The speed of sound underwater is also measured to compare the theoretical speed of sound through water in order to detect the possibility of a large error.

3.4.1. Water

The pulser is placed in reflection mode to perform the measurements. The connections between the pulser, transducers and the water filled tank are the same as in Figure 3.2.

The received signal is shown in Figure 3.12.

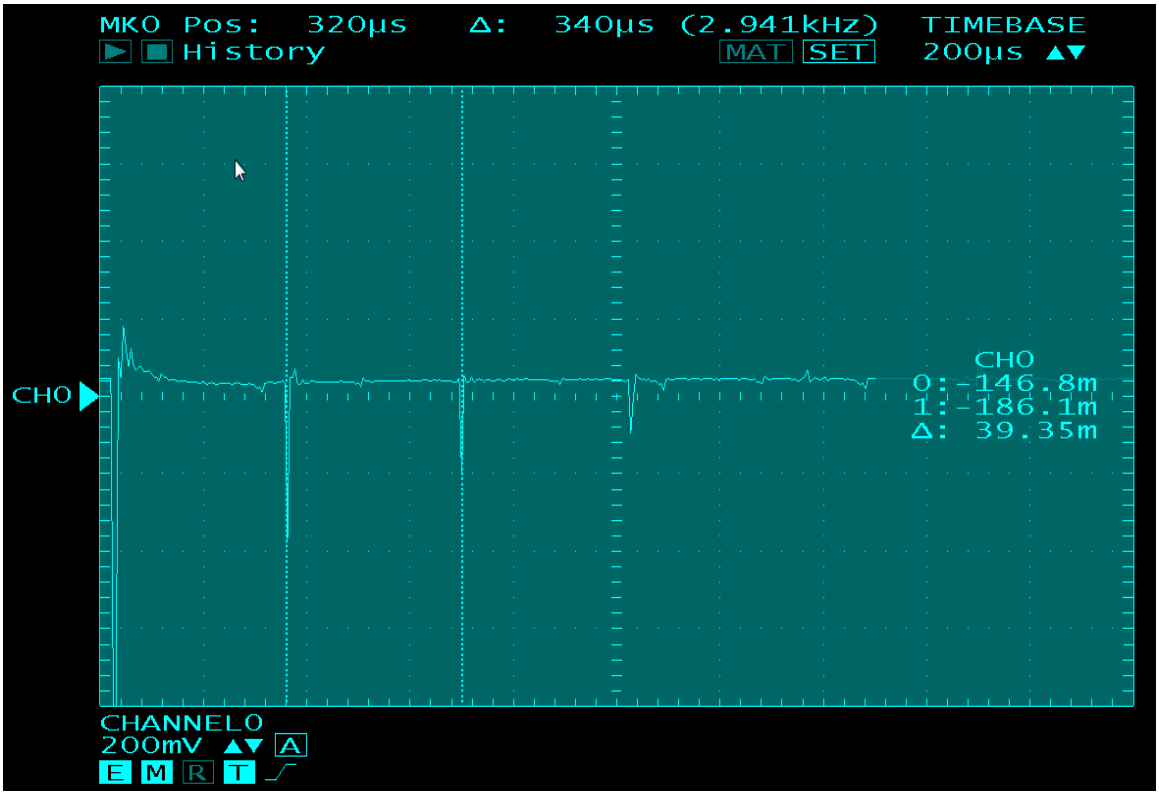

Fig. 3. 12. Reflected signal through sound test system

The width of the aquarium is 25*cm*, and thus the distance the transmitted ultrasound traveled is $2\times 25cm = 50cm$, as the pulser is working in reflection mode. The speed of sound is calculated using the following function:

$$v = \frac{s}{t} \qquad [3.2]$$

The speed of sound through water is $v = \frac{50cm}{340\mu s} = 1470.59m/s$. According to literature, the speed of sound in water at 20℃ is $1481\,m/s$. The difference between the measured and theoretical speeds is small and the accuracy of the measurements is acceptable.

3.4.2. Water saturated sand

The next step, which is critical to the results of the entire experiment, is to measure the speed of sound through the water saturated sand. The water saturated sand is sand from an actual oil field, 100% saturated with water. It is a simulation of the porous media in the oil field. Prior to taking measurements, the sand needed to be soaked in water for 12 to 24 hours to ensure it was fully saturated. The measurement procedure is shown in Figure 3.13.

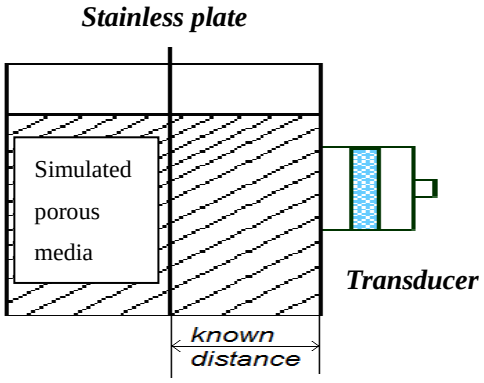

Fig. 3. 13.Sound speed measurement experimental set-up

The visual tank is filled with 100% water saturated sand. A steel plate is inserted in to the media with a known distance from the transducer. The signal is transmitted into the water saturated sand to get the echo signal from the plate; the sound speed is calculated based on the TOF which is determined from the signal record. The ultrasound signal took 100 μs to travel 17.5 cm (the stainless plate was placed 8.75 cm away from the transducer). The speed of sound in the water saturated sand is $v = \frac{17.5cm}{100\mu s} = 1750m/s$. This speed is faster than the speed of sound in pure water

because the movement and vibration of the sand particles is faster than the movement and vibration of the water particles.

To illustrate the fact the resulting speed of sound from the experiment can be used in an imaging system; several experiments were taken place as shown in 3.13 to measure the accuracy of the system with the water saturated sand condition. The steel plate is inserted into the water saturated sand at different positions and the plate's position is changed to vary the distance between it and the transducer. Then different echo signals with different TOF's are recorded. Each time the interval between the transmitted and reflected echo signal is measured at a different positioning of the steel plate, the measured speed of sound will be applied to calculate the distance from the attached surface to the steel plate. The actual distances between the surface, where the transducer is placed, and the steel plate at various positions, are also measured to compare the calculated distances. The comparisons and relative error rates are listed in Table 3.1.

signal	Time interval	Calculated distance	Actual distance	Relative error rate
1	73μs	6.39cm	6.5cm	1.69%
2	100μs	8.75cm	8.6cm	1.74%
3	134μs	11.725cm	11.6cm	1.08%
4	190μs	16.625cm	16.5cm	0.76%

Table. 3. 1. Distance measurement in the water saturated sand

The relative error rate ranged from 0.76% to 1.74% which is acceptable for practical applications. The measured speed of sound through the water saturated sand, based on lab experiments, can be applied to the next ultrasound imaging system.

3.4.3. Oil saturated sand

The speed of sound experiment in the oil saturated sand is a repetition of the water-sand speed of sound experiment. The only difference is the use of the oil saturated sand instead of the water saturated sand. The oil sample used in the experiment is a high viscosity crude oil from the oil field. Prior to performing measurements, the sand is well stirred with the oil and soaked for 12 to 24 hours to ensure the sand is fully saturated with oil. The measured ultrasound signal takes 50 μs to travel 6.8 cm (the plate is 3.4 cm from the transducer). The speed of sound in the water saturated sand is $v = \frac{6.8cm}{50\mu s} = 1360m/s$.

Based on the Hook's law, the sound's speed though liquid, solid, and gases can be expressed as the following function:

$$c = (E / \rho)^{1/2} \qquad [3.3]$$

Where ρ is density (kg/m^3, lb/ft^3) of the media and E is the bulk modulus elasticity (Pa, psi). Table 3.1 shows the density and bulk modulus elasticity of water and oil.

Substance	Bulk Modulus Elasticity - E - 10^9 (N/m^2)	Density - ρ - (kg/m^3)
Water	2.15	999.8
Oil	1.35	9.2

Table. 3. 2. Density versus bulk modulus elasticity [69]

As we can see the oil's bulk modulus elasticity is much smaller than the water's bulk modulus elasticity, the sound speed through oil is slower than it is traveling through water [69], so that the sound speed trough oil saturated sand is slower than water saturated sand.

To measure the accuracy of the acoustic system containing the oil-sand in the tank, the same measurements are repeated and the water saturated sand is replaced with 100% oil saturated sand shown in Figure 3.14.

Fig. 3. 14. Accuracy measurement system with oil saturated sand

Table 3.2 shows the comparison between the calculated distances from the attached surface of the steel plate, which is inserted in the oil saturated sand at different positions, and the actual, measured distances. The measured speed of sound is applied to the distance calculation and the comparison between the calculated distance and actual distance and relative error rate are given in Table 3.2.

Signal	Time interval	Calculated distance	Actual distance	Relative error rate
1	54 μs	3.67cm	3.6cm	1.9%
2	68 μs	4.62cm	4.55cm	1.53%
3	83 μs	5.644cm	5.58cm	1.147%
4	90 μs	6.12cm	6.2cm	1.29%

Table. 3. 3. Distance measurement with oil saturated sand

The relative error rates ranging between 1.147% and 1.9% are acceptable. The measured speed of sound through the oil-sand, based on the lab experiment, can be applied to the next ultrasound imaging system.

3.5. Resolution Measurements

Two main resolution measurements are required to determine the testing range of the ultrasound system. The first one is the depth measurement and the second one is the transducer's scattering shape measurement.

3.5.1. Depth Resolution Measurement

This depth resolution measurement is used to measure how far the 100 kHz ultrasonic signal can penetrate the simulated porous media in the laboratory scale model. The purpose of this measurement is to determine the range of the ultrasound signal and to ultimately determine the maximum area of the system. This determines how many transducers should be applied to measure a gas bubble in an actual oil field.

3.5.1.1. Water saturated sand

The transducer is attached to one of the narrower glass walls of the aquarium with the water saturated sand, and the steel plate is moved to different positions to obtain feedback signals. The distance is also measured between the attached surface and steel plate when no obvious echo signal is received from the system. Figure 3.15 shows the received signal from the plate when it is 27.5 cm away from the attached surface. Since the pulser is working in reflection mode, the distance the ultrasound signal traveled is $2 \times 27.5cm = 55cm$. This means that with our 100 kHz ultrasonic transducer, the signal is able to travel 55 cm in water saturated sand before the energy gets absorbed in the medium because of scattering and attenuation. This depth is 27.5 cm when the pulser is in reflection mode transmitting through the water saturated sand.

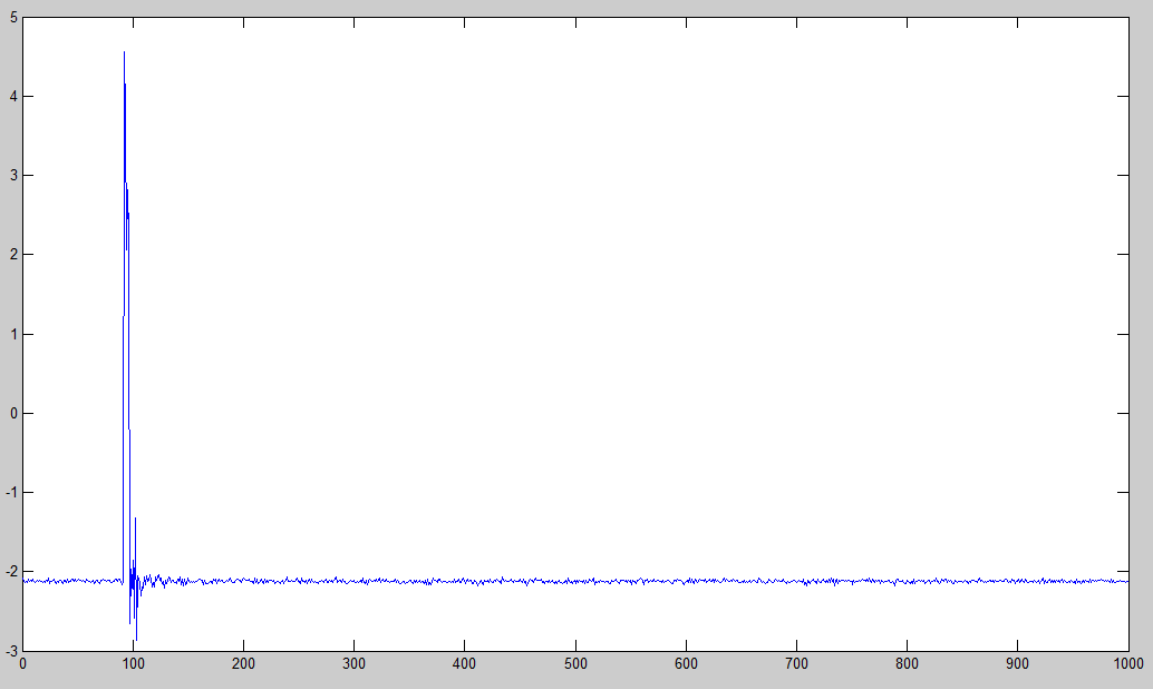

Fig. 3. 15. Reflected signal from the steel plate 27.5cm away from the underwater saturated sand

3.5.1.2. Oil saturated sand

The measurements are repeated with the high viscosity crude oil saturated sand to obtain the resolution of the system with the oil saturated sand. Due to the very high viscosity of the crude oil, it is very difficult for the ultrasonic signals to penetrate the porous media. Accordingly, the depth resolution for the oil saturated sand is relatively low, requiring signal processing techniques to extract the weak echo signal from the background noise.

Figure 3.16 shows the signal when the steel plate is 7 cm away from the attached surface. There is no noticeable reflected signal which can be extracted from the background noise. The depth resolution of the system is 7 cm when transmitting through the oil saturated sand when the pulser is working in reflection mode.

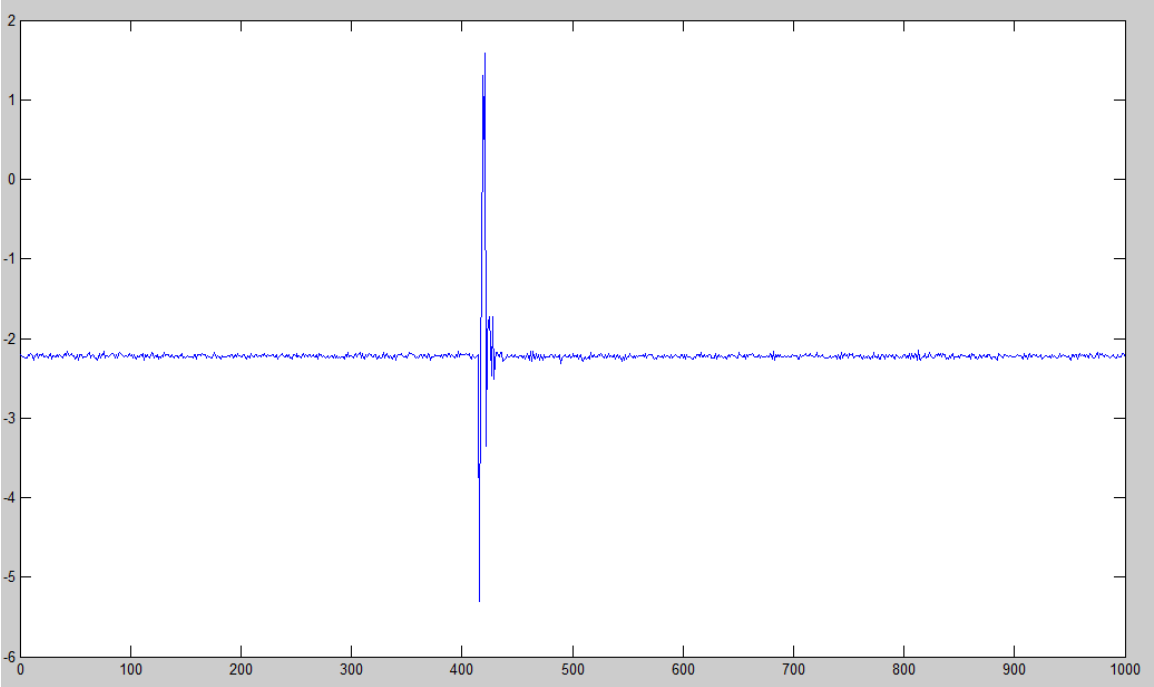

Fig. 3. 16. Reflected signal from the steel plate 7 cm away with oil saturated sand

3.5.2. Spatial Sampling Rate Measurement

The directional shape of the emitted ultrasound pulse and its resolution used for measuring the small slot are related to the spatial sample rate (the distance between two data collection points) of the laboratory scale model. The small slot can be considered a discontinuity in the surface of the reflector. Several measurements are performed to determine the directional shape of the emitted ultrasound pulse. The following section discusses the measurement steps and results.

3.5.2.1. Measurement Environment and Steps

Figure 3.17 shows the 1 cm × 1 cm square grids attached on the bottom of the aquarium. They show the exact positions of the transducer and reflector which include the horizontal distance between the transducer and reflector and the vertical distance between the centre of the transducer and reflector. The combination of the collected reflected signal and the position help form the shape of the signal's scattering.

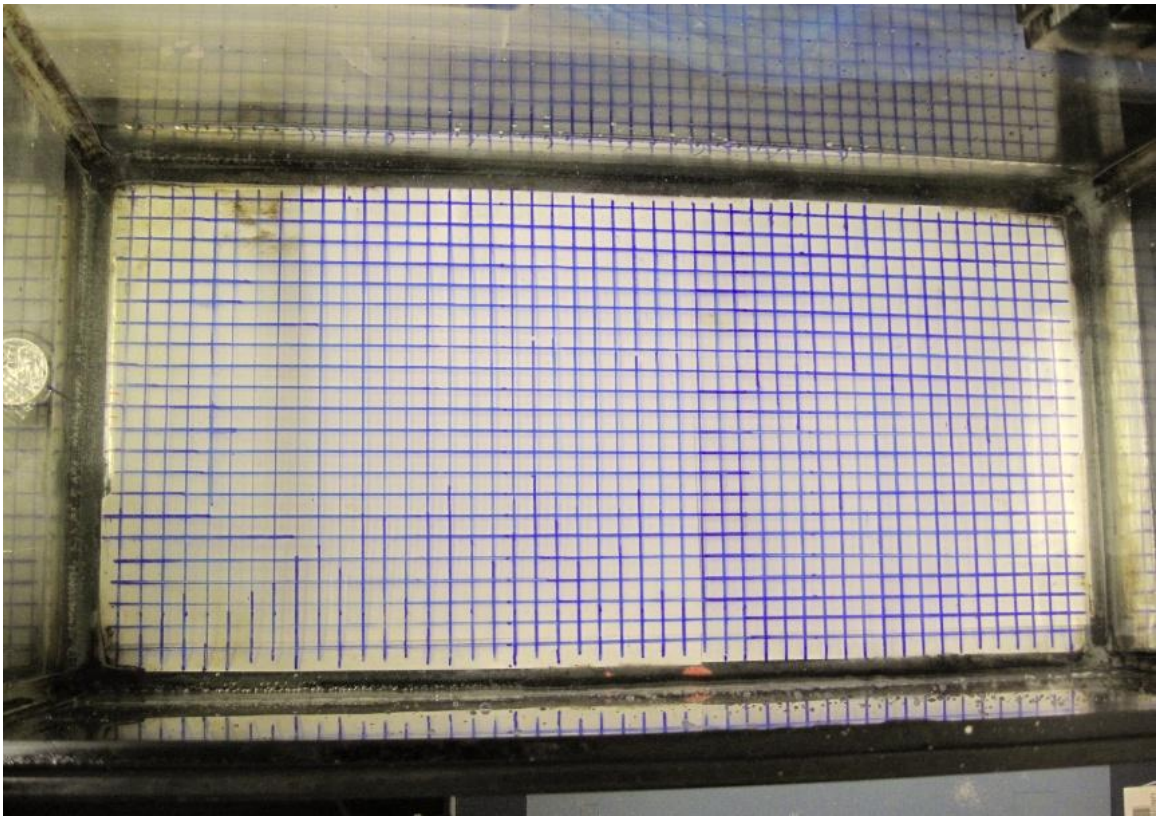

Fig. 3. 17. Experiment environment for the scattering shape measurement

The transducer is attached to one of the glass walls of the aquarium and the reflector is inserted into the water media on the axis through the centre of the transducer at 1 cm intervals. The reflector is moved vertically to the axis and parallel to the glass wall where the transducer is attached. The received reflected signals from all positions of the reflector are analyzed to determine the shape of the scattering. The spatial sampling rate can be finalized based on this scattering shape. The measurement steps are as follows:

1. Attach the transducer onto one of the glass walls of the aquarium, placing it in the middle of the wall.
2. Insert the reflector into the water on the centre axis 1cm away from the

transducer and record the reflected signal.

3. Move the reflector in a direction parallel to the glass wall and record the reflected signals at every position until the signal disappears, then record the distance the reflector is moved.

4. Repeat the measurement process at every 1 cm interval as the reflector is moved away from the glass wall to which the transducer is attached.

5. Record the reflected signal and the position where the signal disappeared.

3.5.2.2. Reflected Signals and Discussion

The following section describes, step by step, the reflected signals when the reflector is moved away from the transducer. How the spatial sampling rate is determined is also discussed.

3.5.2.2.1. Reflected Signals

The transducer is attached to the centre of the left glass wall of the aquarium as shown in Figure 3.18. The reflector is moved along the centre axis, which is defined as the central axis of the transducer. All the reflected signals are recorded at every position of the reflector.

Figure 3.18 shows the reflected signal from the opposite glass wall of the aquarium without any reflector inserted in the water.

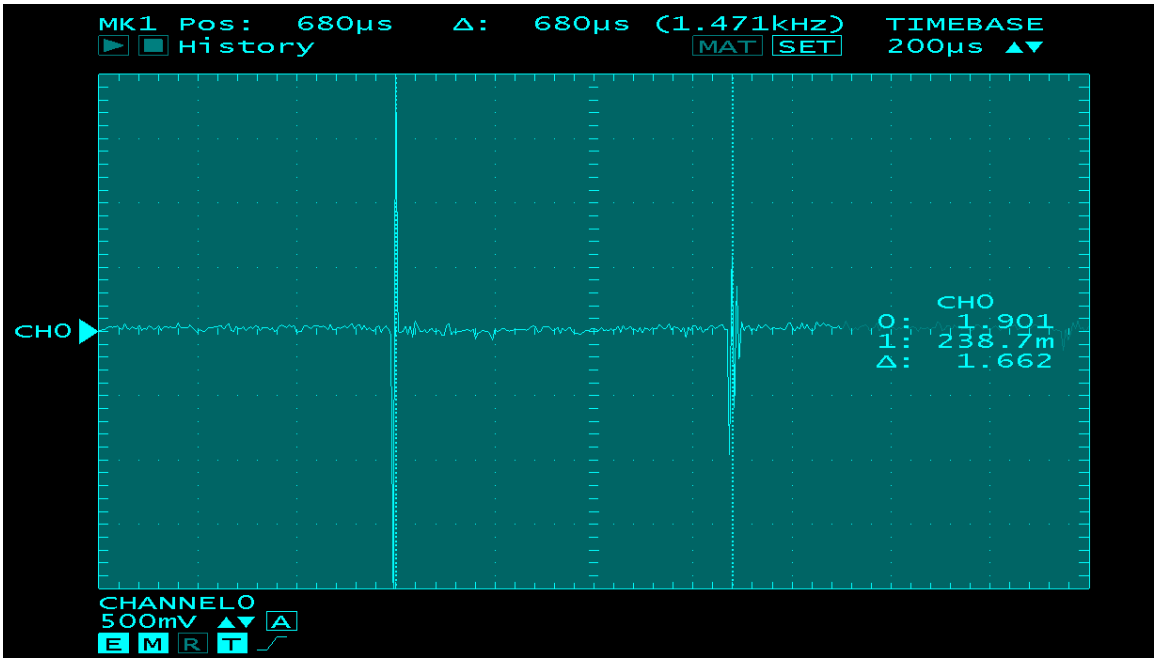

Fig. 3. 18. Reflected signal from the opposite glass wall

The opposite glass wall is 50 cm away from the transducer and the TOF of the ultrasound signal is 680 µs. Figure 3.19 shows the reflected signal when there is a reflector inserted in the water. The object is placed 5 cm horizontally away from the transducer and 1 cm away from the central axis.

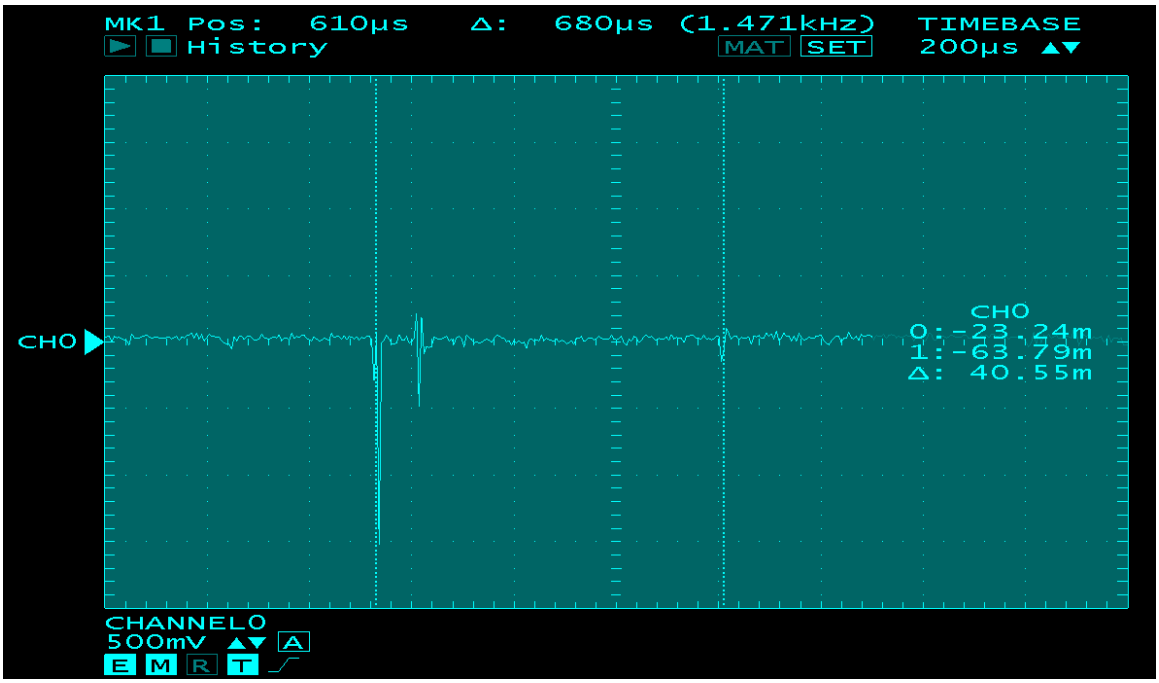

Fig. 3. 19. Reflected signal from the reflector positioned 5cm away from the transducer and 1cm away from the central line

A peak signal is observed in Figure 3.20 which has a time interval of 680 µs from the transmitted signal. This peak signal is the reflected signal from the opposite glass wall. The second peak signal in Figure 3.19, which follows the transmitted signal, is the reflected signal from the reflector. Despite the fact the reflector is not on the central line of the transducer, it can still reflect the ultrasound signal transmitted by the transducer.

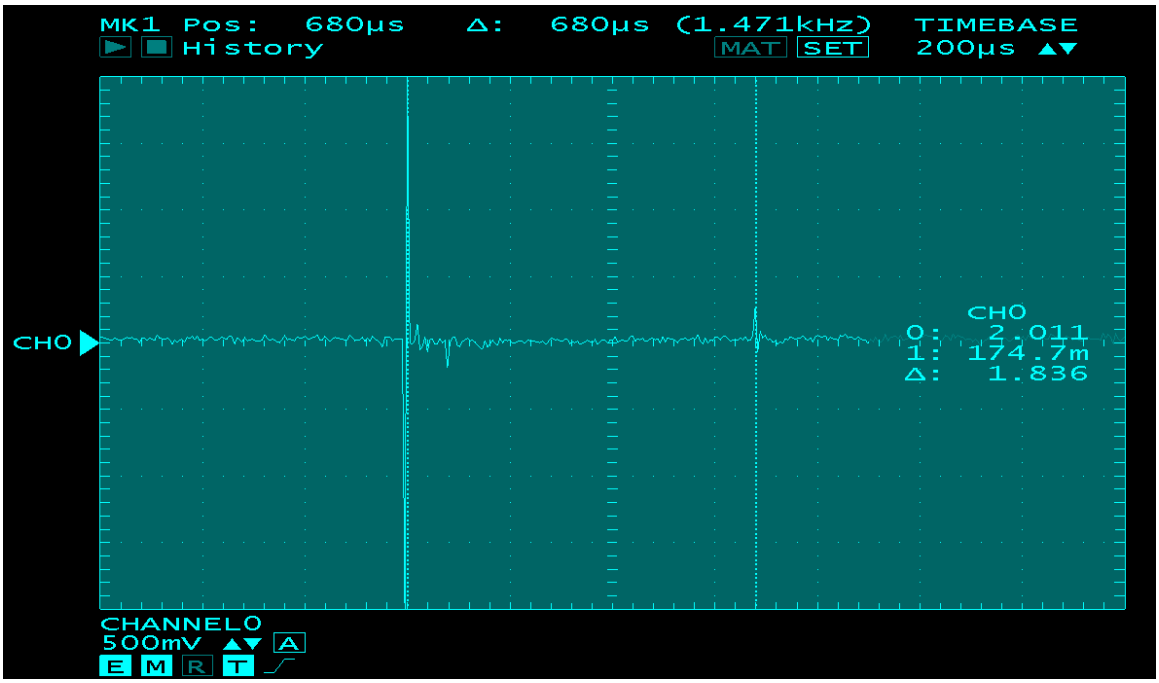

Fig. 3. 20. Reflected signal from the reflector positioned 5 cm away from the transducer and 1.5 cm away from the central line

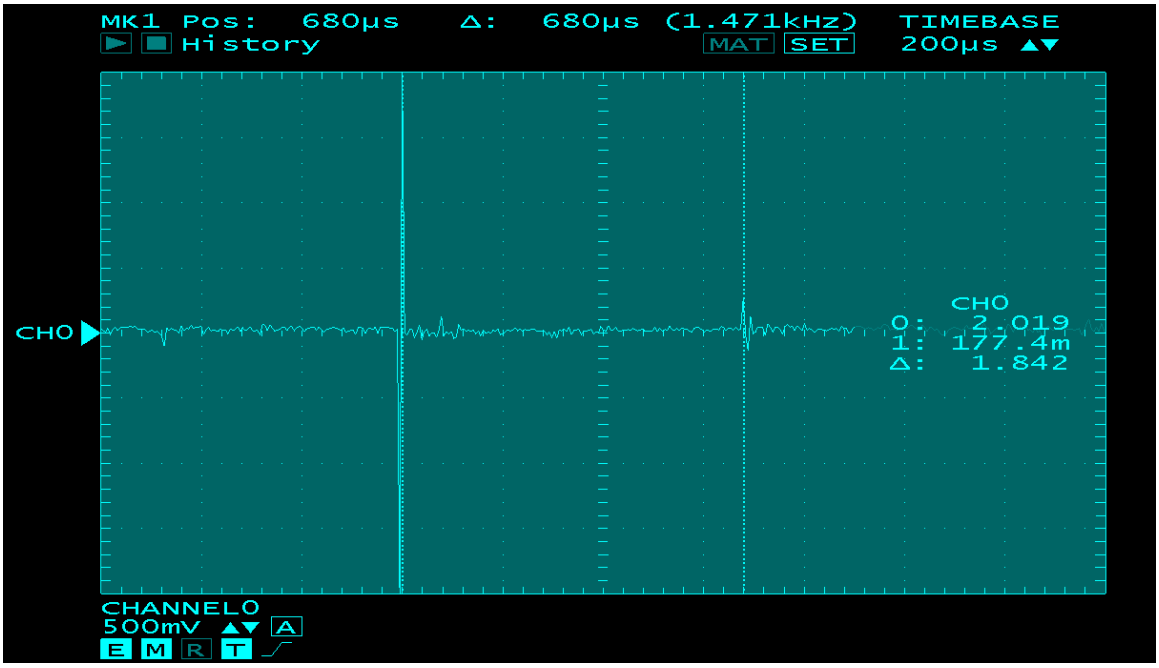

Fig. 3. 21. Reflected signal from the reflector positioned 5 cm away from the transducer and 2 cm away from the central line

Figure 3.20 shows the reflected signal from the reflector when it is positioned 1.5 cm away from the central line.

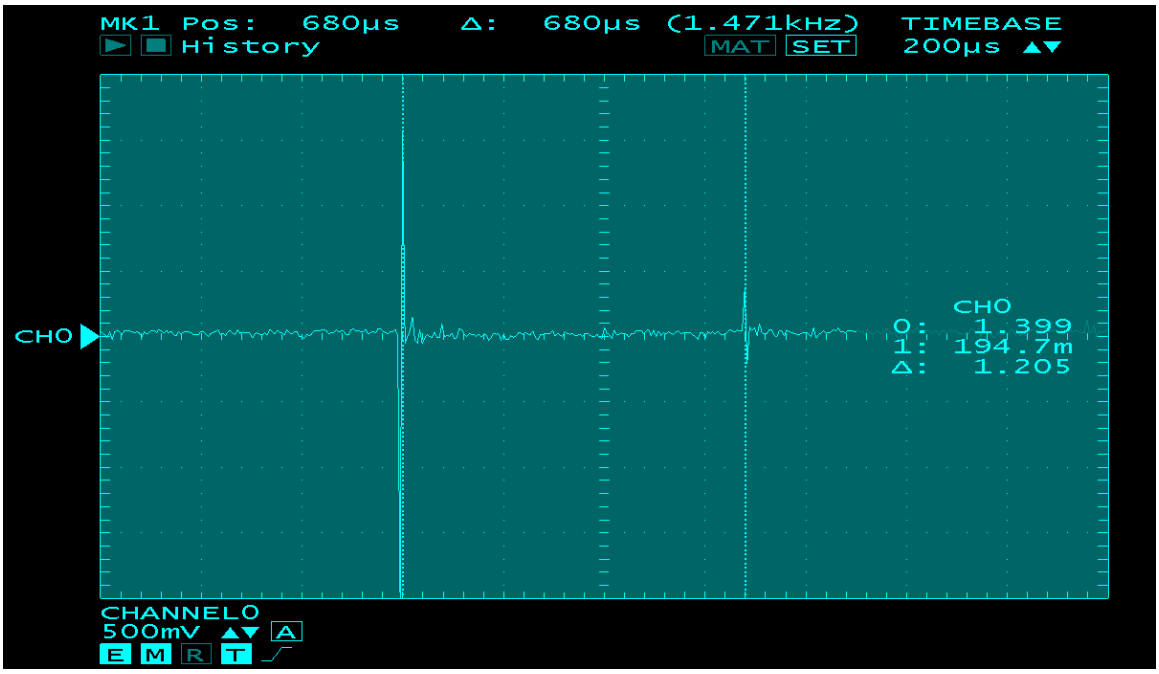

Fig. 3. 22. Reflected signal from the reflector positioned 5cm away from the transducer and 2.4cm away from the central line

When the object is moved 2.4 cm from the central axis, the reflected signal from the object is no longer recorded, as shown in Figure 3.22. The diameter of the scattering shape of the transducer is 2.4 cm when the reflective surface is 5 cm away from the transducer.

The same procedure is repeated after moving the reflector 10 cm away from the transducer. Figure 3.23 presents the collected reflected signals.

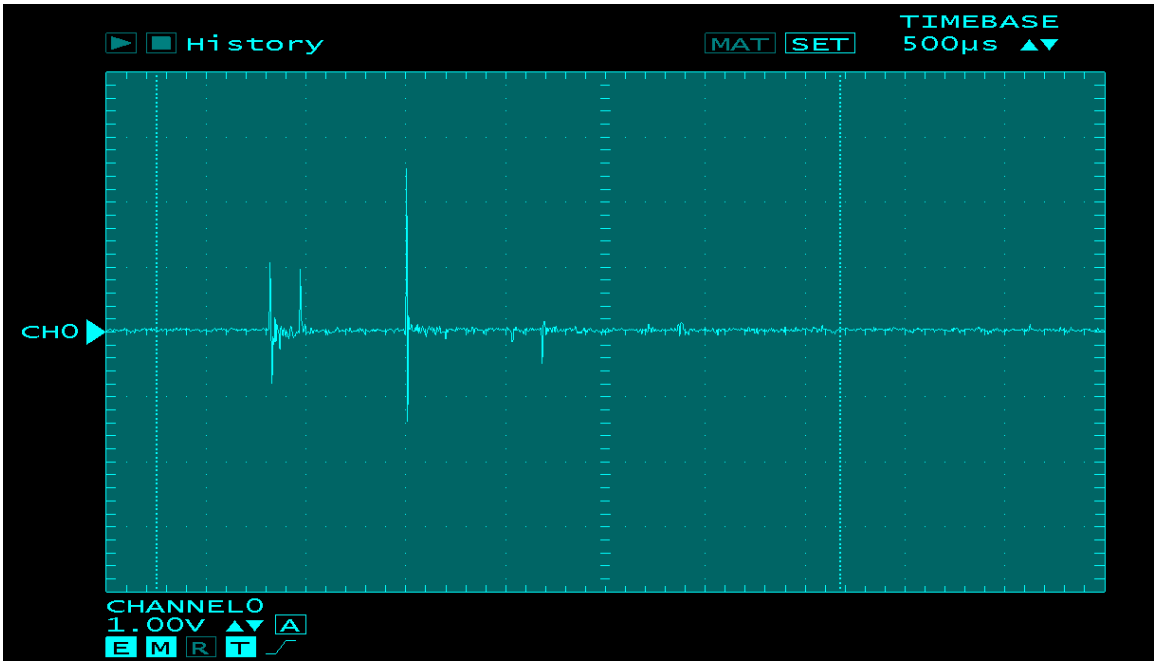

Fig. 3. 23. Reflected signal from the reflector positioned 10 cm away from the transducer and 1cm away from the central line

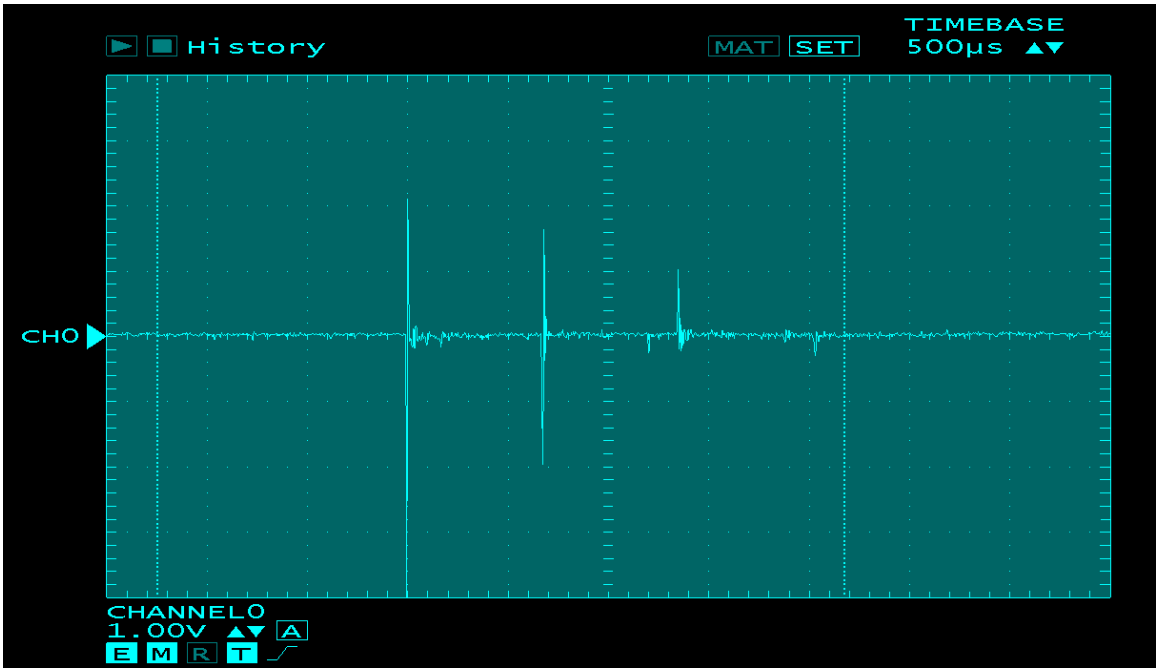

Fig. 3. 24. Reflected signal from the reflector positioned 10 cm away from the transducer and 2.5 cm away from the central line

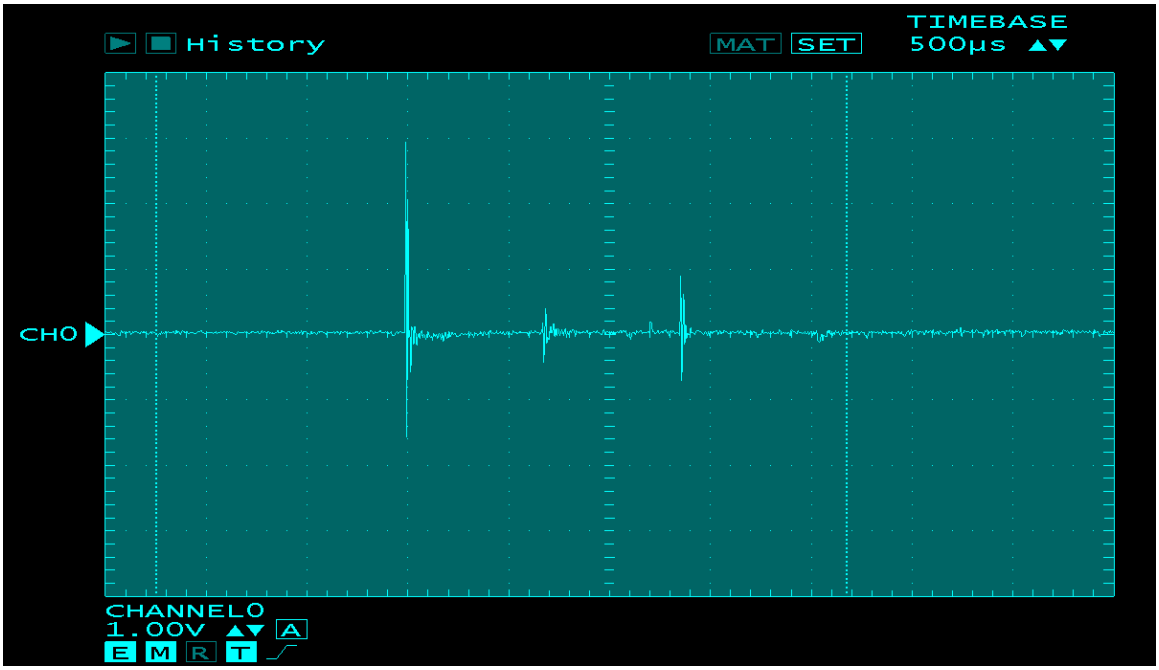

Fig. 3. 25. Reflected signal from the reflector positioned 10 cm away from the transducer and 3.3 cm away from the central line

The reflected signal from the reflector disappears when it is 3.3 cm away from the central line. The diameter of the scattering shape of the transducer increased 0.9 cm with the reflected surface moving 5 cm further away from the transducer. The following function can describe the relationship between the diameter of the scattering shape and the distance between the transducer and the reflective surface:

$$r = \frac{0.18 \times d + 1.5}{2} \qquad [3.4]$$

Where r is the radius of the reflective surface and d is the distance between the transducer and the reflective surface.

Subsequently, by moving the reflector 15 cm from the transducer, the following signals are recorded.

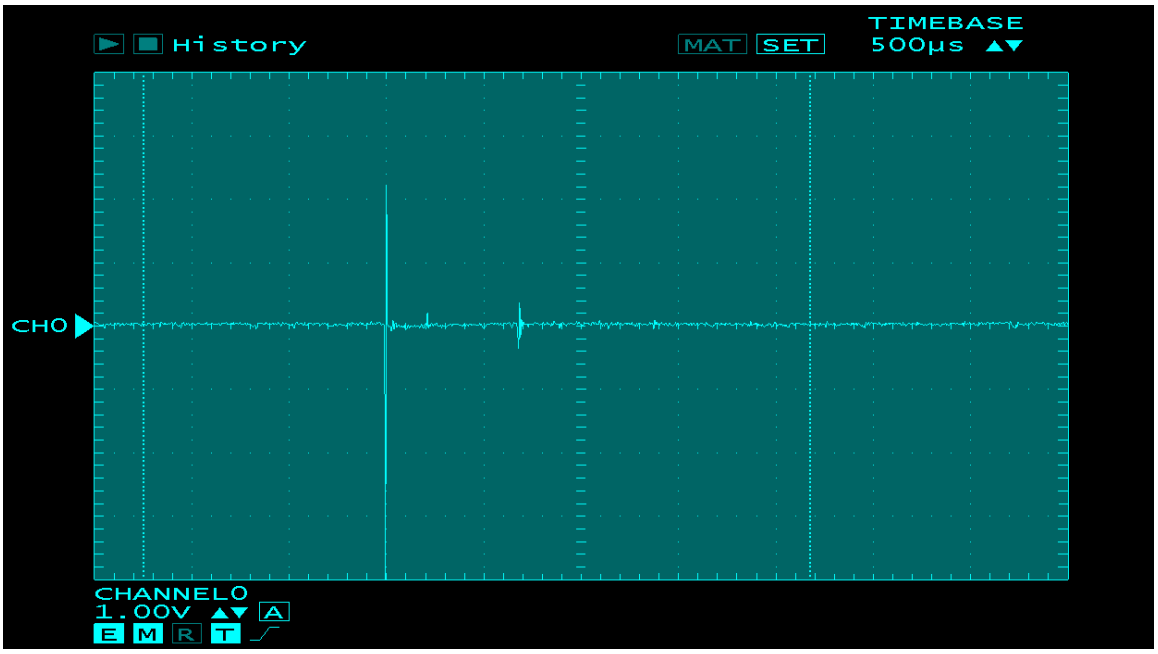

Fig. 3. 26. Reflected signal from the reflector positioned 15 cm away from the transducer and 1cm away

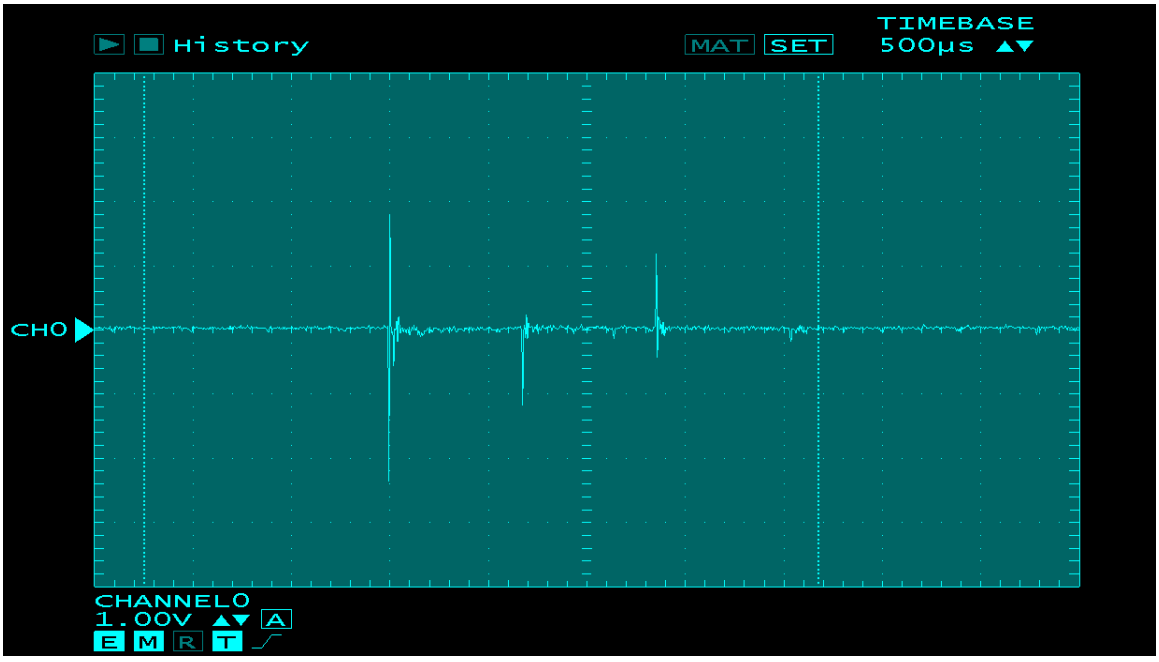

Fig. 3. 27. Reflected signal from the reflector positioned 15 cm away from the transducer and 3 cm away from the central line

The reflected signal from the reflector disappears when it is on the surface which is 3 cm away from the transducer. The diameter of the scattering shape decreases as the reflector moves between 10 cm to 15 cm away from the transducer. This can be attributed

to increasing attenuation and path loss, with the distance between the transducer and reflector becoming longer. This causes the strength of the ultrasound signal to decrease. Thus, the diameter of the scattering shape is shortened.

3.5.2.2.2. Spatial Sampling Rate Determination

Another factor to be considered when determining the spatial sampling rate of this system is how small of a slot can be measured by the system. A series of measurements are taken to determine the shape of the slot the system can see. The measurement procedure is described:

1. Place two identical reflectors in the water at a measured distance from the transducer. Create a slot between the two reflectors and verify that the centre of the slot is on the central axis.
2. Increase the size of the slot until the reflected signal from the opposite glass wall can be measured. At the same time, record the reflected signal and the size of the slot between the two reflectors.
3. Move the two reflectors together in the direction perpendicular to the central line. Repeat steps 1 and 2 with every position.

The results when the objects are on the 5 cm reflective surface are shown in Figures 3.28 to 3.31.

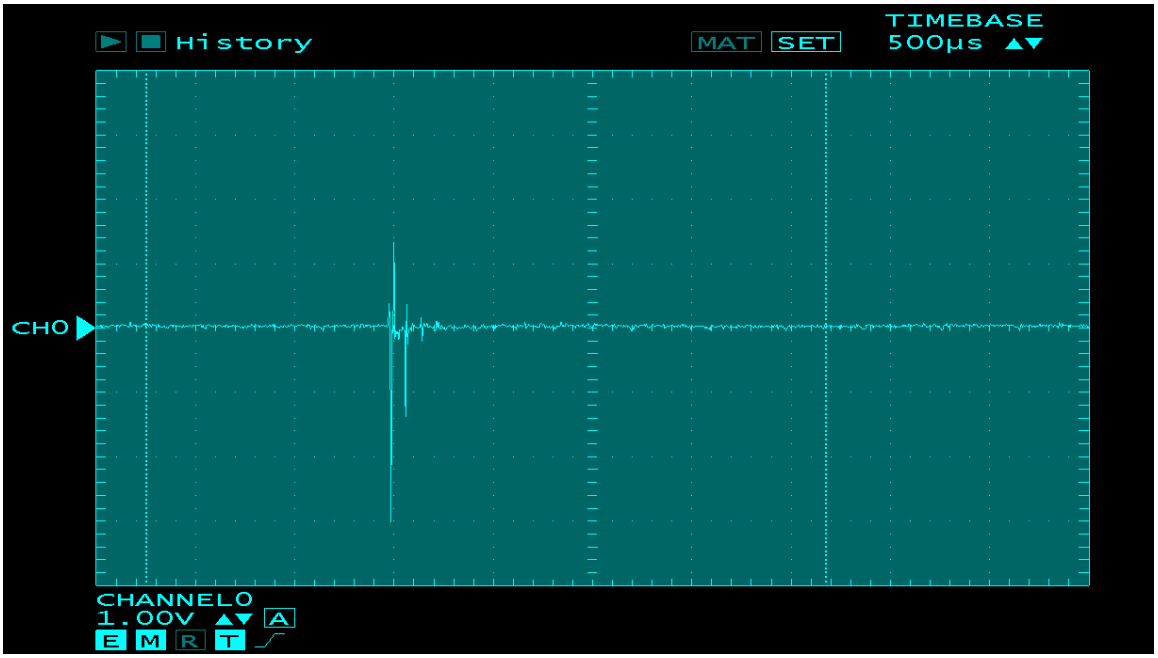

Fig. 3. 28. Reflected signal from the 0.4 cm wide slot positioned 5 cm away from the transducer and on the central line

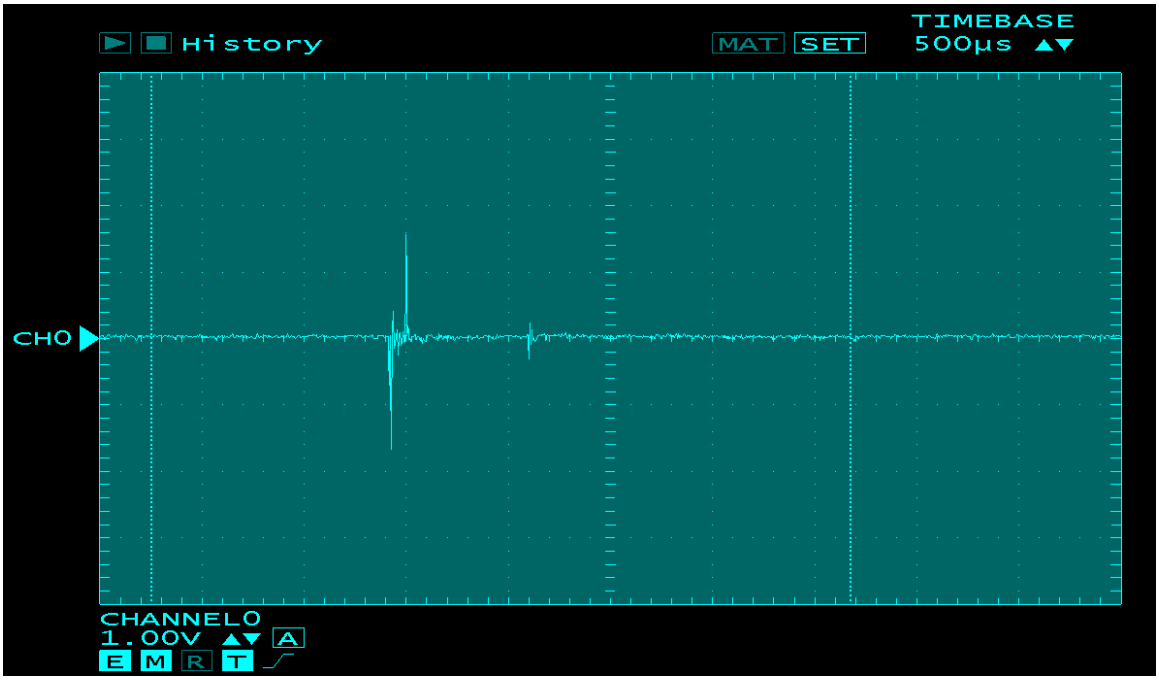

Fig. 3. 29. Reflected signal from the 1 cm wide slot positioned 5 cm away from the transducer and on the central line

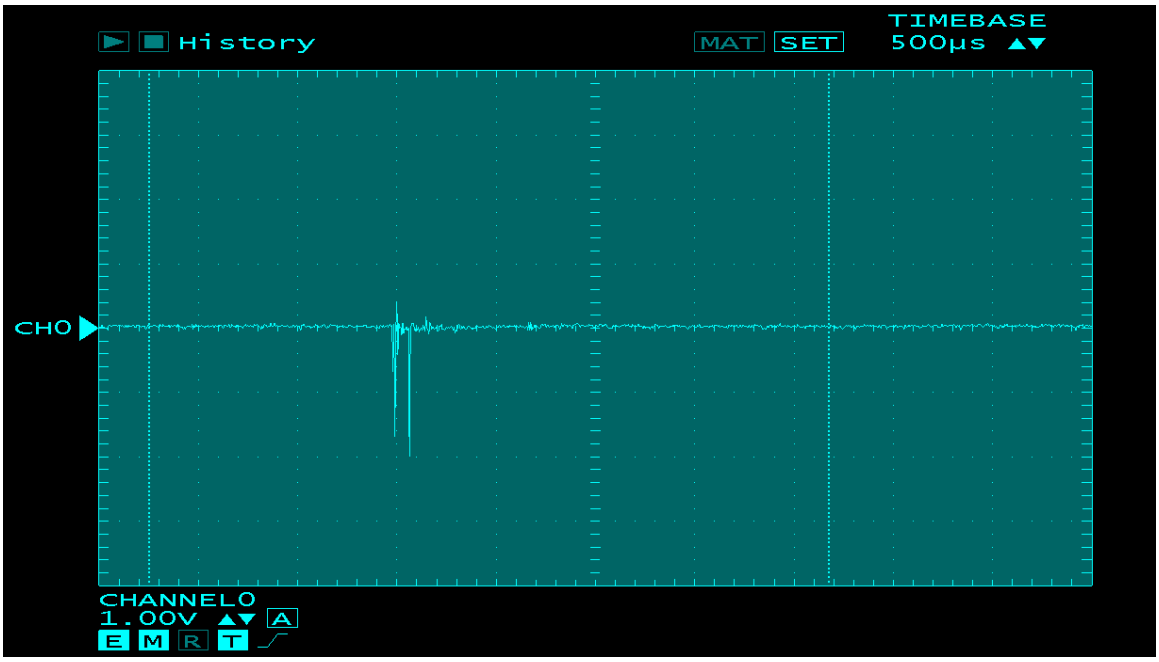

Fig. 3. 30. Reflected signal from the 0.4 cm wide slot positioned 5 cm away from the transducer and 1cm away from the central line

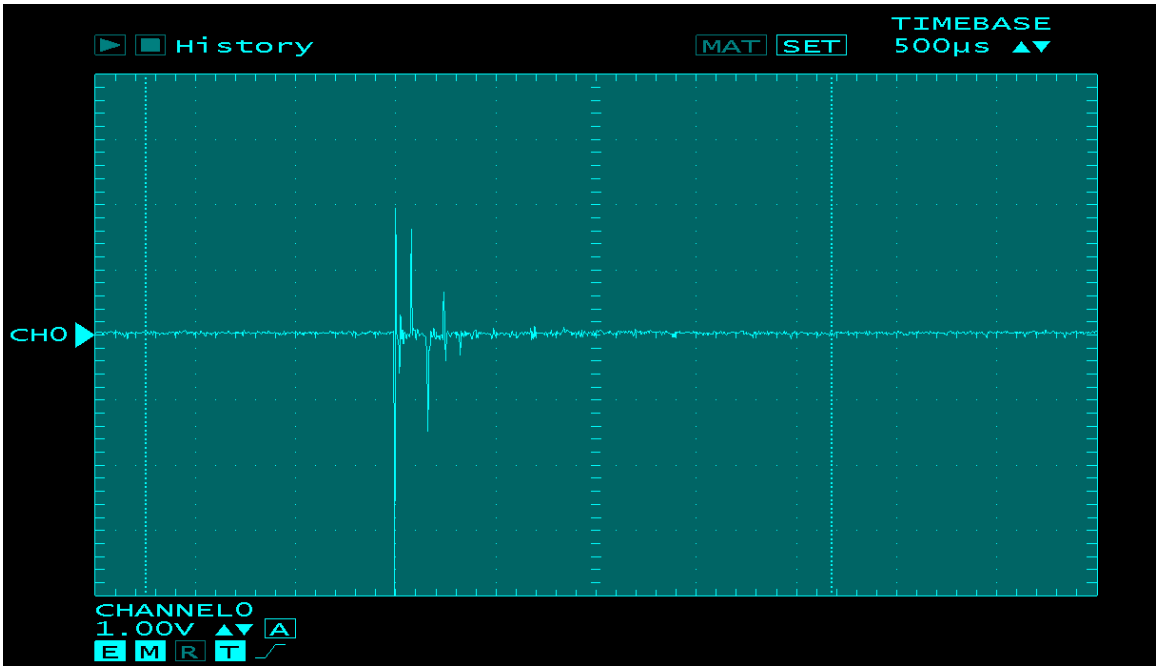

Fig. 3. 31. Reflected signal from the 1 cm wide slot which is 5 cm away from the transducer and 1 cm away from the central line

Figures 3.28 and 3.29 compare the reflected signals at a distance of 5 cm from the transducer. In Figure 3.28, the slot between the two reflectors is 0.4 cm wide. No obvious reflected signal from the glass wall can be noted. In contrast to Figure 3.29, a

reflected signal from the glass begins to appear with a slot width of 1 cm in Figure 3.29. In Figures 3.30 and 3.31, the objects are moved along the reflective surface 1 cm toward the side wall. Figure 3.30 shows the signal received by the transducer with a slot width of 0.4 cm, while Figure 3.31 has a 1 cm wide slot. After the two reflective objects are moved 1 cm away from the central axis, no obvious reflected signal is recorded from the opposite glass wall.

Figures 3.32 and 3.33 illustrate the same process 10 cm away from the transducer.

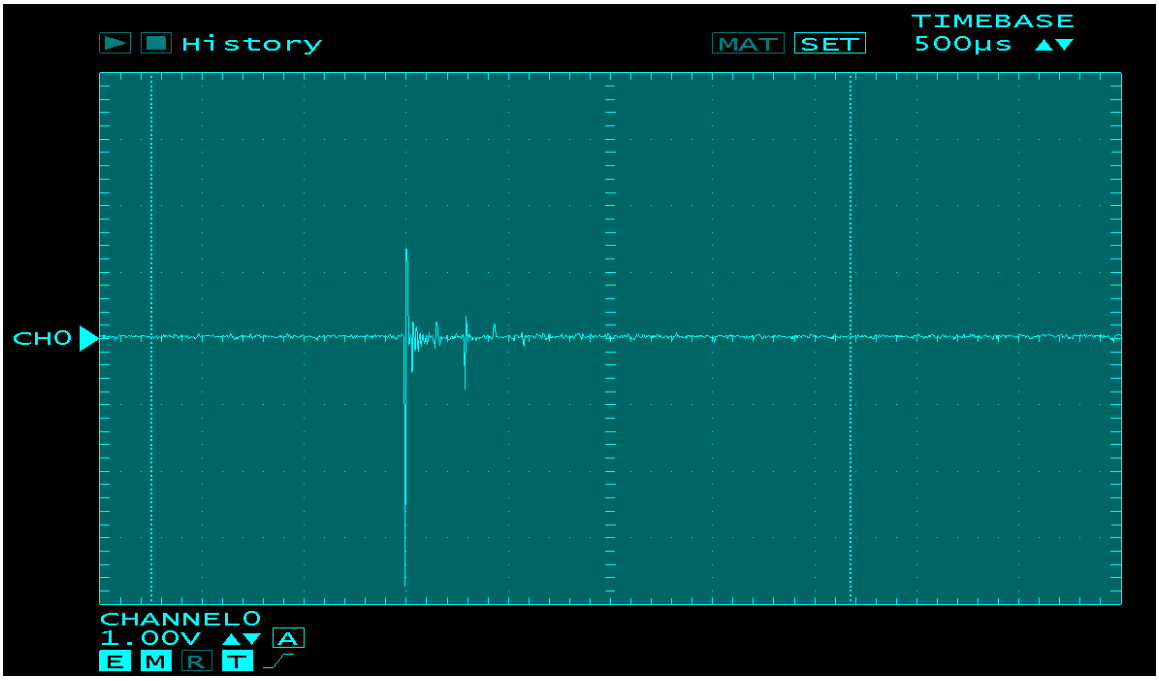

Fig. 3. 32. Reflected signal from the 0.4 cm wide slot, which is 10 cm away from the transducer and on the central line

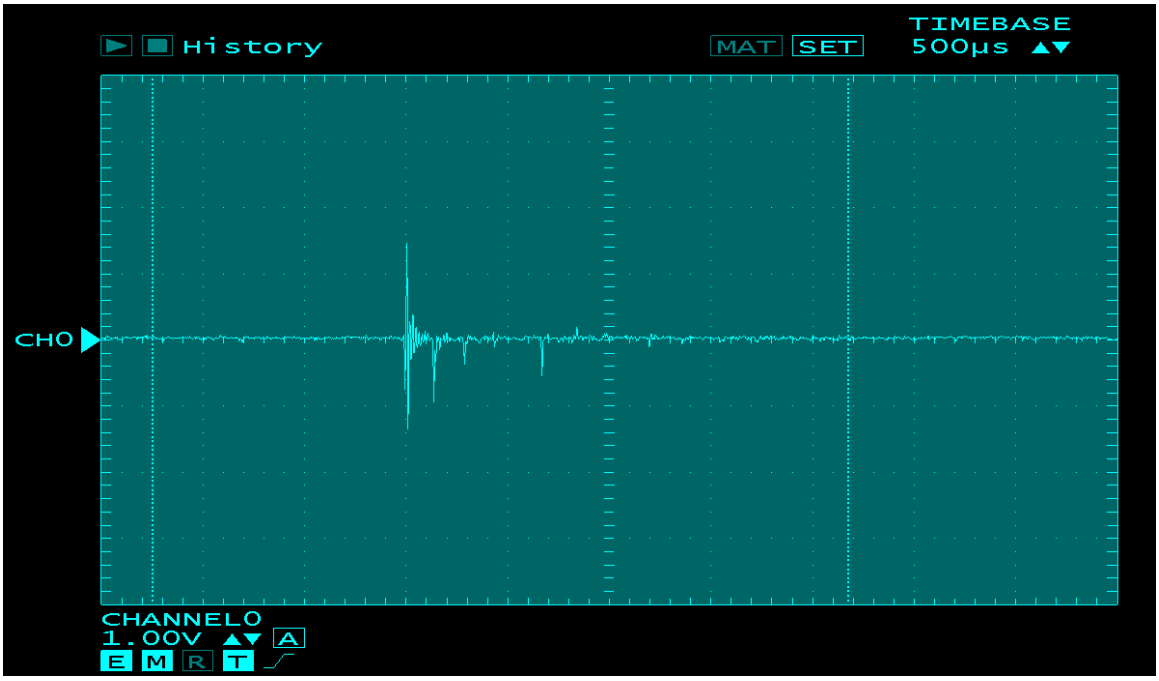

Fig. 3. 33. Reflected signal from the 1 cm wide slot, which is 10 cm away from the transducer and on the central line

When the width of the slot in Figure 3.32 is 0.4 cm, no obvious reflected signal from the glass wall is detected. In Figure 3.33, the slot is 1 cm wide and a reflected signal from the opposite wall begins to appear.

The experimental results show that the transducer can detect a slot which is more than 1 cm wide but resolution is unperceivable if the slot is smaller than 1 cm. The size of the slot can be measured without interfering with the echo signal if the vertical distance between the slot and transducer is more than 1 cm. One centimeter is in the range of the scattering shape of the transducer, which means the transducer can measure the reflected signal from the slot which is 1 cm away from the vertically measured location. If the shape of the object is gradually changed, the scattering phenomenon will not interfere with the distance measurement since the ultrasound speed is too fast to compare a change

of only a few millimeters. Therefore, if we set the spatial sampling rate at 1 cm, it is possible for signal strength to be collected for image processing purposes.

4. Digital Signal Processing (DSP)

In order to estimate the distance between the transducer and the reflector object, digital signal processing is used to extract the times when the excitation and echo signal occur to calculate the TOF. For this purpose, the wavelet transform technique is applied.. In addition, in order to extract a relatively weaker echo signal from the strong background noise, the de-noising algorithm by wavelet transform is used to suppress the noise. This chapter provides a detailed explanation of the approach used in DSP. The last part of this chapter contains further explanation of the 2D imaging algorithm used to extract the shape of the interface between two different media.

4.1. Wavelet Transform

A wavelet is a mathematical function whose amplitude can begin at zero and oscillate from peak to peak [63]. A wavelet transform uses a class of wavelets to localize a given function according to its space and scale [64]. A class of wavelets is created based upon function $\psi(x)$, which is known as a "mother wavelet". The "daughter wavelets" are scaled versions of the "mother wavelet" and are created with dilation. They are a series of functions having the same shape as the mother wavelet but different lengths. The length of a "daughter wavelet" is related to the center frequency of the function. Hence, the "daughter wavelets" can be viewed as different versions of the "mother wavelet".

In contrast to the Fourier transform, which provides a description of the overall

regularity of a signal, the wavelet transform provides information about temporal and scale properties of the signal and is well-adapted to finding the location and spatial distribution of singularities [65]. For a signal series containing sharp spikes, such as seismic or ultrasound data, the frequency changes dramatically when the amplitude spikes. The temporal information available from the wavelet transform combines the change in the signal's frequency with amplitude variations as a function of time. This mathematical property fulfills the requirements of this study – to extract and localize the peaks in a signal.

4.1.1. Basic Principles

Shifting and scaling are two fundamental operations of the wavelet transform. They are functions of two parameters (one is time or space, the other is scale) used to translate a mother wavelet. When the mother wavelet is translated in time, or space, by a variable shift b and scaled by an amplitude parameter, the scale *a*, so that [67]:

$$\psi_{a,b}(t) = \frac{1}{\sqrt{a}}\psi(\frac{t-b}{a}) \qquad [4.1]$$

The pair *(a,b)* vary along the signal series plane [67].

A wavelet transform operates on a signal by revolving the mother wavelet at any position and shifting the mother wavelet to determine if the signal contains the similar frequency information at this position (indicated by the shift index). Next, the original signal is combined with the scaled mother wavelet at several positions. This measures the

similarity between the original signal and a scaled version of the mother wavelet at a given position. The convolution measures similarities in the frequency (scaling) and location (shifting) content of the signal and wavelet.

In order to obtain a continuous wavelet transform (CWT), the process begins by convolving the signal series with every version of the mother wavelet. The frequency content of the mother wavelet is continuously varied according to a series of dilation and shift indices. The wavelet transform function is as follows:

$$W(a,b) = \frac{1}{\sqrt{a}} \int_{-\infty}^{+\infty} f(x)\psi(\frac{x-b}{a})dx \qquad [4.2]$$

The outcome of this process *W(a,b)* is called the wavelet coefficient. Since it is a convolution process, the larger the wavelet coefficient, the greater the convolution between the signal series and the scaled version of the mother wavelet (dilated by *a* at the position *b*). Indices *a* and *b* determine the frequency and position of the wavelet, defining the operation as a time-frequency transform. The time-scale domain of the wavelet transform is shown in Figure 4.1.

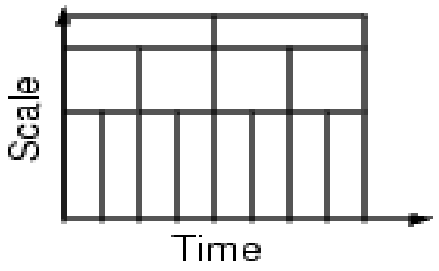

Fig. 4. 1. Wavelet transform time scale domain [67]

The wavelet analysis begins with a high-frequency mother wavelet. The frequency content of the mother wavelet decreases with increasing dilations. A large

convolution between the signal and the lowest frequency version of the mother wavelet is viewed as low frequency components of the signal, and a large convolution with the high frequency version of the mother wavelet is considered a small discontinuity, such as a spike. Figure 4.2 demonstrates the convolution process of a temporal signal with two versions of a mother wavelet.

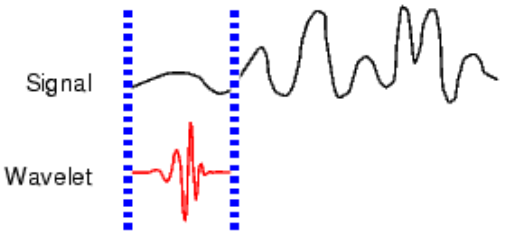

Beginning with low scale high frequency

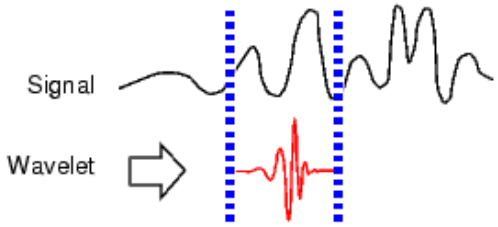

Shifting along x axis

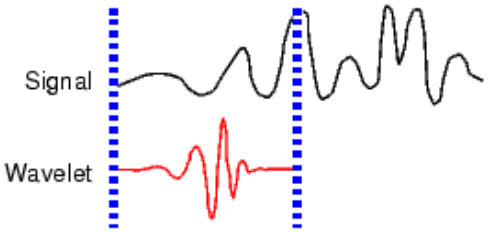

Beginning with high scale low frequency

Fig. 4. 2. Continuous wavelet transforms [67]

Although the continuous wavelet transform (CWT) provides a good mapping from a temporal signal to its time-frequency domain, some limitations still exist. A

“continuous process” means the whole process is continuous with regard to shifting and scaling. The CWT will operate on every scale, from that of the original signal, up to a maximum value determined by available computational resources. The CWT is also continuous in terms of shifting, as the wavelet is shifted smoothly over the full domain of the analyzed function. Figure 4.3 illustrates the continuous shifting in the CWT process.

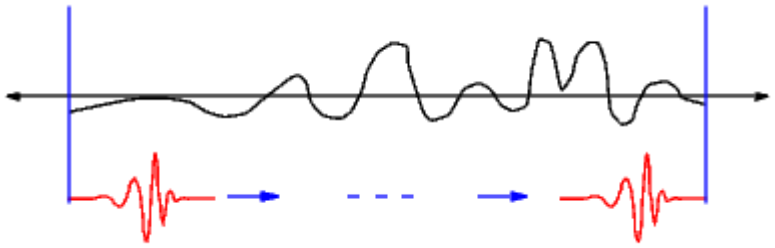

Fig. 4. 3. Continuous shifting in CWT [68]

Calculating wavelet coefficients at every possible scale can be arduous and can generate a large amount of data. To significantly reduce calculations for the CWT without losing the data’s important components, scales and positions for the wavelet transform are chosen based on the power of two; dyadic scales and positions [68]. This makes the analysis more efficient and accurate. An analysis of the wavelet transform, based on the selected scales and positions, is called a discrete wavelet transform (DWT).

In digital signal processing, the convolution of two time domain signals is equal to the multiplication of the signals in the frequency domain. The convolution of the temporal signal with a wavelet, which has a specific frequency band determined by a scale index, can be viewed as a band pass filter in the frequency domain. The wavelet transform convolves the original signal with a mother wavelet filter in the frequency

domain and can be interpreted as the original signal being filtered by the mother wavelet in the time domain. Based on this characteristic, the DWT can be illustrated as shown in Figure 4.4.

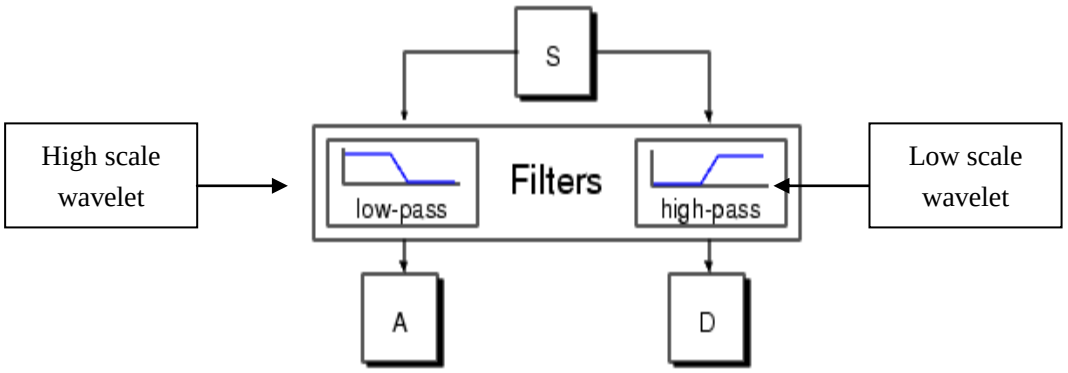

Fig. 4. 4. DWT Scheme [68]

The time domain filter shown in Figure 4.4 represents the shape of the mother wavelet. The signal obtained from the low-pass filter is called an approximation because it shows the gross feature of the signal [68] and the signal passing through the high-pass filter is called the detail signal [68]. The filtering process is called de-composition. If we require a more specific signal which shows more detailed information, the approximation is filtered by a low-pass, high-pass filter pair. The schematic for this algorithm is shown in Figure 4.5.

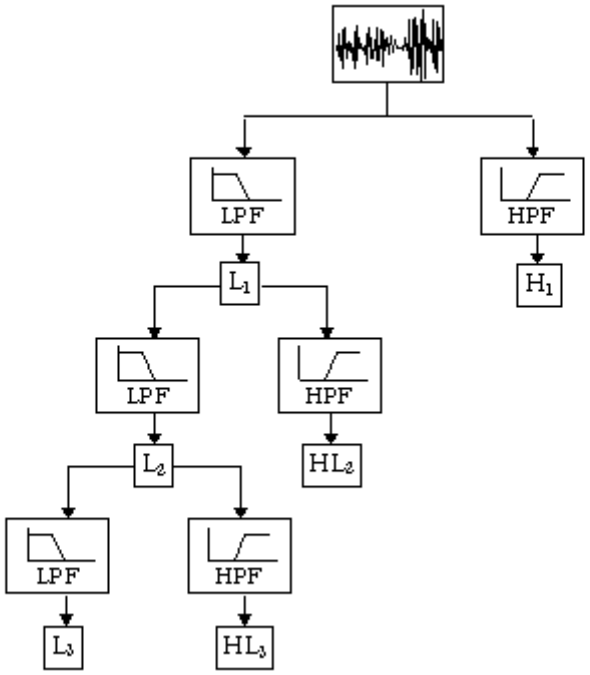

Fig. 4. 5. Multi-decomposition algorithm [68]

This is a very practical filtering algorithm that yields a fast wavelet transform. Processing a signal through the transform produces the wavelet coefficients.

4.1.2. Choice of Mother Wavelets

There are many existing mother wavelets, such as Haar, Daubechies, Morlet, and Coiflet wavelets, which are used for various applications. Each mother wavelet has its own characteristics and properties used to resolve different problems. The time duration, number of cycles, shape of the decay and central frequency of the mother wavelet all contribute to its resolution after applying the wavelet to the temporal signal.

Compared to the acoustic signals emitted from other systems, less uncertainty is recorded in the signals from the experiments. For instance, the shape of the transmitted

signal, the expected shape of a received signal (which should be a dilated version of the transmitted signal with a smaller amplitude due to attenuation and energy loss during propagation) and the actual shape of the received signal (which is slightly different from the theoretical shape), were all known factors since they could be measured. The main purpose of the wavelet transform is to measure the similarity between the temporal signal and mother wavelet at different scales and positions by convolution, to achieve the final goal of localization. The most similar and least complicated mother wavelet is the transmitted signal. Hence, the mother wavelet used in the signal analysis was the transmitted signal emitted from the transducer. Figure 4.6 shows the transmitted signal from the system.

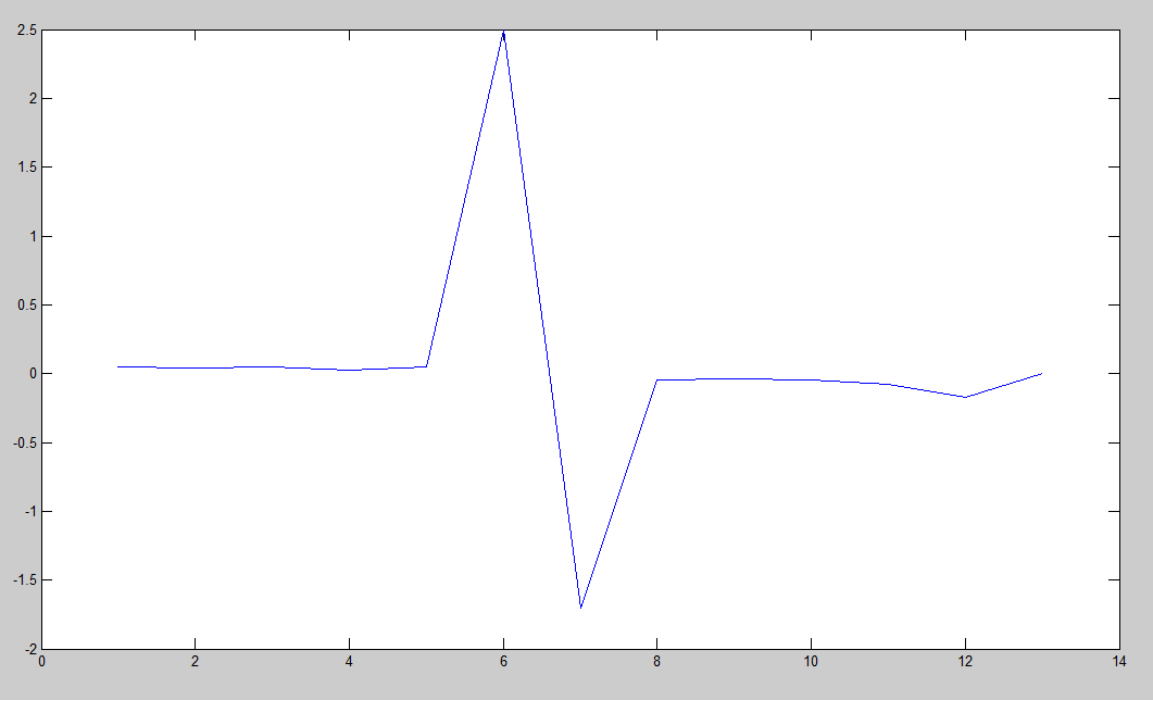

Fig. 4. 6. Transmitted signal

14 data points are sampled to represents the transmitted signal. Since the frequency of the ultrasound is 100 kHz and the sampling rate is 500 kHz, 14 data points

are enough to represent the shape and frequency of the transmitted signal. The following procedure is used to create the specific wavelet applied to the experimental signal:

1. Collect the transmitted signal.
2. Truncate it to a length which contains all the information regarding the transmitted signal, such as: shape, number of cycles, central frequency and amplitude.
3. Adjust the truncated signal to a format which satisfies the entire criterion of a mother wavelet.
4. Apply the mother wavelet to the experimental data to finish the wavelet transform.

Figure 4.7 shows the creation of the mother wavelet based on the transmitted signal shown in Figure 4.6.

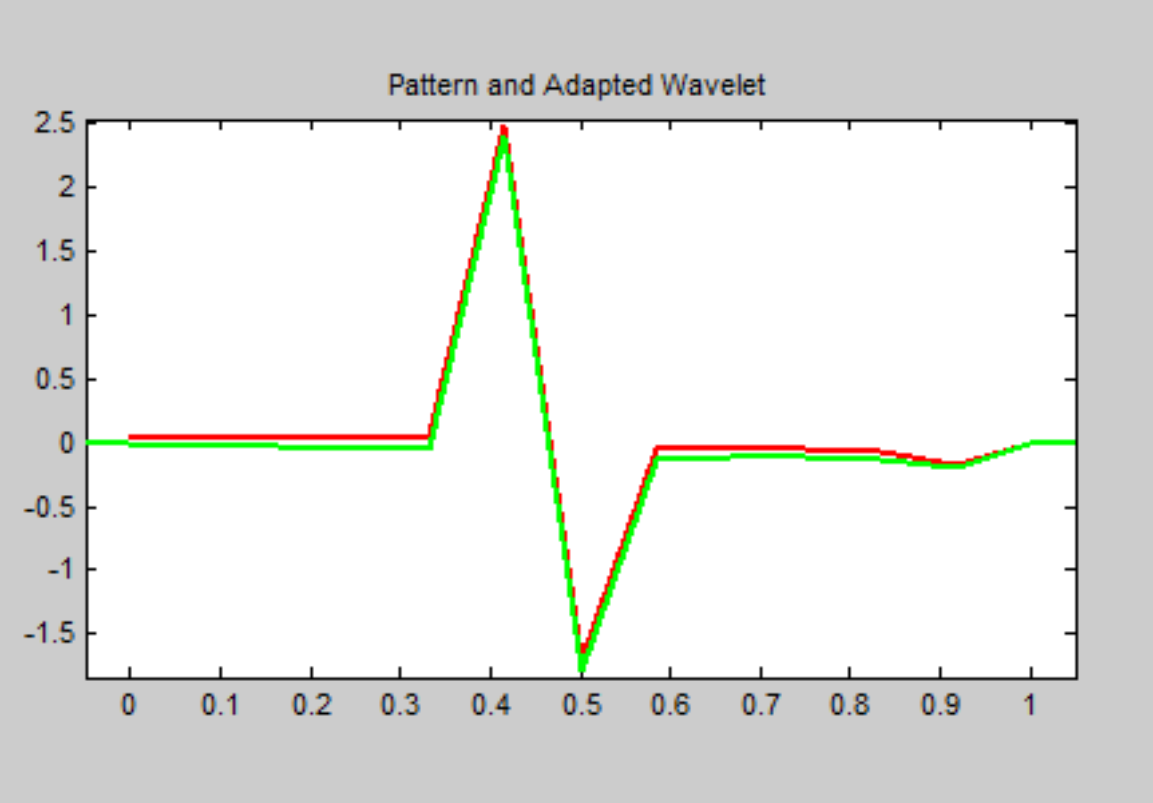

Fig. 4. 7. Mother wavelet and transmitted signal

In Figure 4.7, the red line shows the original transmitted signal, while the green line is the adapted mother wavelet based on the transmitted signal.

4.1.3. The Application of Wavelet Transforms in Signal Testing

Since a wavelet transform maps a temporal signal into the frequency-time domain where the signal's frequency changes with a variation in time, it is therefore very useful in the analysis of ultrasound signals. In the field of digital signal processing, the noise and the gross feature of the signal are represented by low-frequency signals [68]. The spikes in the high end of its frequency spectrum are created by events such as discontinuities, singularities and spikes. Localizing the high end of the frequency

spectrum assists with compression and imaging. The most important information contained in an ultrasound signal is when spikes occur during a relatively smooth period in the signal. We must obtain the precise position of the spikes to complete the imaging process. Compared to a classical Fourier transform, which represents the frequency components of a signal but cannot indicate location, wavelet transforms not only identify the frequency components but also provide location information. The positioning information obtained from a wavelet transform is a critical prerequisite for the imaging process. The time-frequency analysis algorithm has many applications in ultrasound signal analysis.

4.2. Analysis of Transient Ultrasound using a Wavelet Transform

This section explains how a wavelet transform is applied to ultrasound signals. The wavelet transform overcomes two problems in the ultrasound signal analysis process. The first problem, which is a unique property of the wavelet transform, is the ability to localize the transient signal, and the second problem is de-noising.

4.2.1. Localization of the Transient Signal

Localization is the main problem to be solved in an ultrasonic system. An accurate positioning of the echo signal contains information regarding the time of arrival (TOA) and the time of flight (TOF), which is very important in obtaining the object's position and recreating its image. The most important aspect of localizing the transient signal is

matching the temporal signal with a high-frequency wavelet to obtain the position of the most similar portions of the signal and wavelet. Sudden changes in the signal lead to a spike corresponding with higher frequency components. To obtain the location of a spike, a temporal signal is transformed into a wavelet and its coefficients are obtained. The position of the highest wavelet coefficient number determines the location of a spike. A DWT system filters the signal through a series of high-low frequency filter pairs and, normally, the frequency spectrum filtered by the highest frequency filter contains the most information regarding the locations of the spikes.

The received signal is filtered through many pairs of high-low frequency paired filters and the resulting output of the highest frequency filter contains the largest coefficients of the wavelet transform. The signal passed by the highest frequency filter is called the detail level one signal. The coefficients of the detail level one signal represent the amplitude of the high frequency components and are used to locate the spikes in the original received signal. Figure 4.8 shows the working process of a DWT.

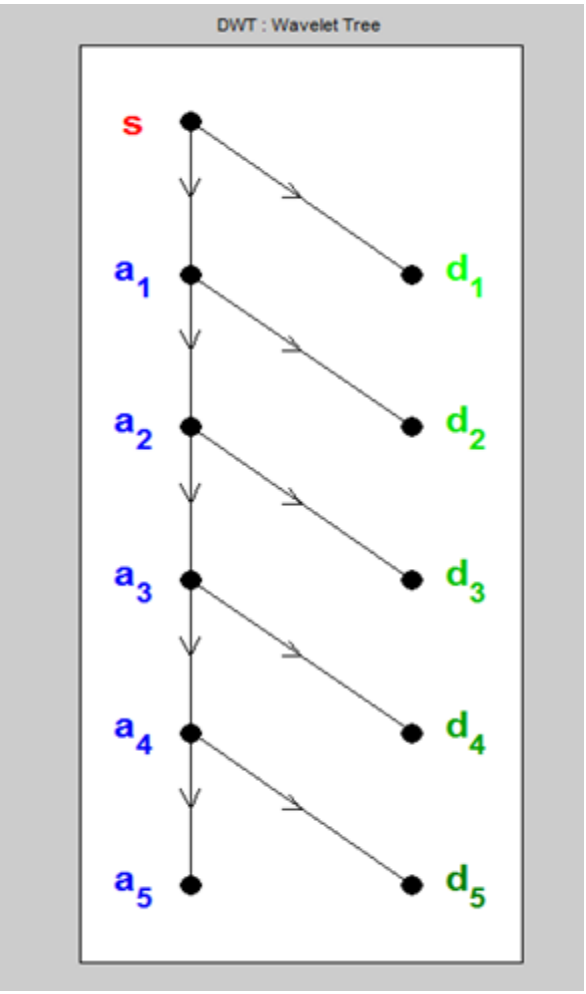

Fig. 4. 8. Wavelet decomposition process [68]

Figure 4.8 outlines the process for wavelet transform-based localization. The signal d1 in this figure is the original signal filtered by the highest frequency filter, and the high frequency components contain further detailed information in the signal series.

A pulse-echo signal will be analyzed using the wavelet transform to illustrate how the wavelet transform processes an actual pulse-echo signal, recorded from the experimental measurements. Figure 4.9 shows the actual pulse-echo signal produced by the system. The signal in Figure 4.9 is the sixth signal from the left side of the water tank which was used to measure the shape of the air-filled balloon buried in the water

saturated sand.

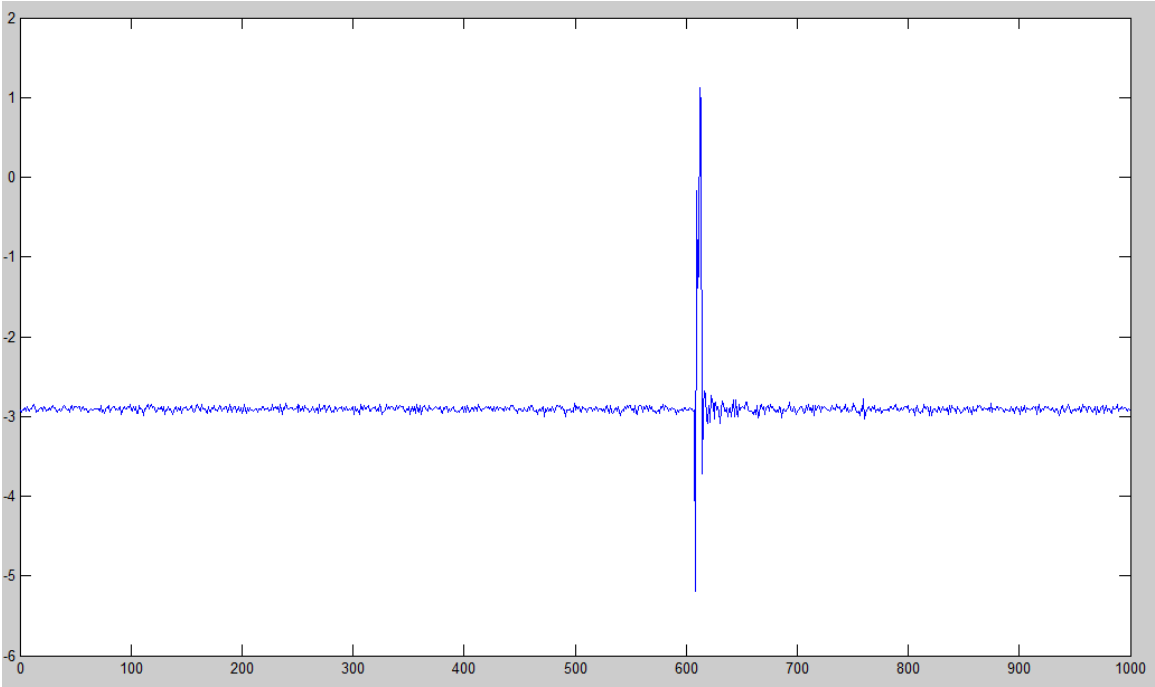

Fig. 4. 9. Actual signal from the acoustic system

The original signal can be extracted from the actual signal in Figure 4.9. However, extraction of the echo signal is not as simplistic as extracting the original signal. To localize the echo signal, it was processed with the wavelet transform. The location of the spikes could be extracted from the detail level one coefficients. Theoretically, higher coefficients of the detail signal correspond to the occurrence of high frequency components, which could be viewed as spikes.

Figures 4.10 and 4.11 show the full decomposition of the actual signal in Figure 4.9 and its wavelet coefficients at the detail level one composition.

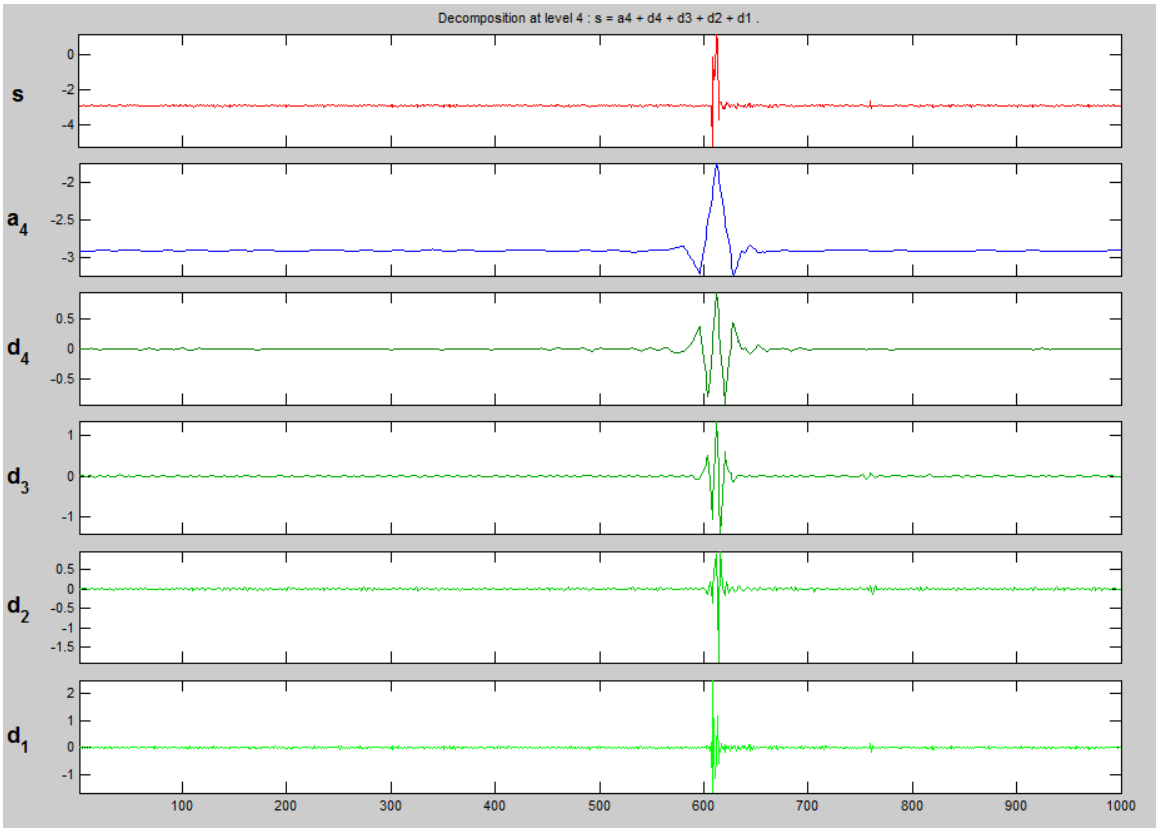

Fig. 4. 10. Wavelet decomposition of the signal

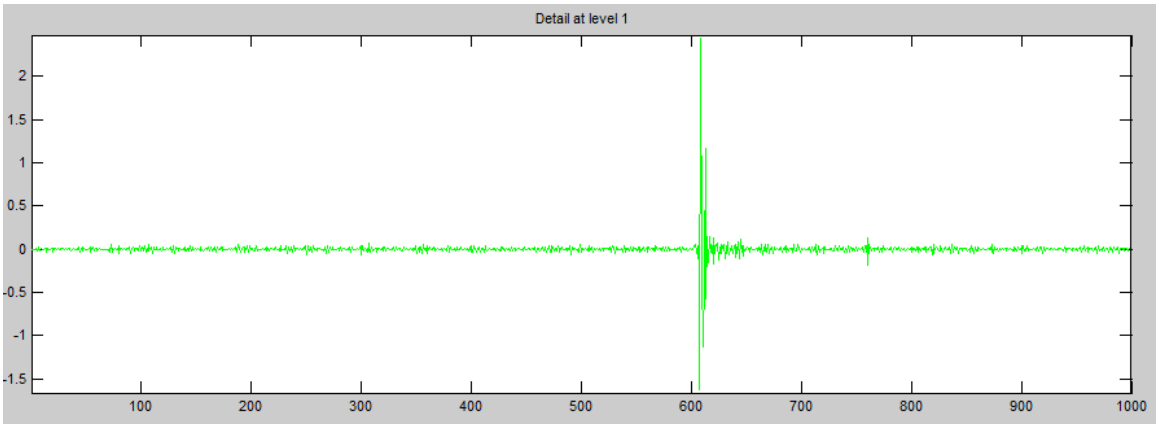

Fig. 4. 11. Detail of the signal

The detail level one signal in Figure 4.11 has a large wavelet coefficient around position 780. This indicates the location of the discontinuity present in the original signal. The next step is to extract the spike signal in the detail level one coefficient series to localize the peak signal in the ultrasonic system. Its corresponding coefficient index is the

location of the peak in the original ultrasound signal. After establishing the location of the spike, the TOF (the time interval between the original pulse and reflected pulse) can be expressed and calculated using the following equation:

$$t = \frac{P_2 - P_1}{f} \qquad [4.3]$$

Where P_2 and P_1 are the positions of the echo ultrasonic and original signals and f is the sampling frequency during the data acquisition process.

4.2.2. De-Noising

Another important application of the wavelet transform in pulse-echo ultrasonic signal processing is de-noising. Since localization of the received echo signal is an important task in the system, distorting the localization of the received signal may lead to incorrect measurements. The simulated porous media is viewed as a high noise background when the ultrasonic signal goes through it and it may lead to distortion of the signal. Hence, de-noising the received signal is a very important step with regard to the entire signal process.

As mentioned in Section 4.2.1, only large coefficients contribute to a singularity in the signal. Hence, selective elimination of the small coefficients will not lead to a loss of important information. Each coefficient contains a signal and superimposed noise. At the same time, the noise pollutes all the wavelet coefficients to some degree. Therefore, a threshold value is applied to the coefficients and only the coefficients whose magnitudes

are greater than the threshold are recognized as valid values, while magnitudes smaller than the threshold are reduced to zero. Discarding the smaller coefficients could improve the whole SNR without losing important components, since the significant coefficients are still maintained to describe the original signal. The wavelet transform based de-noising process involves the following procedures:

1. Transformation: Transform the noisy data to the wavelet coefficients C_a^b which represent the signal at various scales at position b.
2. Shrinkage: Apply the threshold value to the coefficients in order to eliminate the relatively less important small coefficients.
3. Reconstruction: Reconstruct the de-noised signal by the shrunken wavelet coefficients.

Figures 4.12 and 4.13 show the process of the wavelet based de-noising procedures. The signal in Figure 4.12 shows a real signal received by the system. The signal from the left side of the water tank was used to measure the distance between the water tank's surface and the steel plate inserted in the water saturated sand.

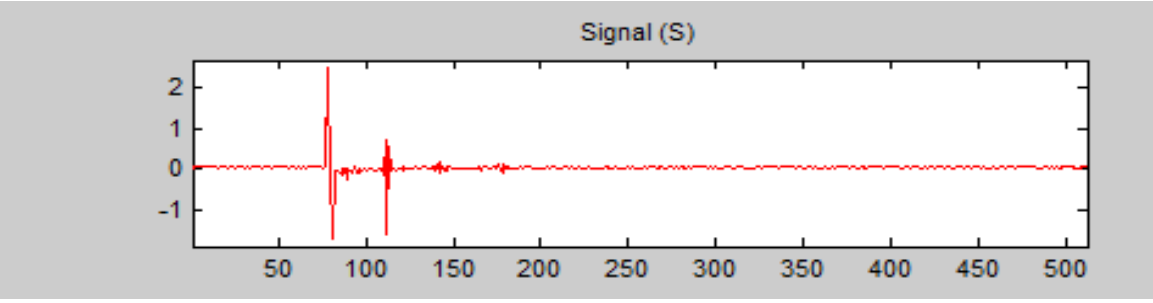

Fig. 4. 12. Pulse-echo signal from the steel plate

Only one obvious echo signal could be easily discerned from the original signal.

Figure 4.13 shows the de-noising process of the original signal by the wavelet transform and Figure 4.14 shows the reconstructed de-noised signal.

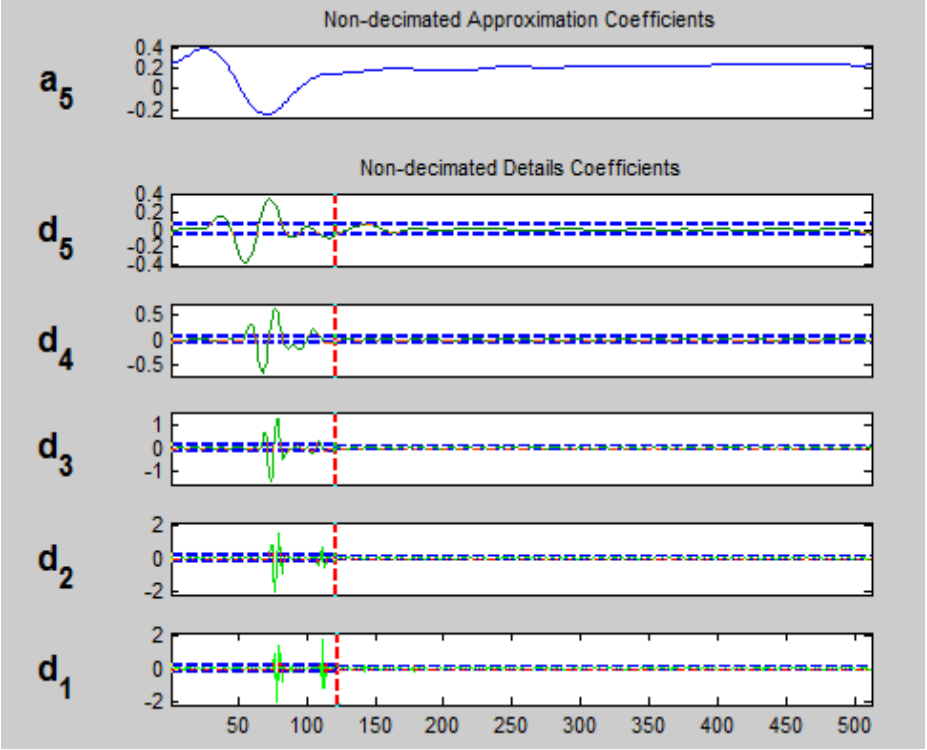

Fig. 4. 13. Decomposition and threshold process

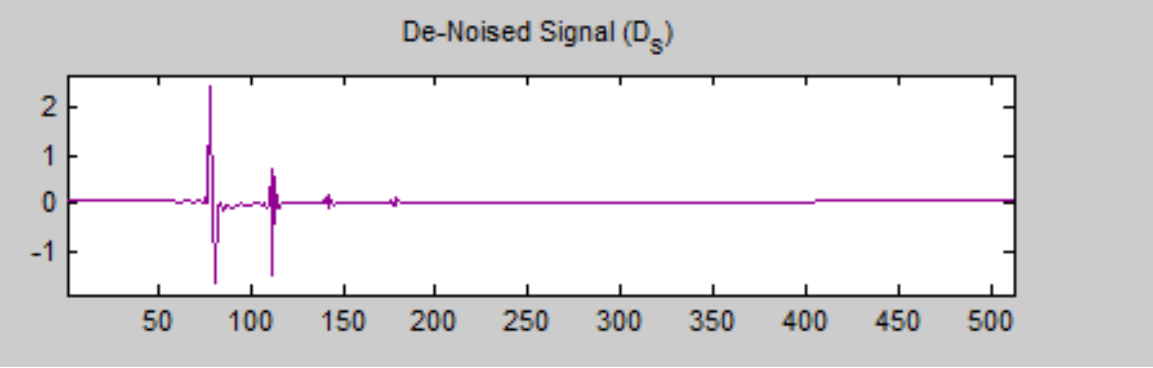

Fig. 4. 14. Reconstructed signal

Actually, there are 3 echo signals present in the reconstructed de-noised signal recorded by the system. The wavelet transform effectively reduces the background noise detected by the system. The last two received signals are used to measure the level of attenuation reducing the amplitude of the ultrasonic wave due to the water saturated sand.

4.3. Imaging

The last step in ultrasonic signal processing is imaging. The image of the object is obtained by collecting signals from various locations, localizing each echo signal's position, calculating the distance between the transducer and the reflector object and synchronizing the distances from multiple received signals.

4.3.1. B-Scan Presentation

Ultrasound data can be displayed in three different formats; A-scan, B-scan and C-scan presentations. Each provides a different perspective and evaluates the environment of the material being inspected. The A-scan presents the received signal energy as a function of time. The relative size of the reflector is estimated in an A-scan by comparing the signal amplitude from an unknown reflector to that of a known reflector. In a B-scan presentation, the TOF is displayed with the position of the transducer. The C-scan presentation is produced with an automatic data acquisition scheme. The amplitude of the received signal, or the TOF, is recorded at regular intervals as the transducer scans over the object and is displayed as a shade of gray for each position where data is collected.

Data obtained from the lab-scale VAPEX process experiment was collected by measuring ultrasonic signals at fixed positions in a container filled with media to detect a buried air-filled balloon or a dry sand bag. The TOF was calculated by employing the

signal processing process and the speed-time function using collected data. Figure 4.15 shows how the B-scan presentation displays the signal in an ultrasonic system.

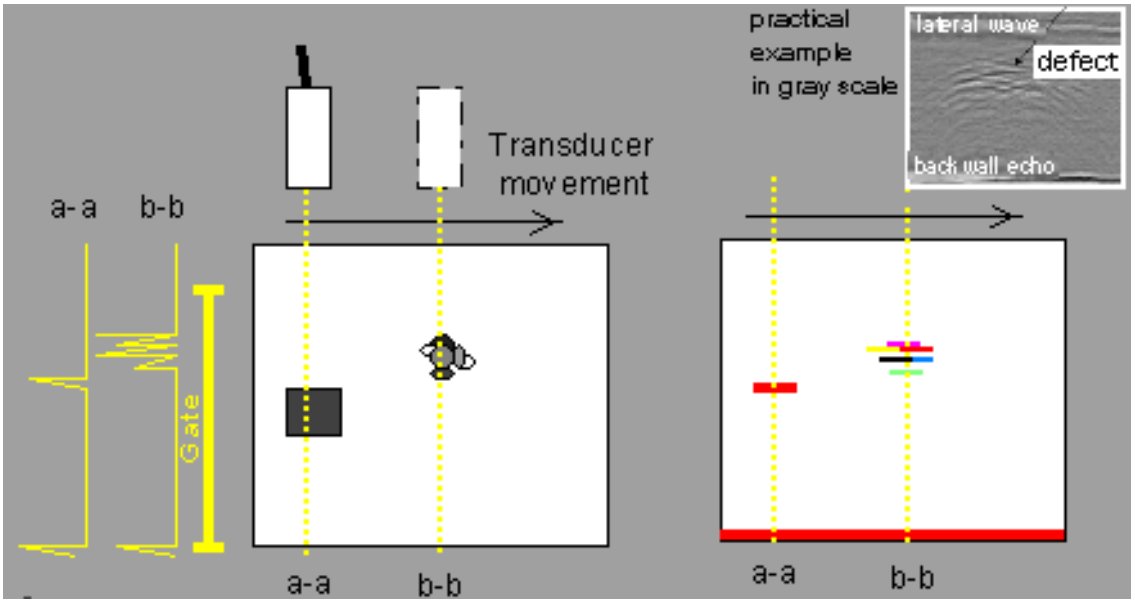

Fig. 4. 15. B-scan presentation

The transducer is detected over one of the surfaces of the container in Figure 4.15. The signals in the left part of the figure are the two pulse-echo signals the transducer received from the two data collecting points a-a and b-b. The middle part of the figure shows the movement of the transducer along the surface under the object. The right side of the figure is the B-scan profile of the system. In the B-scan presentation profile, the horizontal axis represents the distance between the transducer's location where the data is collected and the transducer's original position when it emitted the signal. The B-scan presentation shows the position of the transducer in the system. The vertical axis shows the TOF of the received signal, which is related to the distance between the surface where the transducer is located and the reflector.

4.3.2. 2D Imaging

The B-scan presentation shows the position of the transducer as a function of the TOF. The TOF is used to calculate the distance between the transducer and reflector using the time-speed function. Therefore, the position-time map can be converted into a position-distance map.

The final objective of this thesis is to obtain a 2D image of either the air-filled balloon or the dry sand bag, which are buried in the opaque porous media in the laboratory-scale model. To draw a picture of a buried object, we need to know the depth of the object interpolated from different data collection points, which is the basis of a 2D imaging system. The procedure for 2D imaging within an acoustic system is as follows:

1. Mark the position of the data collection points along one side of the water tank (the distance between two points should be incremental).
2. Conduct a pulse-echo measurement at each data collection point along the surface of the water tank and map the collected data to a B-scan presentation.
3. Repeat the same procedure on the opposite surface of the water tank.
4. Calculate the distances by multiplying the measured time of flight by the speed of sound.
5. Map the temporal position B presentation to the distance position plane.
6. Synchronize the distance data from both surfaces into one plane and display

the position and shape of the buried objected on the plane.

Figure 4.16 shows how the 2-D imaging process works in the system.

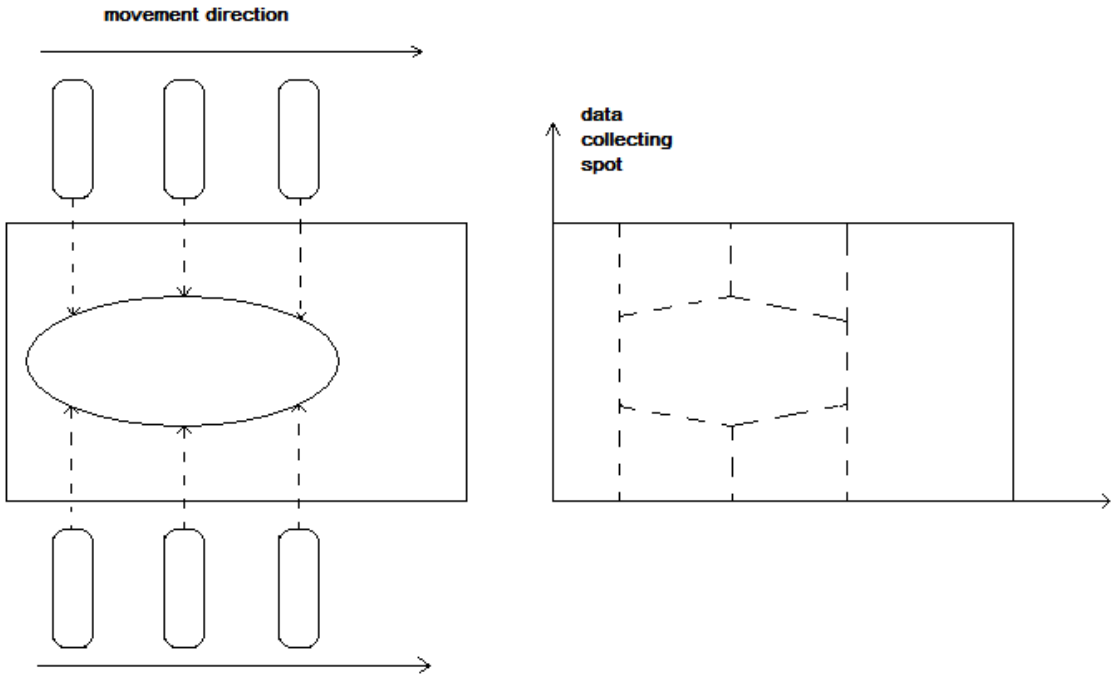

Fig. 4. 16. 2-D imaging

4.4. Errors

Three main sources of error could occur in signal processing to generate the 2D maps: noise, attenuation, and error in distance measurement between two data collection points.

4.4.1. Noise

Noise is any unwanted signal randomly added to the original signal. In an ultrasonic system, background noise is a major problem which influences the precision of the detector. The propagating media used in the experiment were either water saturated

sand or oil saturated sand, which combines sand particles and increases the level of scattering. When the ultrasonic wave goes through a medium which inhibits propagation, the reflected signal may be as weak as the background noise. Consequently, the echo is not obvious and useful information cannot be extracted with the desired level of precision. Figure 4.17 displays a signal collected within the oil saturated sand. Due to the high viscosity of crude oil, it is difficult for signals to penetrate into the mixture with an ultrasonic wave. A great deal of energy is lost due to attenuation. The amplitude of the echo signal is particularly low, making it difficult to be distinguished from background noise.

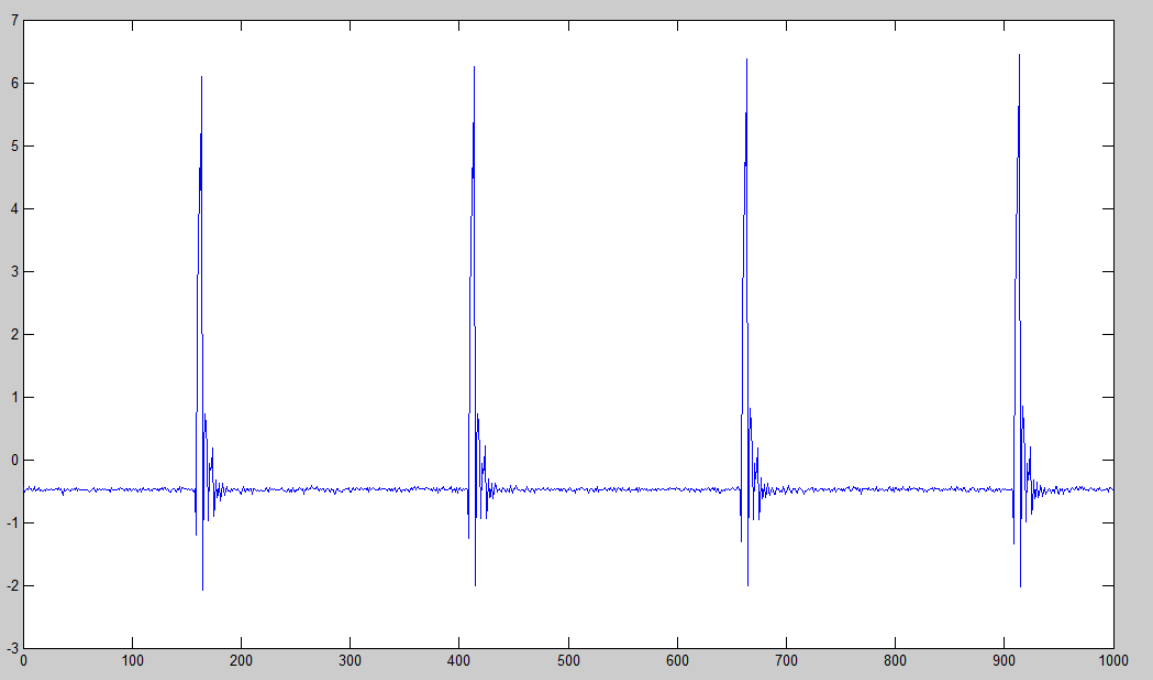

Fig. 4. 17. Pulse-echo signal from oil saturated sand

Four transmission impulse periods are presented in Figure 4.17 but no obvious reflection can be identified in the signal graph. We are unable to attain any information from the signal which propagates through the oil saturated sand without performing the

de-noising process. Background noise has a strong effect on the signal, therefore, it is the main source of any errors that might occur in producing the images of the simulated vapor chamber.

4.4.2. Attenuation

Another important factor which may lead to an erroneous outcome is attenuation. The ultrasonic signal decays as a function of distance. A sharp-spiked, high-amplitude signal becomes wider and smaller after propagating through a medium over a given distance. The main problem regarding attenuation of the ultrasonic signal is that it gains a wider and more triangular shape and the actual location of the signal becomes more difficult to extract, which critically influences the precision of the experimental result. Figure 4.18 shows the original signal and its echo over a long distance.

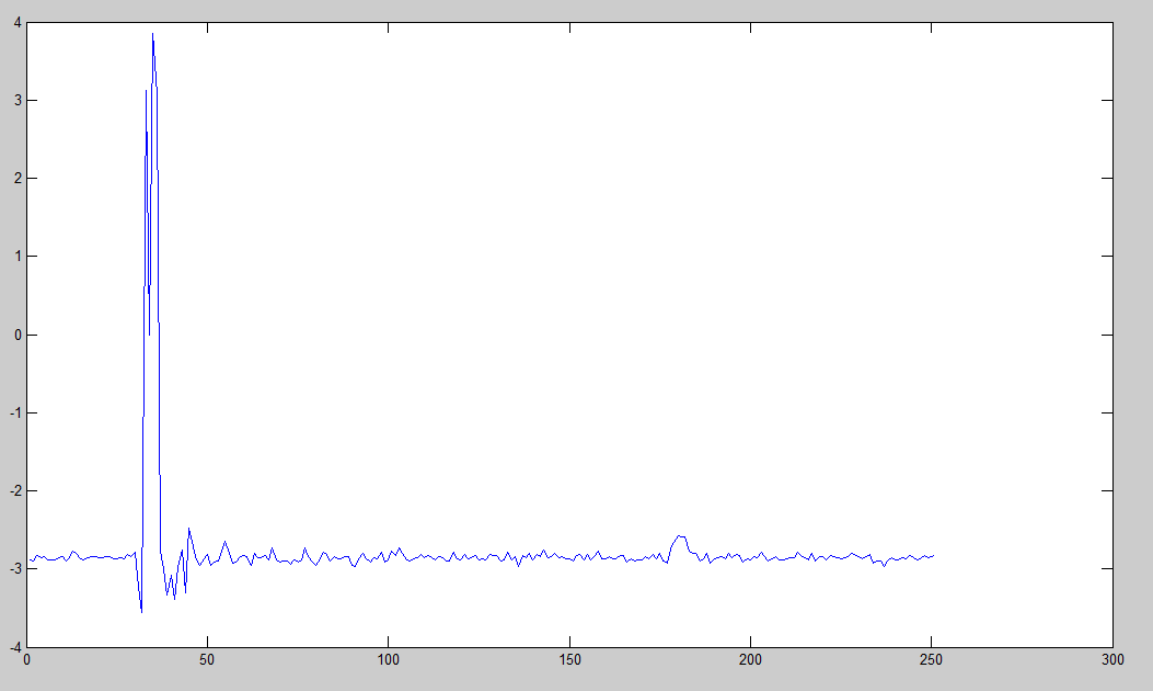

Fig. 4. 18. Reflection signal from a glass wall 25cm away

The signal recorded in the Figure 4.18 is a reflection from the glass on the side of the tank opposite from the transducer. The width of the water tank is 25 cm, so the reflected signal is the echo of the original signal after it travelled 50 cm in the water saturated sand. After the ultrasonic signal traveled 50 cm, the echo became a smooth, wide signal making it difficult to distinguish from the background noise and the precise location is not as clear.

4.4.3. Distance between Two Collection Points

The actual shape of a simulated vapor chamber (i.e., spherical shape balloon) inside the laboratory-scale model is a smooth curve. Since the data collection was performed at unique points located on each side of the physical model, the result from the ultrasound testing system appears to be more of a polygon. The generation of the polygon is based on the horizontal distance between every data collection point on the water tank's surface and the balloon, which represents the interface between the media and the simulated air chamber. The missing parts between the two signal collection points may lead to an error in the imaging result if an irregular shape between two points occurs. Therefore, the distance between two collection points can be considered another source of inaccuracy in the system.

5. Application of Acoustic Imaging Techniques in Monitoring the Solvent Chamber in VAPEX Experiments

A series of experiments were conducted to generate images of the experimentally simulated vapor chambers. Reliable image results of the interface between different media demonstrate the feasibility of acoustic imaging techniques to monitor the solvent chamber in VAPEX in a simulated lab environment. The results of these experiments are discussed in this chapter.

5.1. Imaging of a Sealed Dry Sand Bag Embedded in Water Saturated Sand

The first experiment measures the shape of a sealed dry sand bag buried in a water-saturated sand pack. The signal was acquired at fixed positions marked on two opposite glass walls of the physical model, which were along the two longer glass walls, 1 cm apart (i.e. a quarter of the length of the diameter of the transducer). The main purpose of this experiment was to measure the interface between the dry sand and the water saturated sand. The schematic of the imaging experiment is shown in Figure 5.1.

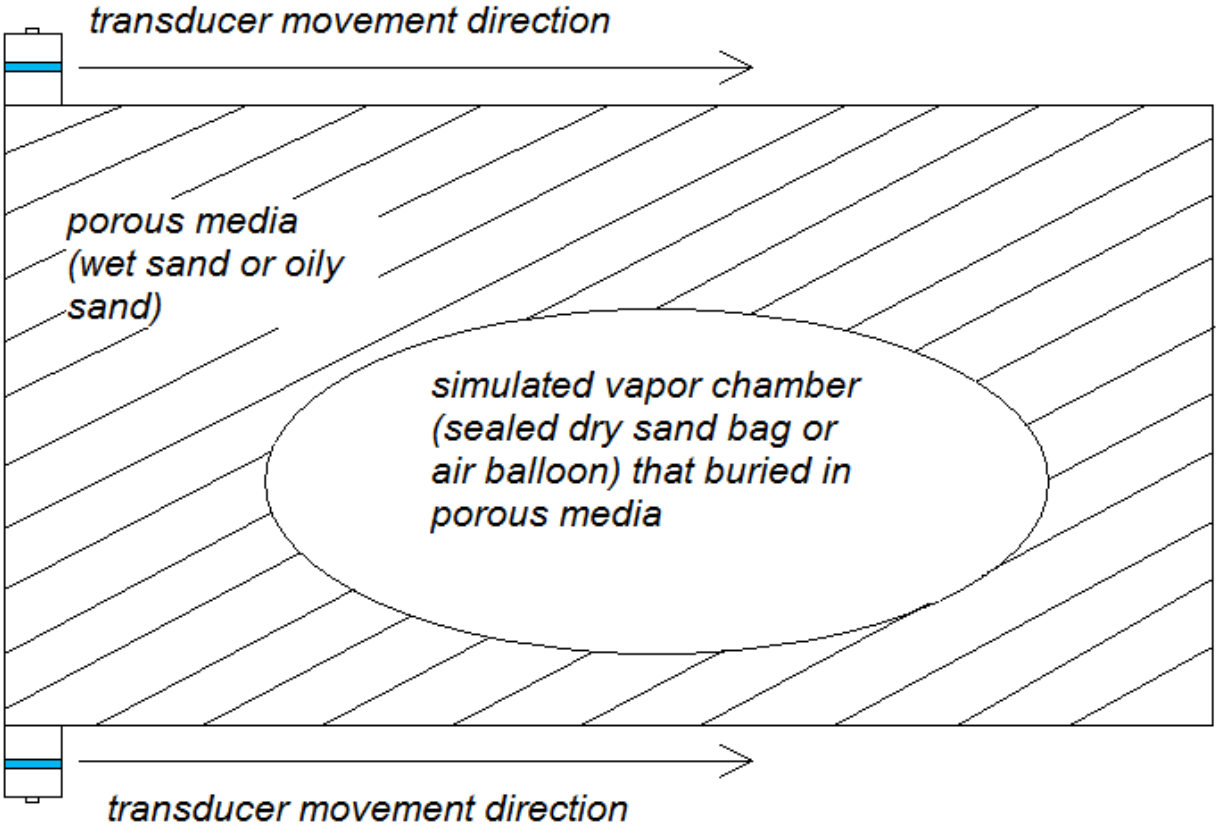

Fig. 5. 1. Schematic of image testing of simulated vapor chamber in porous media

5.1.1. Steps in Experiment 1

1) Fill the physical model with 100% water-saturated sand
2) Fill a plastic bag with dry sand and seal the bag
3) Place the sealed dry sand bag into the 100% saturated water saturated sand
4) Pack the water saturated sand
5) Set the pulser to reflection mode
6) Send and receive ultrasonic signals at fixed positions on the physical model
7) Localize the excitation and echo signals from the signal record

8) Calculate the distance and perform imaging

5.1.2. Image Results

Since the experimental environment used to measure the location of the dry sand bag was a water-saturated sand pack, the speed of sound used for further calculation was 1750 m/s, which is the speed obtained from the previous measurement. Figures 5.2 and 5.3 show a typical reflected signal from the water tank containing a buried dry sand bag. Figure 5.2 shows the signal when no dry sand bag was placed between the two opposite surfaces of the physical model. Figure 5.3 shows the echo signal from the interface between the water-saturated sand pack and the dry sand bag.

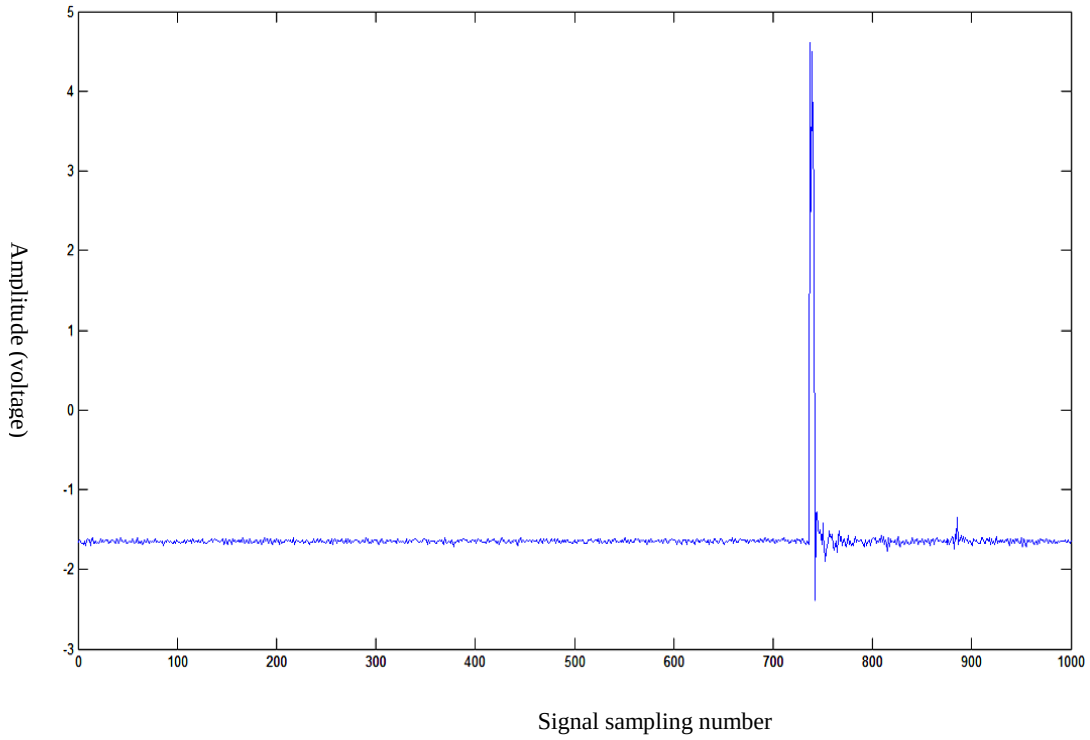

Fig. 5. 2. Reflected signal without a sealed dry sand bag buried in water saturated sand

The signal in Figure 5.1 is shown from the third collection point from the left side. Following the signal processing steps, we can extract the positions of the transmitted pulse and the echo pulse as 744 and 886. The TOF time slot between the transmitted signal and the reflected signal is $\frac{886-744}{500000}=292\mu s$ so the distance between the attached surface and the reflective surface is $\frac{1750m/s\times 292\mu s}{2}=25.5cm$. The true width of the water tank is 25 cm and the error is acceptable.

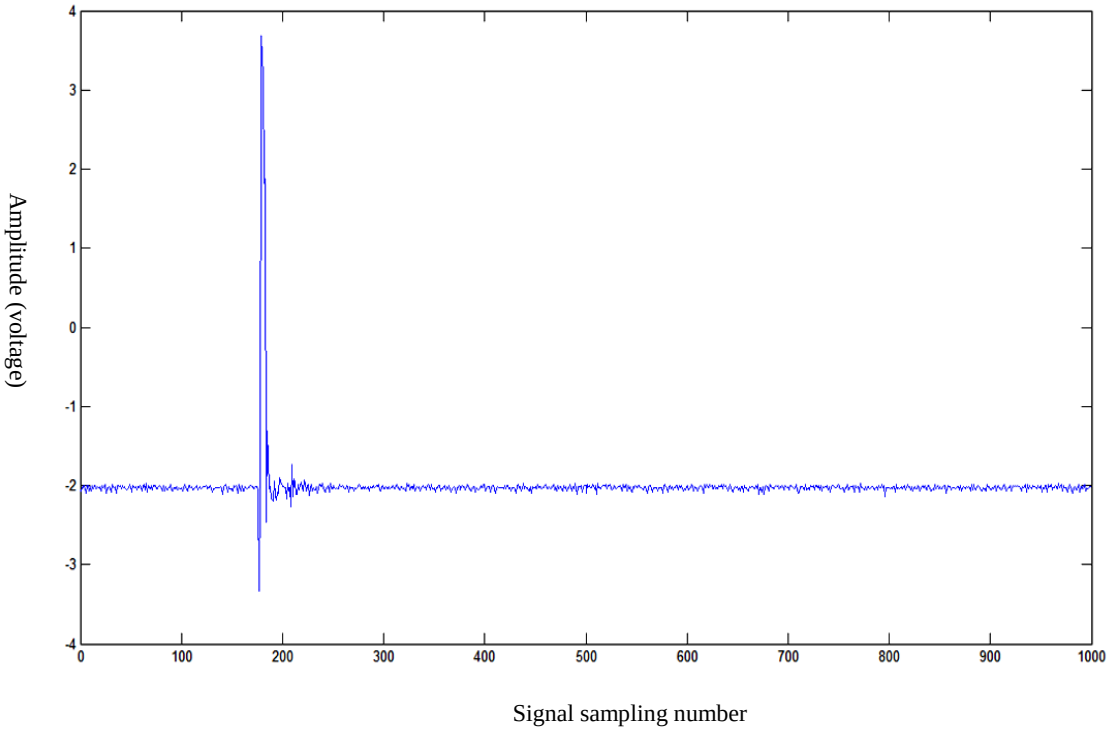

Fig. 5. 3. Reflected signal from the sealed dry sand bag

The signal in Figure 5.3 is from the 14th collection point on the left side of the physical model. The time slot between the transmitted signal and the reflected signal is 48 μs so the distance between the attached surface and the reflective surface is $\frac{1750m/s \times 48\mu s}{2} = 4.2cm$. The outcome of the experiment shows the dry sand bag is 4.2 cm away from the physical model's surface upon which the transducer is attached.

Data from 30 points per side of the water tank are processed. Figure 5.4 shows the measured shape of the dry sand bag buried in the water-saturated sand pack measured by the acoustic system. The upper side of Figure 5.4 corresponds to the left of the water tank.

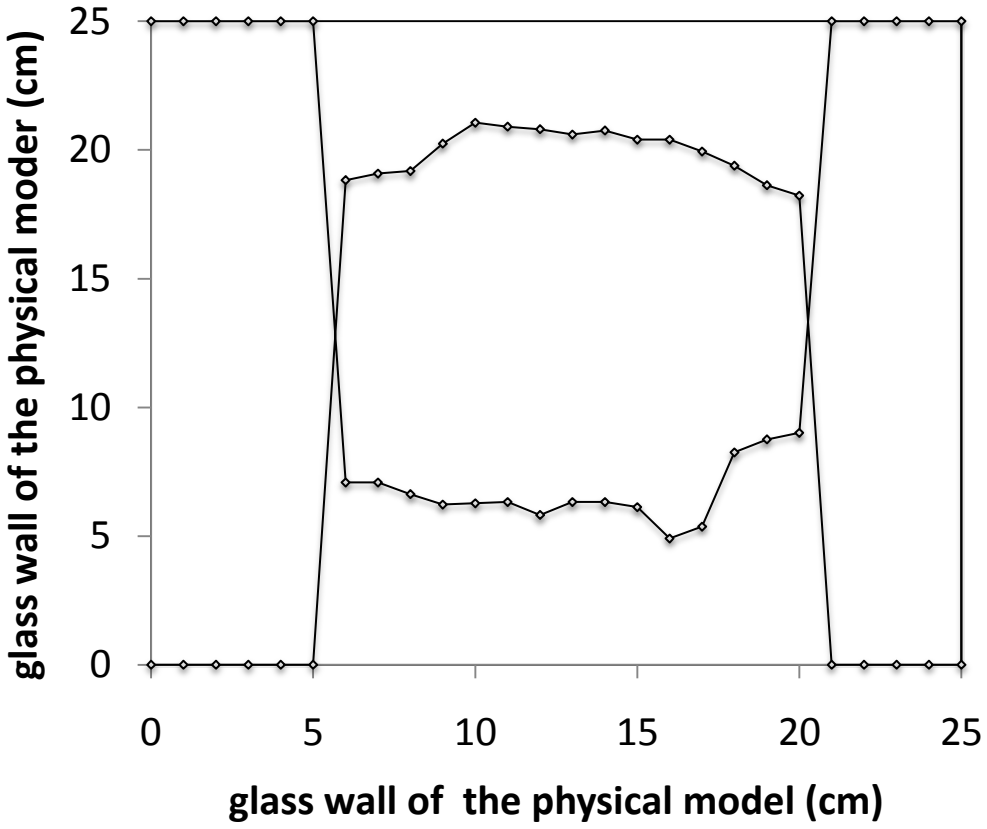

Fig. 5. 4. Shape of the dry sand bag

5.2. Imaging of an Air Balloon in Water Saturated Sand

The second experiment measures the shape of the air balloon in the water-saturated sand pack. Three different-shaped air balloons were used to mimic the growing process of a vapor chamber in the VAPEX process. The signals were collected at every interval of 1 cm (1/4 length of the diameter of the transducer). The main purpose of this experiment is to detect the air/water saturated sand interface. The resolution of this technique is illustrated in the three experiments, which measured three different-shaped air balloons. The outcomes are analyzed to distinguish the difference between the three resulting images.

5.2.1. Steps in Experiment 2

1) Fill the aquarium with 100% water-saturated sand
2) Put an air balloon into the 100% saturated water saturated sand
3) Pack the water saturated sand down
4) Set the pulser to reflection mode
5) Send and receive ultrasonic signals at every fixed position on the aquarium
6) Localize the excitation and echo signals from the signal record
7) Distance calculation and imaging
8) Put another air balloon with a different shape into the water saturated sand
9) Send and receive ultrasonic signals at every fixed position on the aquarium
10) Localize the excitation and echo signals from the signal record
11) Distance calculation and imaging
12) Tie two air balloons together
13) Put the tied air balloons into the 100% saturated water saturated sand
14) Send and receive ultrasonic signals at every fixed position on the aquarium
15) Localize the excitation and echo signals from the signal record
16) Distance calculation and imaging

5.2.2. Image Results

Since the experimental environment used to measure the location of the air balloon is still 100% water-saturated sand, the speed of sound used for further calculation

is 1750 m/s, which is the same as the measurement of the dry sand bag. Figure 5.5shows a typical reflected signal from the water tank with an air balloon buried in the sand pack. The reflector that reflects the ultrasound is the interface between the water saturated sand and the air balloon.

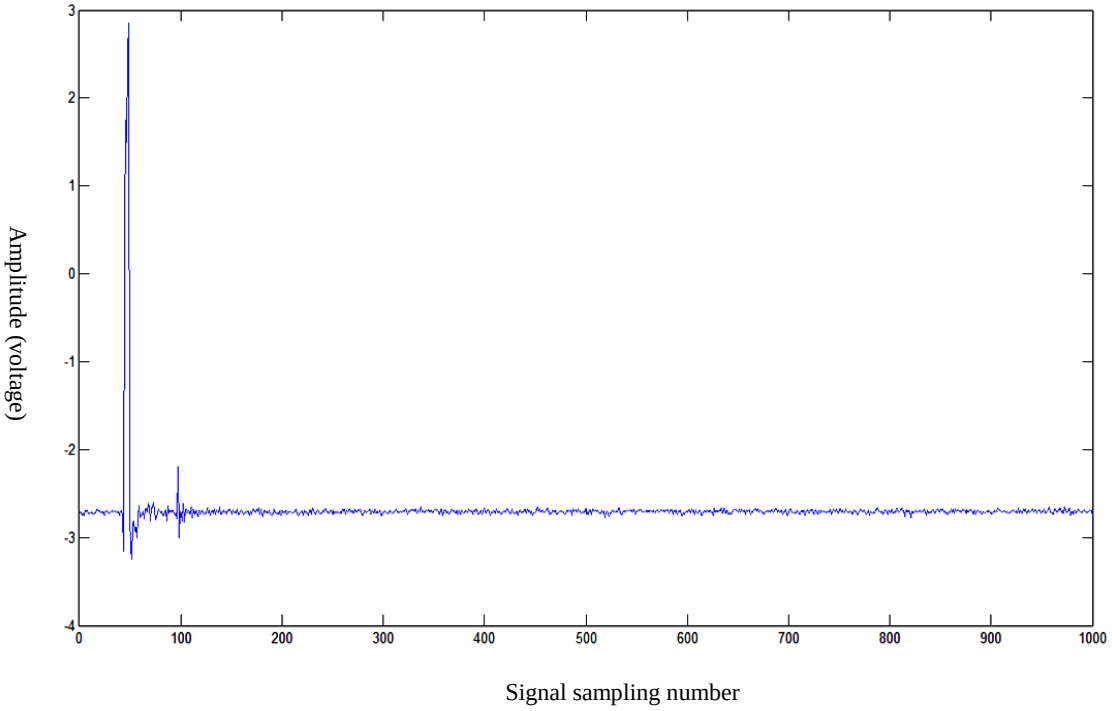

Fig. 5. 5. Reflected signal from the air balloon

The signal shown in Figure 5.4 is from the 15th collection point on the left side of the water tank. The time slot between the transmitted signal and the reflected signal is 96 μs, therefore the distance between the attached surface and the reflective surface is $\frac{1750m/s \times 96\mu s}{2} = 8.4cm$. The results of the experiment show that the detected air balloon's surface is 8.4 cm away from the water tank surface upon which the transducer is attached.

Data from 25 points per side of the water tank are processed. Figure 5.6 shows the

measured shape of the first air balloon buried in the 100% water saturated sand measured by the acoustic system. The upper side of the figure corresponds to the left of the water tank.

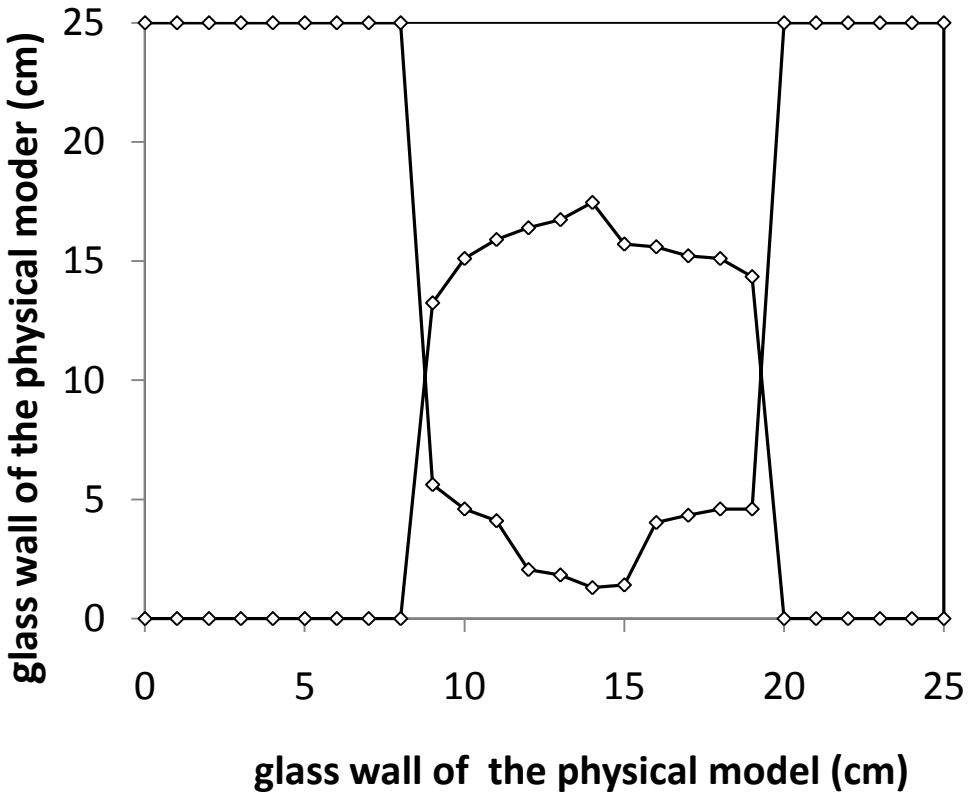

Fig. 5. 6. Shape of the first air balloon

Data from 25 points per side of the water tank are processed. Figure 5.7 shows the measured shape of the second air balloon buried in the water saturated sand from the acoustic system. The upper side of the figure corresponds to the left of the water tank.

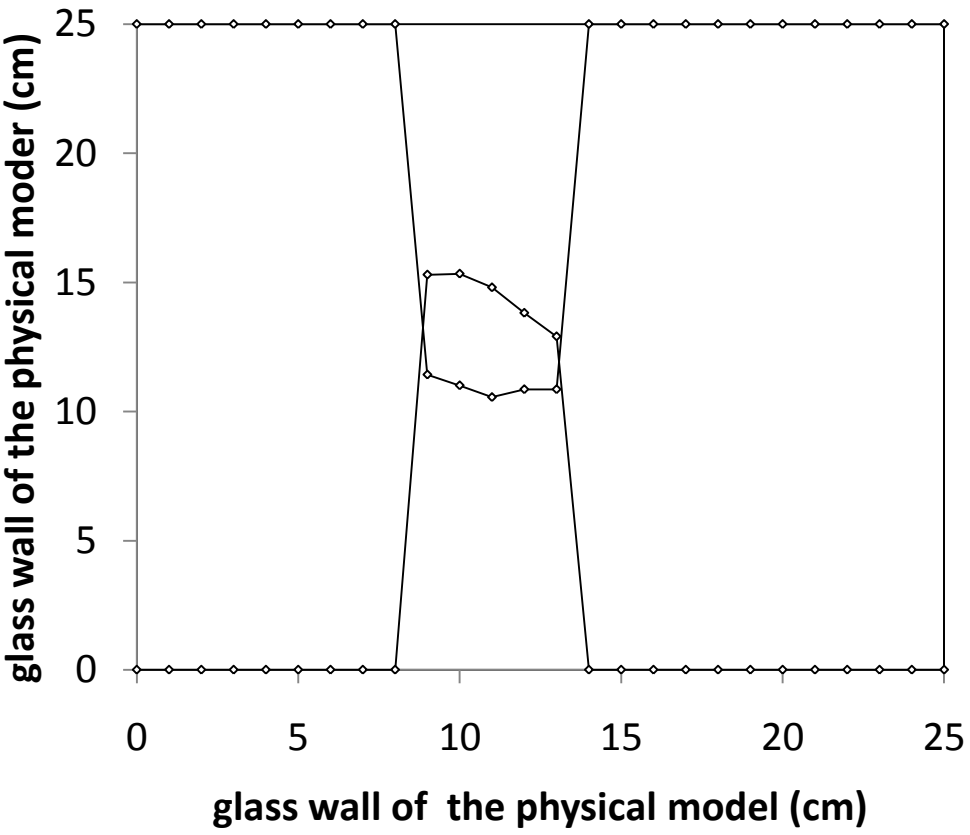

Fig. 5. 7. Shape of the second air balloon

Data from 25 points per side of the water tank are processed. Figure 5.8 shows the measured shape of the two tied balloons buried in the water saturated sand from the acoustic system. The upper side of the figure corresponds to the left of the water tank.

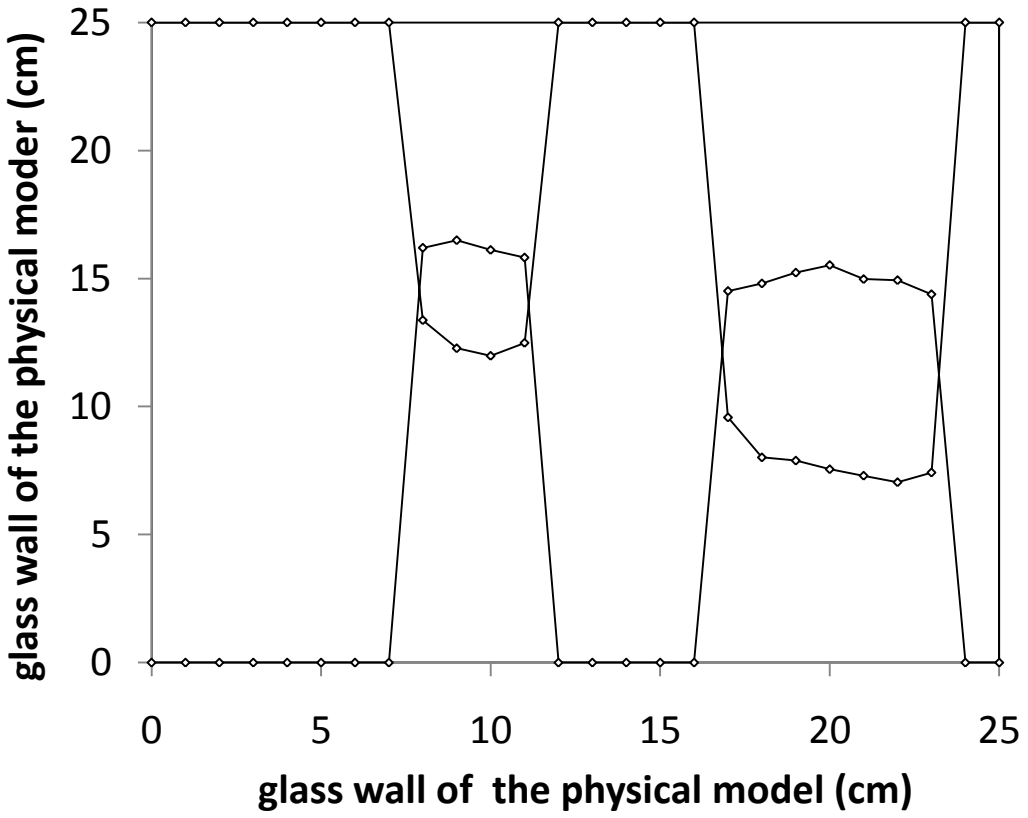

Fig. 5. 8. Shape of two tied air balloons

5.3. Imaging of Air Balloon in Oil saturated sand

The final experiment detects the shape of the air balloon in the oil saturated sand. An air balloon is buried in the crude oil saturated sand in a plastic container smaller than the water tank. A smaller plastic container is selected due to the limited amount of crude oil that can be used in the experiment and also due to the relatively poor propagation of the ultrasound through the oil saturated sand. The main purpose of this experiment is to measure the interface between the air and the oil saturated sand and the accuracy of the ultrasound detection technique in the “oil field”.

5.3.1. Working Procedure

1) Fill the aquarium with 100% saturated crude oil saturated sand
2) Bury an air balloon in the crude oil saturated sand
3) Set the pulser to reflection mode
4) Send and receive ultrasonic signals at every fixed position on the aquarium
5) De-noise the acquired signal by wavelet transform
6) Localize the excitation and echo signals from the signal record
7) Distance calculation and imaging

5.3.2. Image Results

Since the experimental environment used to measure the location of the air balloon is 100% oil saturated sand, the speed of sound used for further calculation is 1360m/s. Figure 5.9 shows a typical reflected signal from the water tank with an air balloon buried within it. The interface is between the 100% oil saturated sand and air balloon.

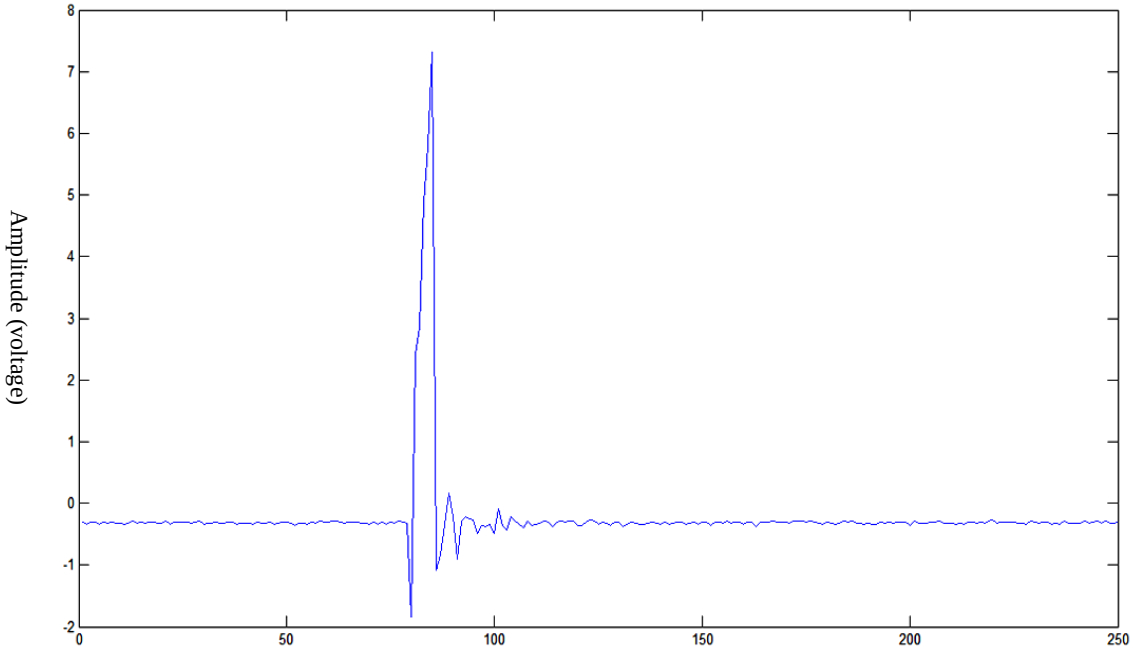

Fig. 5. 9. Reflection signal from oil saturated sand and air balloon interface

According to Figure 5.9, the first spike of this signal series is the transmitted pulse, whose position is easily observed, but the accurate position of the reflected signal is difficult to determine since there are few smaller spikes following the transmitted pulse, so wavelet transom is applied to the signal. Figure 5.10 shows level 1 detail wavelet transform coefficients after a 5^{th} level wavelet transform.

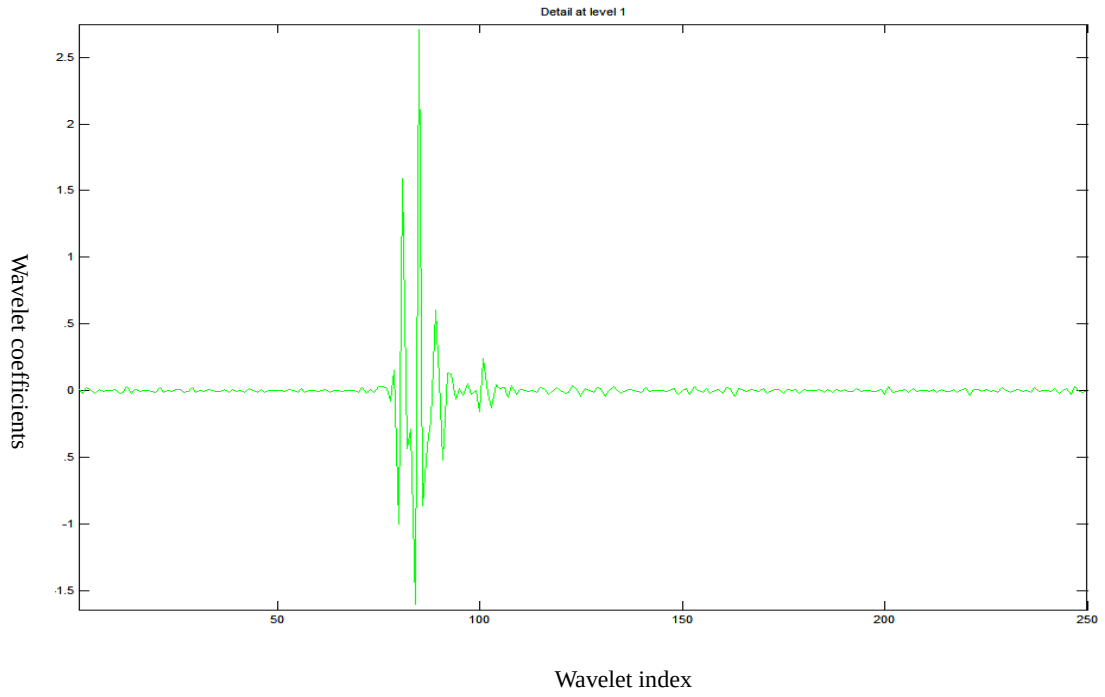

Fig. 5. 10. Wavelet transform coefficients at detail level 1

When observing Figure 5.10, we can more easily denote the position of the reflected signal. The precise position index of the reflected signal is 101 so the time slot between the transmitted and reflected signal is 32 μs. This is multiplied by the speed of sound and divided by two to obtain the distance between the attached surface and the reflective surface, $\frac{1360m/s \times 32\mu s}{2} = 2.176cm$. The outcome of the experiment shows the air balloon is 2.176cm away from the plastic container's surface upon which the transducer is attached.

Data from 20 points per side of the tank are processed. Figure 5.11 shows the measured shape of the two tied balloons buried in the 100% oil saturated sand from the acoustic system. The upper side of Figure 5.11 corresponds to the left side of the tank.

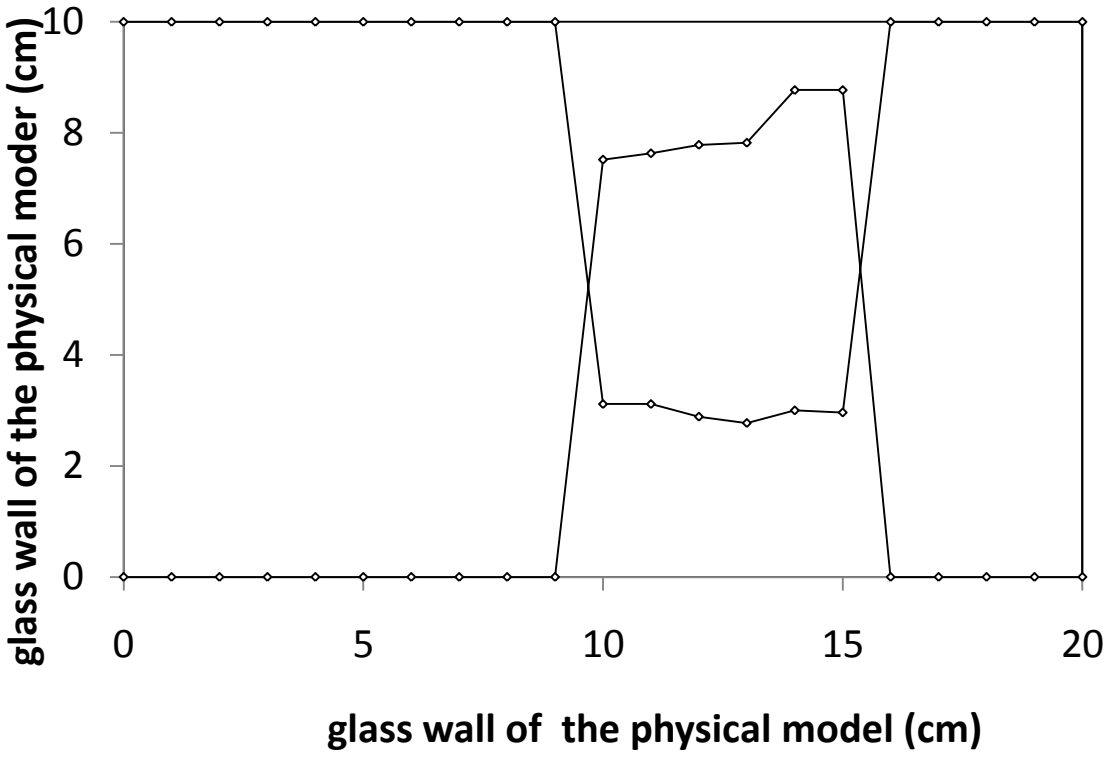

Fig. 5. 11. Shape of the air balloon buried in the oil saturated sand

5.4. Accuracy

The submerged air balloon and the dry sand bag are detected by the transducer to produce a 2-D image. The vertical location of the objects and transducer are measured relative to the bottom of the water tank. Unfortunately, we could not measure the exact shapes of the submerged air balloon and dry sand bag due to the invisibility of the media.

The accuracy of the system cannot be determined by comparing the shape of an object with 2-D measurements by the transducer in air. A series of measurements are made through the oil-sand media by varying the position of a steel plate, since its exact position can be determined by the transducer. The measured and actual distances between

the transducer and the object in the oil saturated sand are compared in Tables 3.1 and 3.2 which are shown in chapter 3.

Since the same speed of sound and signal processing algorithm were used to process the signal with respect to calculating the TOF and the distance from the transducer to the reflector object, the error rate range of the distance from the air balloon or the dry sand bag will be similar to the error rate range for the steel plate experiments. During the entire size imaging process, a huge error will take place when an irregular shape change occurs in between the two data collection points.

A second method to determine the accuracy of a measurement is to measure an object's position and shape in water. The media is transparent and the position of the object in the water is easily determined. A grid map is attached to the bottom of the water tank as when the spatial resolution was measured. The position and shape of an object in the water can easily be seen from the top of the tank.

As in Figure 3.14, it shows the experimental enclosure with a grid map attached to the bottom of the water tank. It is used here show the exact shape and position of the buried object in water. The propagating media is water, so the speed of sound used in the calculations is assumed to be 1470.59 m/s. A sand bag is placed in the water; the grid map on the bottom is to help us to determine the accuracy of the system. The sand bag's shape and position are shown in Figure 5.12.

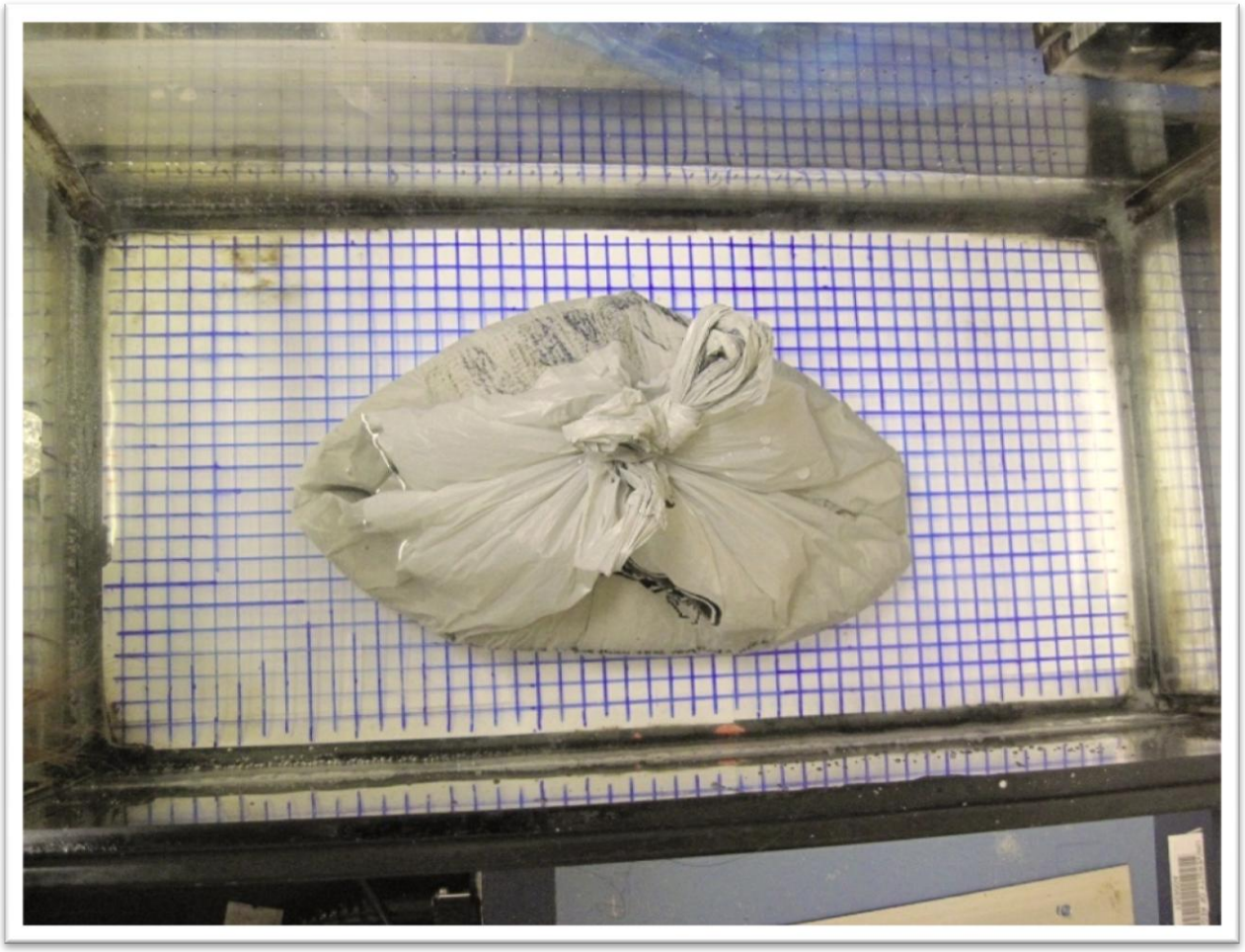

Fig. 5. 12. Shape and position of the sand bag in the water

The measurement procedure used to locate the sand bag in the water is the same as the previous measurements which detected either a sand bag or an air balloon in the water-sand or the oil saturated sand. The result of this experiment is shown in Figure 5.13.

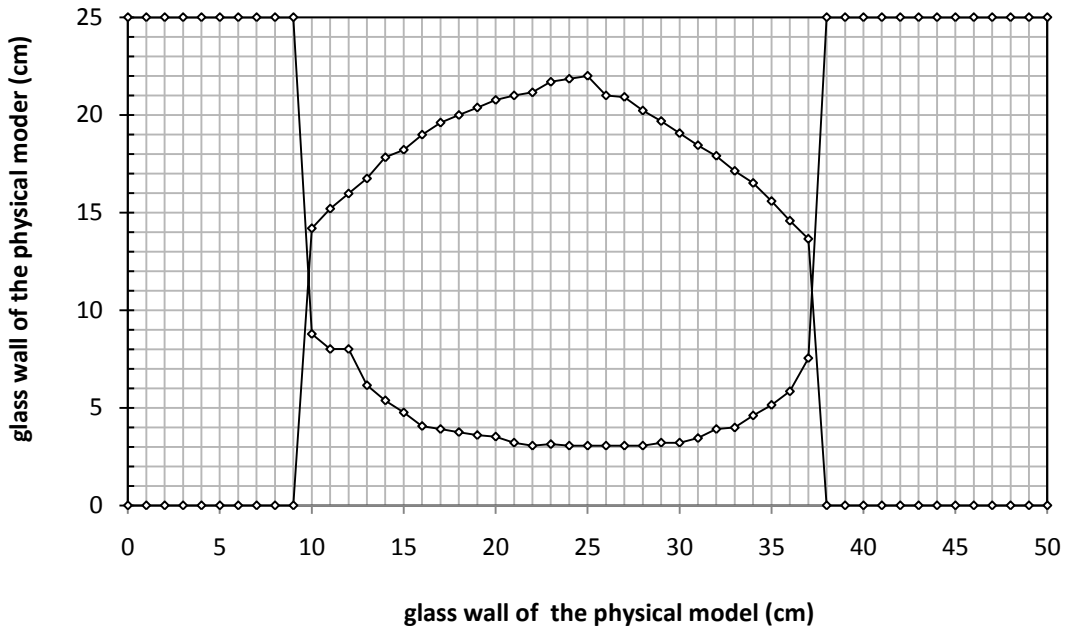

Fig. 5. 13. Result of the shape and position test

The above noted result was quite accurate and reliable according to the comparison between the result and the actual shape of the sand bag.

5.5. Discussion

The shapes of the air bubbles in the 2-D images were more polygonal than spherical and further research is required to either improve the experimental apparatus or digital image processing is needed to obtain realistic images, including the possibility of extending the measurements to 3-D images.

5.5.1. Resolution Improvement

The experiments fail to reveal the actual air contours of the air balloon or sand bag which are evenly distributed. If the whole contour is divided by the points from the collected signals, a curly line between the two points should be obtained. However, the

contour appearing in the image is a straight line between the two collected points due to the fact the signals are collected at discrete points. There are two main approaches to improving the resolution in order to make the polygon more like a real ellipsoid. The first approach is to shorten the distance as much as possible between the two fixed points, or to design an automated detection system in order to have the transducer travel along the attached surface. The second approach is to use a numerical method to interpolate the positions between two fixed points.

5.5.2. 3-D Imaging and Growth Monitoring

The imaging process of previous experiments produced two-dimensional images because the signals were only collected by the transducer, which was attached to the opposite surfaces of the media container at the same height. For a three-dimensional image, the height, length and width are required. To make this system a three-dimensional system, the signals should be measured at different heights as well. The measurement points where the transducer should be positioned are going to be a grid system. The height and reflected signals from the additional positions will also be processed.

To monitor the growth of the vapor chamber, the entire measurement procedure should be repeated frequently. For example, it could be done hourly or at set time intervals as determined by the research.

6. Conclusion, Limitations and Recommendations

6.1. Conclusion

An analysis of the existing ultrasonic system provides us with evidence that the application of ultrasonic testing system in porous media to test the shape and growth of a vapor chamber during the VAPEX process is feasible in a simulated lab scale. The wavelet transform has a time-frequency mapping ability which can extract the discontinuity of the ultrasound signal record.

Experimental results showed that lower frequencies had a relatively strong ability to propagate through the high energy scattering and loss media such as the water-sand and oil saturated sand. However, when the ultrasound frequency drops below 100 kHz, the resolution is too low to accurately detect any echo signal. Hence, there is a tradeoff between higher resolution and less attenuation. For lab scale purposes, a 25 cm×50 cm water tank containing water saturated sand was used, and the plastic container for the oil saturated sand was 10 cm ×15 cm. In the relatively small lab scale environment, a more accurate resolution is required to monitor the 2-D shape of a gas bubble in a lab scale sized VAPEX process compared to less attenuation with a low frequency ultrasound wave. Therefore, a 100 kHz ultrasound wave was selected to achieve the specified resolution in the lab scale model. The experimental image data results show reliable pictures of objects with various shapes buried in the media. It demonstrates that an ultrasonic system could be used as a tool to monitor and detect the interface between two

different media. An ultrasound provides reliable results with which to test the/steel interface, water saturated sand/air interface, water saturated sand/dry sand and oil saturated sand/air interface. On this basis, it is feasible to apply an ultrasonic system to monitor the growth of the vapor chamber during the VAPEX process.

The wavelet transform algorithm, a frequency analysis technique, was employed to localize the singularity and de-noise the received signal. This transform, unlike the classical Fourier transform, can map the frequency change of a signal with a variation of time rather than just identify the frequency components of a signal. This property is useful in the discontinuity analysis in an ultrasound signal record. At the same time, the wavelet transform coefficients could be modulated by setting a threshold to help reduce noise, without losing important signal information. This wavelet transform is clearly able to process the ultrasound signal which travels through a noisy environment and viscous media, such as the oil saturated sand.

In this system, the performance evaluation of the wavelet transform algorithm is based on localization and de-noising results from actual signals produced within the system. According to the corresponding results shown in Chapter 4, the wavelet transform algorithm was able to accurately localize the discontinuous portion of the ultrasound signal. It also effectively reduced background noise to distinguish the valuable information contained in the signal.

The accuracy of the entire system is evaluated based upon the distance measurement between the transducer and reflector, and the imaging result of an object

buried in water, rather than the shape of the buried object in the simulated porous media. The opaque environment leads to uncertainty of the location of the buried object, and an inability to measure the actual reflector's shape, which is used to compare the imaging results in order to analyze the error rate. Since the principles of shape and distance measurements are the same, the range of the measurement error rate under simulated porous media situations is based on the distance measurement between the transducer and reflector at the data collection points. This will be the same error rate range produced from the steel plate distance test experiments and those obtained from the water environment. The imaging error may be governed by an irregular shape change in between two data collection points.

Analyses of the experimental results, including the ultrasonic speed tests, the shape of the pulse-echo signal through the media, the experimental results from the distance experiments, the localization of the pulse-echo signal, the reconstructed de-noised signal and the image result from the experimental system, show that the ultrasound experimental system is able to reliably predict the location and the shape of the vapor chamber during the VAPEX process at lab scale. The wavelet transform is evidently a very effective signal processing algorithm when dealing with ultrasound signals.

6.2. Limitation

Although the experimental results show that reliable simulated vapor chambers'

images in water saturated sand and oil saturated sand could be generated by using ultrasound testing system, some limitations to this study exist.

1. The work in this study was strictly lab scale and the VAPEX process was idealize to be represented by air chamber and sealed dry sand bag placed in water saturated sand and oil saturated sand. In actual VAPEX the construction of various compounds will influence the acoustic sensitivity, additional testing is required for this situation.
2. Effects of ultrasound's frequency change were not considered in this study.
3. Spatial resolution was limited to the physical size the transducer and the depth of the object because the acoustic sign disperses with distance.

6.3. Recommendations

The application of an acoustic system to monitor the growth of a vapor chamber during the VAPEX process is a fairly new research area. The evaluation of the feasibility of such a technique is based upon empirical results from lab scale simulations, as only a limited number of researchers apply the ultrasound technique in an industrial area to image the gas bubble or interface between two different materials underground. The measurement data in this thesis was collected from a fairly small and simple model. Thus, it would be worthwhile to study and evaluate this technique in a larger and more complicated environment.

When the ultrasound testing signal passes through a highly viscous media such as

the oil-saturated sand pack, the length that the ultrasound sound can travel is relatively short, this could lead to a lower resolution to detect the reflector which is with a long distance from the transducer. A higher power signal or a lower frequency signal is recommended to fit the purpose of imaging in a larger physical model.

In order to accurately monitor the growth of a vapor chamber in the VAPEX process, a 2-D image is inadequate. Further height information regarding the position of the transducer is required in order to form 2-D images at different heights so as to produce a 3-D image. Furthermore, to make the entire system more accurate, the distance between the data collection points could be arranged more closely, or scanned automatically.

REFERENCES

[1] Froster, D.G., “Lessons Learnt from over 20 years of 4-D Deployment”, SPE 113542, Indian Oil and Gas Technical Conference and Exhibition, Mumbai, India, March 4-6, 2008.

[2] Christiansen, R.L., Kim, H., “Rapid Measurement of Minimum Miscibility Pressure Using the Rising Bubble Apparatus”, SPE 13114, SPE Annual Technical Conference and Exhibition, Houston, TX, USA, September 16–19, 1987.

[3] Steeghs, P., Drijkoningen G., “Seismic Sequence Analysis and Attribute Extraction”, Geophysics, 66: 1947-1947, 2011.

[4] Ober, C.C., Oldfield, R., VanDyke, J. and Womble, D. E., “Seismic Imaging on Massively Parallel Computers”, International Exposition & 67th Annual Meeting Society of Exploration Geophysicists, Dallas, TX, USA, November 2-7, 1997.

[5] Emerick, A.A., De Moraes, A.J., Rodrigues, J.R.P., “History Matching 4D Seismic Data with Efficient Gradient based Methods”, SPE 107179, SPE Europec/EAGE Annual Conference and Exhibition, London, United Kingdom, June 11-14, 2007.

[6] Mikkelsen, P.L., Guderian, K., Du, G., “Improved Reservoir Management through Integration of 4D Seismic Interpretation, Draugen Field, Norway”, SPE 96400, Offshore Europe 2005, Aberdeen, Scotland, U.K., September 6-9, 2005.

[7] Huang, X., Meister, L., Workman, R., “Reservoir Characterization by Integration of Time-Lapse Seismic and Production Data”, SPE 38495, SPE Annual Technical Conference Exhibition, San Antonio, TX, USA, October 5-8, 1997.

[8] Huang, X., Bentley, L.R., Laflamme, C., “Integration of Production History and Time-Lapse Seismic Data guided by Seismic Attribute Zonation”, SPE 68819, SPE Western Regional Meeting, Bakersfield, CA, USA, March 26-30, 2001.

[9] Fornel, A., Roggero, F., Noetinger, B., “Using Time Domain Seismic Attributes for History Matching”, IEA-International workshop and symposium of the International Energy Agency, Vedbaek, Denmark, September 4-7, 2007.

[10] Wu, J., Mekerji, T., Journel, A.G. “Improving Water Saturation Prediction with 4-D Seismic”, SPE 95125, SPE Annual Technical Conference and Exhibition, Dallas, TX, USA, October 9-12, 2005.

[11] Arts, R., Brouwer, J., Hofstee, C., Kooijman, J., Drijkoningen, G., “Continuous 4D Monitoring is Now Reality”, SPE 99927, SPE Intelligent Energy Conference and Exhibition, Amsterdam, The Netherlands, April 11-13, 2006.

[12] http://en.wikipedia.org/wiki/Well_logging, as seen on October 17, 2010.

[13] Chopra, P., Papp, E., Gibson, D., “Geophysical Well Logging”, http://crcleme.org.au/Pubs/OPEN%20FILE%20REPORTS/OFR%20144/13Wells.pdf, as seen on October 18, 2010.

[14] Kane, J., Herrmann, F.J., Toksoz, M. N., “Wavelet Domain Linear Inversion with Application to Well Logging”, Expanded abstract in the Proceedings of the 71th annual meeting of the Society of Exploration Geophysicists, May 11, 2001.

[15] Prokoph, A., Agterberg, F.P., “Wavelet Analysis of Well-Logging Data from Oil Source Rock, Egret member, Offshore Eastern Canada”, AAPG Bulletin, V.84, No. 10, p.

1617-1632, October 2000.

[16] Herrmann, F. J., “Multiscale Analysis of Well- and Seismic Data”, Mathematical Methods in Geophysical Imaging V, V. 3453, p. 180-208, SPIE, 1998b.

[17] Kimball, C. V., “Sonic Well Logging with Multiwave Processing”, Schlumberger, WO 2011/081951, November 2011.

[18] Nugraha, H.B., Langi, A. Z. R., “A Procedure for Singularity Measurement using Wavelet”, Asia-Pacific Conference on Circuits and Systems, 1 , April 7 – 10, 2002.

[19] Donoho, D.L., “De-nosing by Soft-Thresholding”, IEEE Trans. Inform. Theory, V. 41, No. 3, p. 613-627. May, 1995.

[20] Saito, N., Coifman, R.R., “Extraction of Geological Information from Acoustic Well-Logging Waveforms using Time-Frequency Wavelets”, Geophysics, V 62, No. 6,p. 1021-1993, November-December, 1997.

[21] White, J. E., “Underground Sound: Application of Seismic Waves”, Elsevier Science Publ. Co., Inc. 1983.

[22] Paillet, F. L., Cheng, C. H.,, “Acoustic Waves in Boreholes”, CRC Press, Inc., 1991.

[23] Murphy,W., Reischer, A., Hsu, K., “Modulus Decomposition of Compressional and Shear velocities in Sand Bodies”, Geophysics, V. 58, p. 227–239, 1993.

[24] Winkler, K. W., Murphy, W. F., III, “Acoustic Velocity and Attenuation in Porous Rocks, in Ahrens, T. J., Ed., Rock Physics and Phase Relations”, a Handbook of Physical Constants: Am. Geophys, Union, 20–34, 1995.

[25]Kimball, C. V., Marzetta, T. L., “Semblance Processing of Borehole Acoustic Array Data” Geophysics, V. 49, p. 274–281, 1984.

[26] Hsu, K., “Wave Separation and Feature Extraction of Acoustic Well-Logging Waveforms using Karhunen-Loeve Transformation”, Geophysics, V. 55, p.176–184, 1990.

[27] Desai, M., Shazeer, D.J., “Acoustic Transient Analysis using Wavelet Decomposition”, Proceedings of the IEEE Conference on Neural Networks for Ocean Engineering, p. 29–40, 1991.

[28] An, P., “Sand Mapping Using Multi-Wavelet Seismic Trace Decomposition and Reconstruction”, SPE 104115-MS, International Oil & Gas Conference and Exhibition, Beijing, China, December 5-7, 2006.

[29] Liu, X., Zhang, X. “Wavelet Transform and Seismic Signal Analysis”, Earthquake, V. 22, No. 3, 2002.

[30] Foster, D.J., Lane, F.D., Mosher, C.C., Wu, R., “Seismic Processing 9: Wavelet Transforms”, Wavelet Transforms for Seismic Data Processing, http://www.es.ucsc.edu/~wrs/publication/seg/seg1997/ea199713181321.pdf, as seen on October 18, 2010.

[31] Nestor, R., Ray, S. Chan, A., Jensen, J., “Well-Log Feature Extraction using Wavelet and Genetic Algorithm”, AAPG Annual Meeting, Houston, Texas, USA, March 10-13, 2002.

[32] Yue, W., Guo, T., Liu, Z., “Identifying Reservoir Fluids by Wavelet Transform of Well

Logs", SPE 88559, SPE Asia Pacific Oil and Gas Conference and Exhibition, Perth, Australia, October 18-20, 2004.

[33] Strauss, M., Sapir, M., Glinsky, M.E., Melick, J.J., "Geologic Lithofacies Identification using the Multiscale Character of Seismic Reflections", Journal of Applied Physics, V. 94, I. 8, p.5350 – 5358, October, 2003.

[34] Li, X., Ulrych, T.J., "Well Log Analysis using the Wavelet Transform", http://www.eos.ubc.ca/research/cdsst/members/8_97.pdf, as seen on October 20, 2010.

[35] Yang, X., Zhao, J., Li, J., Liu, J., Zeng, S., "The Application of the Wavelet Transform to the Prediction of Gas Zones", Wavelet Analysis and its Applications, Lecture Notes in Computer Science, V. 2251/2001, 430-434, DOI: 10.1007/3-540-45333-4_54, 2001.

[36] Hloupis, G., Vallianatos, F., "Denoising Seismic Data using Wavelet Methods: a Comparison study", Geophysical Research Abstract, V. 11, EGU2009-6165-1, 2009, EGU General Assembly, Vienna, April, 2009.

[37] Cvetkovic, M., Pralica, N., Marfurt, K.J., Chávez-Pérez, S., "Some Applications of Wavelet Transform in Seismic Data Processing", SEG Expanded Abstract, November, 2008.

[38] Johnson, D.J., "Probing Porous Media with Superfluid Acoustics", Journal of Physics, V. 87, Issue S1, p. S112-S112, 1990.

[39], Morin, M.E., Panella, J., Baker, D.A., Engle, J., "Ultrasound Detection of a Carcinoid Tumor", Abdominal imaging, V.4, No. 1, December, 1979.

[40] Stewart, P. A., Wladimiroff, J. W., Gussenhoven, W. J. "Antenatal Real-Time

Ultrasound Diagnosis of a Congenital Cardiac Malformation", Eur J Obstet Gynecol Reprod Biol 1983;14:233-7, 1983.

[41] Lalor J., Devane D. McParland P., "Ultrasound Screen for Fetal Abnormality in Ireland: a National Survey", Irish Journal of Medical Science, V. 176, No. 3, 2007.

[42] Karpelson, A., "Ultrasonic Measurement of Air Gap Between Metal Walls Using Bending Waves", http://www.ndt.net/article/v12n09/karpelson.pdf , as seen on October 28, 2010.

[43] Binda, L., Saisi, A., "Application of NDTs to the Diagnosis of Historic Structures", NDTCE'09, Non-Destructive Testing in Civil Engineering Nantes, France, June 30 – July 3, 2009.

[44] Hasenstab, A., Osterloh, K., "Defects in Wood Non-Destructive Locating with Low Frequency Ultrasonic Echo Technique", NDTCE'09, Non-Destructive Testing in Civil Engineering Nantes, France, June 30 – July 3, 2009.

[45] Sangoju, B., Murthy, S.G.N., Parthasarathy, S., Wiggenhauser, H., Ravisankar, K., Iyer, N.R., Lakshmanan, N., "Reliability of the Impact-Echo Method on Thickness Measurement of Concrete Elements", NDTCE'09, Non-Destructive Testing in Civil Engineering Nantes, France, June 30 – July 3, 2009.

[46] Chassignole, B., Paris, O., Abittan, E., "Ultrasonic Examination of a CVCS Weld", 6th International Conference on NDE in Relation to Structural Integrity for Nuclear and Pressurized Components, Budapest, Hungary, October, 2007.

[47] Teng,Y., Kioke, K., "Synthetic 3D Imaging of Geothermal System Using

Well-Logging Data Set", Proceedings World Geothermal Congress 2005, Antalya, Turkey, 24-29 April, 2005.

[48] Wylie, A.S., Jr., Wood, J.R., "Well Log Tomography and 3D-Imaging of Core and Log Curve Amplitudes in a Niagaran Reef, Belle River Mills Field, St. Clair County, Michigan, U.S. ", ref AAPG Bull., v. 89, No. 4, p. 329-357, April, 2005.

[49] Gardner, G., "Investigations in Geophysice", Society of Exploration Geophysicists.

[50] Leite, L.W.B., Heilmann, Z., Koglin, I., Mann, J., Steht, M.V., Chira-Oliva, P., "Amazon Seismic Data Imaging with the WIT System", 9th International Congress of the Brazilian Geophysical Society held in Salvador, Brazil, 11-14 September , 2005.

[51] Bulter, R.M. and Mokrys, I.J., "Solvent Analog Model of Steam-Assisted Gravity Drainage", AOSTRA Journal of Research, V. 5, No. 1, p. 17–32, 1989.

[52] Allen, F. H. "The Canadian Oil Sands: A Race against the Clock. The Future of Heavy Crude Oils and Tar Sands", 1st UNITAR Conference, Edmonton, Alberta, Canada, June 4-12, 1979; McGraw-Hill: New York, 1981.

[53] ROSMN, A.; Zana, E., "Experimental Studies of Low IFT Displacement by CO2 Injection", SPE 6723, SPE 52nd Annual Fall Meeting, Denver, CO, October 9-12, 1977.

[54] Chen, Y., "Development of Ultrasonic Transducer Testing Austenitic Stainless Steel Weld", 17th World Conference on Nondestructive Testing, Shanghai, China, 25-28 October, 2008.

[55] Coffeen, J. A., "Seismic Exploration Fundamentals the Use of Seismic Techniques in

Finding Oil", PPC book, A division of the Petroleum Publishing Co. Tulsa, Oklahoma, 1978.

[56] Gadallah, M.R., "Reservoir Seismology", Pennwell Books, Pennwell Publishing Company, Tulsa, Oklahoma, January, 1994.

[57] http://en.wikipedia.org/wiki/Seismic_refraction, as seen on October 29, 2010.

[58] http://en.wikipedia.org/wiki/Reflection_seismology, as seen on October 29, 2010.

[59] Gadallah, M.R., Fisher, R.L., "Applied Seismology: A Comprehensive Guide to Seismic Theory and Application", Pennwell Corporation, November 30, 2004.

[60] Mari, J., Arens, G., Chapeller, D. Gaudiani, P., "Geophysics of Reservoir and Civil Engineering", Editions Technip, Paris, 1998.

[61] Boyer, S., Mari, J., "Oil and Gas Exploration Techniques: Seismic Surveying and Well Logging", Editions Technip, 1997.

[62] Debnath, L., "Wavelet Transform & their Applications", Birkhauser, November 16, 2007.

[63] Wee, A., Grayden, D.B., Zhu, Y., Petkovic-Duran, K., Smith, D., "A Continuous Wavelet Transform Algorithm for Peak Detection", Electrophoresis, V. 29, Issue: 20, p.4215-4225, 2008.

[64] Farye, M., "Wavelet Transforms and Their Applications to Turbulence", Annual Reviews Inc, V. 24, p. 395-457, 1992.

[65] Zhang, J., Zheng, C., "Extracting Evoked Potentials with the Singularity Detection Technique", Engineering in Medicine and Biology Magazine, IEEE, V. 16, Issue: 5, p.

155 – 161, Sept.-Oct. 1997.

[66] Kok, M. V. , Yildirim, Y. , Akin, S., “Application of Vapex Process for Light Crude Oil”, Energy Sources, Part A: Recovery, Utilization, and Environmental Effects, V. 30, Issue 1, p. 20 – 26, 2008.

[67] http://www.mathworks.com/help/toolbox/wavelet/gs/f3-1000759.html, as seen on November, 2, 2010.

[68] http://www.mathworks.com/help/toolbox/wavelet/gs/f3-998127.html#f3-1001892, as seen on November, 2, 2010.

[69] http://www.engineeringtoolbox.com/speed-sound-d_82.html, as seen on July 18, 2011.

.

APPENDIX A: Matlab Program for Capturing Real-Time Ultrasonic Signals

```
AI = analoginput('mcc','Dev1');

chan = addchannel(AI,0);

duration = 1; %1 second acquisition

set(AI,'SampleRate',500000)

ActualRate = get(AI,'SampleRate');

set(AI,'SamplesPerTrigger',duration*ActualRate)

set(AI,'TriggerType','Manual')

blocksize = get(AI,'SamplesPerTrigger');

Fs = ActualRate;

start(AI)

trigger(AI)

wait(AI,duration + 1)

data = getdata(AI)
```

APPENDIX B: Matlab Program for Creating Mother Wavelet and its Application to Real Signals

New mother wavelet creation

```
load data1;

IntVAL

plot(X,Y), title('Original Pattern')

new wavelet[psi,xval,nc] = pat2cwav(data1, 'polynomial',6, 'continuous') ;

plot(X,Y,'-',xval,nc*psi,'--'),

title('Original Pattern and Adapted Wavelet (dashed line)')
```

Apply the new mother wavelet to the real signal

```
load data

signal=data(1:500000);

lv = length(signal);

subplot(211), plot(vonkoch);title('Analyzed signal.');

[c,l] = wavedec(signal,5,'newwavelet');

cfd = zeros(5,lv);

for k = 1:5

    d = detcoef(c,l,k);

    d = d(ones(1,2^k),:);
```

```
        cfd(k,:) = wkeep(d(:)',lv);
end
cfd = cfd(:);
I = find(abs(cfd)<sqrt(eps));
cfd(I)=zeros(size(I));
cfd = reshape(cfd,5,lv);
subplot(312), colormap(pink(64));
img = image(flipud(wcodemat(cfd,64,'row')));
set(get(img,'parent'),'YtickLabel',[]);
title('Discrete Transform, absolute coefficients.')
ylabel('level')
```

APPENDIX C: Matlab Program for Excitation and Echo Peak Extraction and TOF Distance Calculation

```
[pks,locs] = findpeaks(signal)

[pks1, locs1] = findpeaks (signal[1:(locs-1);(locs+1):lv])

TOF = (locs1-locs)/SampleRate

d = TOF * velocity
```

APPENDIX D: Matlab Program for 2-D Imaging

For water tank

dleft = [dleft1, dleft2, dleft3, dleft4, dleft5, dleft6, dleft7, dleft8, dleft9, dleft10, dleft11, dleft12, dleft13, dleft14, dleft15, dleft16, dleft17, dleft18, dleft19, dleft20, dleft21, dleft22, dleft23, dleft24, dleft25, dleft26, dleft27, dleft28, dleft29, dleft30]

dright = [25-dright1, 25-dright2, , 25-dright3, 25-dright4, 25-dright5, 25-dright6, 25-dright7, 25-dright8, 25-dright9, 25-dright10, 25-dright11, 25-dright12, 25-dright13, 25-dright14, 25-dright15, 25-dright16, 25-dright17, 25-dright18, 25-dright19, 25-dright20, 25-dright21, 25-dright22, 25-dright23, 25-dright24, 25-dright25, 25-dright26, 25-dright27, 25-dright28, 25-dright29, 25-dright30]

y = 1:30

plot (dleft, y, dright,y)

For plastic container

dleft = [dleft1, dleft2, dleft3, dleft4, dleft5, dleft6, dleft7, dleft8, dleft9, dleft10, dleft11, dleft12, dleft13, dleft14, dleft15, dleft16, dleft17, dleft18, dleft19, dleft20]

dright = [10-dright1, 10-dright2, , 10-dright3, 10-dright4, 10-dright5, 10-dright6, 10-dright7, 10-dright8, 10-dright9, 10-dright10, 10-dright11, 10-dright12, 10-dright13, 10-dright14, 10-dright15, 10-dright16, 10-dright17, 10-dright18, 10-dright19, 10-dright20]

y = 1:20

plot (dleft, y, dright,y)